E.O. Paton Electric Welding Institute of the National Academy of Sciences of Ukraine

International Scientific-Technical and Production Journal

The Paton WELDING JOURNAL

Issue 07 2019

Published Monthly Since 2000

English translation of the monthly «Avtomaticheskaya Svarka» (Automatic Welding) journal published in Russian since 1948

Founders
E.O. Paton Electric Welding Institute, NASU
International Association «Welding»

Publisher
International Association «Welding»

Translators
A.A. Fomin, O.S. Kurochko, I.N. Kutianova
Editor
N.G. Khomenko
Electron galley
D.I. Sereda, T.Yu. Snegiryova

Address
E.O. Paton Electric Welding Institute,
International Association «Welding»
11 Kazimir Malevich Str. (former Bozhenko Str.),
03150, Kyiv, Ukraine
Tel.: (38044) 200 60 16, 200 82 77
Fax: (38044) 200 82 77, 200 81 45
E-mail: journal@paton.kiev.ua
www.patonpublishinghouse.com

State Registration Certificate
KV 4790 of 09.01.2001
ISSN 0957-798X
DOI: http://dx.doi.org/10.15407/tpwj

Subscriptions
$384, 12 issues per year,
air postage and packaging included.
Back issues available.

CONTENTS

DOI: http://dx.doi.org/10.15407/tpwj2019.07.01

STUDY OF PULSED ARC PROCESSES AT PERIODIC SWITCHING OF VOLT-AMPERE CHARACTERISTICS OF ARC POWER SOURCE

G.A. TSYBULKIN
E.O. Paton Electric Welding Institute of the NAS of Ukraine
11 Kazimir Malevich Str., 03150, Kyiv, Ukraine. E-mail: office@paton.kiev.ua

The article discusses the pulsed arc processes carried out by periodic switching of the volt-ampere characteristics of the arc power source having different slope. At the same time, the commutation of the mentioned characteristics itself is realized not forcedly, but automatically based on the information about the current state of the system «power source–arc». The main aim is to find out how effective is this method of gas-shielded pulsed arc welding with consumable electrode. The article presents the results of theoretical investigations and computer modelling of self-oscillating processes, occurring in the system under consideration. A formula was derived for a preliminary evaluation of the pulse repetition rate of the welding current. By varying the value of a certain parameter appearing in this formula, it is possible to set the desired repetition rate of the indicated pulses. 9 Ref., 7 Figures.

Keywords: *pulsed arc welding, consumable electrode, switching of volt-ampere characteristics, computer modelling, pulse repetition rate of welding current*

Pulse process of gas-shielded consumable electrode welding can be realized in different ways [1–7]. Today, it is believed that two methods are the most efficient:

- by means of supply on the arc of additional voltage from special pulse generator, connected in parallel to main arc power source;
- periodic switching of volt-ampere characteristics of arc power source having different slope.

The second method is particularly attractive from point of view that it contains potential possibilities to realize a pulsed welding mode not only due to forced switching of volt-ampere characteristics of arc power source as it is realized in work [5]. For example, it is possible to bring into the «power source–arc» system a feed back providing switching of indicated characteristics automatically based on information on current state of this system.

It is assumed that such a solution will allow getting the new useful properties not typical for the pulsed arc welding system with forced switching of volt-ampere characteristics.

It should be noted that the systems, work of which is based on a principle of change of its parameters depending on current state of the system, in a control theory are referred to a system class with variable structure [8].

This paper will consider the pulsed arc processes formed in a system with automatic switching of volt-ampere characteristics. The aim is to determine how effective the indicated method of pulsed arc welding is.

Figure 1 schematically shows the «power source–arc» system including arc power source (*SP*) with two volt-ampere characteristics, slope of which S_1 and S_2 is different, and welding circuit (*WC*) with consumable electrode. Besides, a logical switching device (*LSD*) was added, which, depending on current state of the system, characterized with output voltage of power source $u_s = u_s(t)$, is connected to a welding circuit or electric circuit with parameter S_1 or with parameter S_2, i.e. changes the structure of the system itself on certain law.

Mathematical description of the system. Based on a scheme, presented in Figure 1, and known properties of arc self-regulation [9] let's make the equations describing the dynamic processes, taking place in the considered system:

$$\left.\begin{aligned} u_x &= u_s + Si, \\ u_s &= u_a + (LD + R)i, \\ u_a &= u_0 + El + S_a i, \\ l &= H - h_0 - \frac{1}{D}(v_e - v_m), \\ v_m &= Mi \end{aligned}\right\}, \qquad (1)$$

where u_x = const is the open circuit voltage; $i = i(t)$ is the welding current; $S = |\partial u_s/di|$ is the absolute value of slope of output volt-ampere characteristic, being equal S_1 or S_2 depending on switch K position;

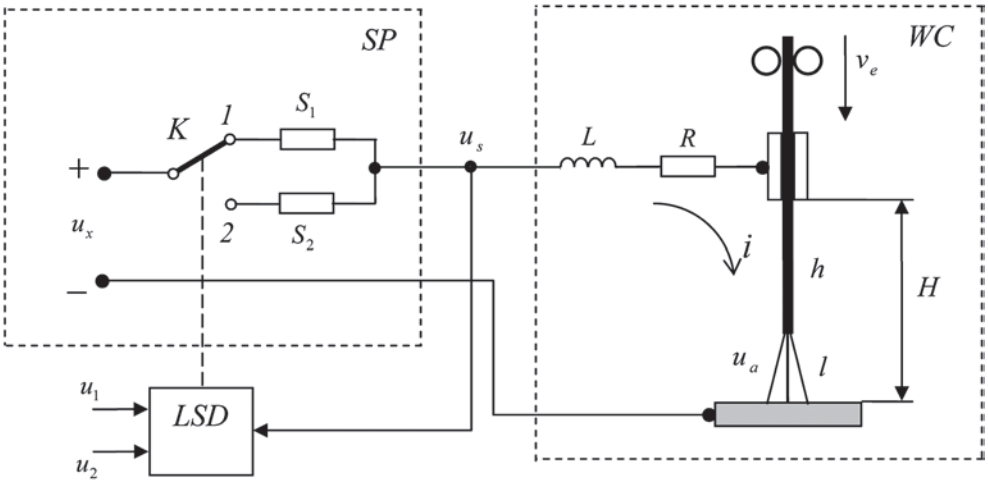

Figure 1. Scheme of «power source–arc» system (see designations in the text)

$u_a = u_a(t)$ is the arc voltage; L is the welding circuit inductance; R is the sum resistance of supply leads, electrode extension and slider contact in a torch nozzle; u_0 is the sum of near-electrode voltage drops; $S_a = |\partial u_a/di|$ is the absolute value of slope of volt-ampere characteristic of arc; E is the electric field intensity in the arc column; $l = l(t)$ is the arc length; H = const is the distance between the edge of current-supplying nozzle and free surface of welding pool; h_0, $h = h(t)$ is the initial and current values of electrode extension; u_e = const, $v_m = v_m(t)$ is the rate of feed and melting of electrode, respectively; $M = dv_m/di$ is the slope of current characteristic of electrode melting; $D = d/dt$ is the operator of differentiation; t is the current time.

Some idealization in relation to the real volt-ampere characteristics of welding current source, namely their approximation to linear functions, was used for compiling equations (1). Figure 2 shows the graphic interpretation of the system of equations (1) in form of a structural scheme. The welding circuit *WC*, included in this system, from point of view of theory of automatic regulation presents itself a closed systems with a natural negative feedback on electrode melting rate v_m, which provides self-stabilization (self-regulation) of arc length $l(t)$ at set rate v_e and set distance H, and relay voltage feedback $u_s(t)$ provides automatic switch of a system structure.

Let's write a law of switching as:

$$S = \begin{cases} S_1, & (u_s \le u_1,\ Du_s < 0), \\ S_2, & (u_s \ge u_2,\ Du_s > 0), \end{cases} \quad S_1 < S_2, \qquad (2)$$

where u_1 and u_2 are the threshold values of $u_s(t)$.

We reduce the system of equations (1) taking into account expression (2) to one differential equation

$$(T_L^2 D + TD + 1)u_s(t) = g, \qquad (3)$$

in which T_L, T are the coefficients determined by the relationships

$$T_L^2 = \frac{L}{EM}, \quad T = \begin{cases} T_1, & (S = S_1), \\ T_2, & (S = S_2), \end{cases} \qquad (4)$$

where

$$T_1 = \frac{S_1 + S_a + R}{EM}, \quad T_2 = \frac{S_2 + S_a + R}{EM},$$

and the right part has a form

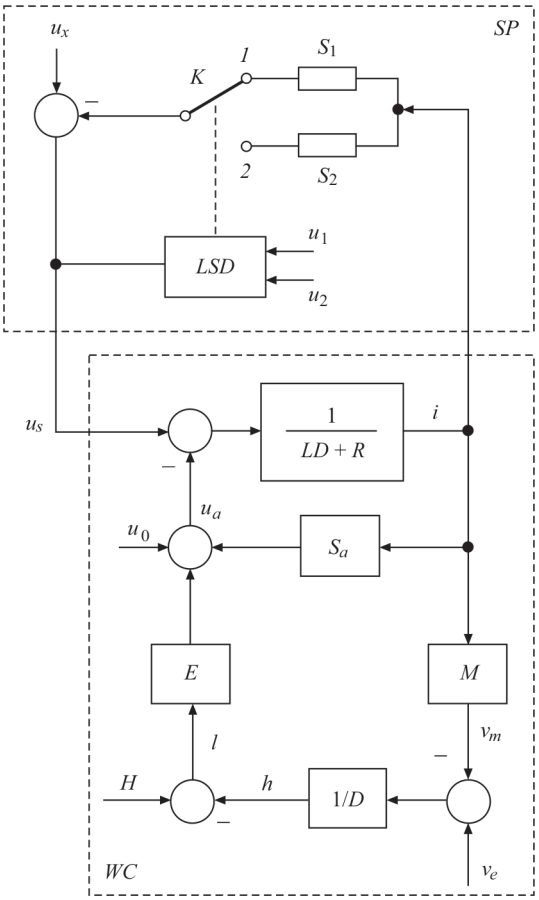

Figure 2. Structural scheme of «power source–arc» system with variable structure (see description in the text)

$$g = \begin{cases} g_1, & (S = S_1), \\ g_2, & (S = S_2), \end{cases} \quad (5)$$

where

$$g_1 = u_x - S_1 \frac{v_e}{M}, \quad g_2 = u_x - S_2 \frac{v_e}{M}.$$

From expressions (4), (5) it can be seen that coefficient T, present in equation (3), and the right part of this equation g has a stepwise change during system switching from one characteristic to another, i.e. in switching of the connections between the system elements. As for value T_L^2 then it, according to (4), is constant and in the majority of practical cases is significantly lower than T since $L << (S + S_a + R)^2/EM$. This allows instead of equation (3) further on using reduced equation

$$(TD + 1)u_s(t) = g. \quad (6)$$

The threshold values u_1 and u_2, included in expression (2), are selected based on the following conditions:

$$u_1 = g_2 + \xi, \quad u_2 = g_1 + \xi, \quad (7)$$

where $\xi > 0$ is the some value selected by technological reasons.

In order to trace the dynamic process, described in equation (6), let's consider sequentially two processes obeying two different differential equations $(T_1D + 1)u_s(t) = g_1$ and $(T_2D + 1)u_s(t) = g_2$.

Let's start from the moment, when switching element K is set in position *1*, as shown in Figure 1. At this stage the welding process takes place according to differential equation $(T_1D + 1)u_s(t) = g_1$. Considering the initial condition $u_s(0) = u_{s0}$ the solution of this equation will have the following form:

$$u_s(t) = (u_{s0} - g_1)\exp\left(-\frac{t}{T_1}\right) + g_1 \quad (8)$$

(point P corresponds to the initial condition $u_s(0) = u_{s0}$ in Figure 3).

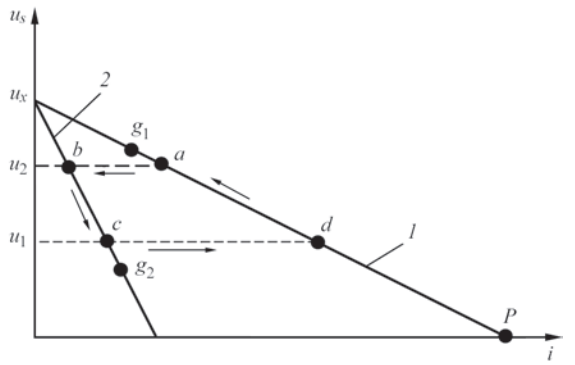

Figure 3. Cyclogram of set self-oscillating mode: *1* — $u_s = u_x - S_1 i$; *2* — $u_s = u_x - S_2 i$ (see designations in the text)

According to (8) $u_s(t)$ voltage with rise of t increases and tends to its set value $g_1 = u_x - S_1 v_e M^{-1}$. However, in moment of time t, when $u_s(t)$ becomes equal to the threshold value $u_2 = g_1 - \xi$, there is switching of the system from characteristic 1 to characteristic *2* according to law (2) (switch K in Figure 1 is set in position *2* at that). A working point of the considered dynamic process (see Figure 3) «stepwise» transfers from point a in point b. At that voltage u_s, being equal to u_2, remains unchangeable, but there is a stepwise decrease of welding current $i = i(t)$. This is the end of the first stage.

The dynamic process on the second stage is regulated by differential equation

$$(T_2D + 1)u_s(t) = g_2.$$

Solution of this equation considering initial condition $u_s(t_1) = u_2$ takes the form

$$u_s(t) = (u_2 - g_2)\exp\left(-\frac{t - t_1}{T_2}\right) + g_2. \quad (9)$$

Based on (9) voltage $u_s(t)$ starting from moment of time t_1 will decrease tending to set value $g_2 = u_x - S_2 v_e M^{-1}$. As soon as $u_s(t)$ becomes equal to $u_1 = g_2 + \xi$ in accordance with (2) there is switching of the system from characteristic *2* to characteristic *1*. At that the working point «stepwise» transfers from point c into point d. Respectively, there is «stepwise» rise of welding current $i = i(t)$.

Now voltage $u_s(t)$ again starts rising in accordance to equation

$$u_s(t) = (u_1 - g_1)\exp\left(-\frac{t - t_2}{T_2}\right) + g_1, \quad (10)$$

where t_2 is the moment of time, when $u_s(t) = u_1$. Rise of $u_s(t)$ will continue until reaching threshold u_2 in point a. Further the processes in the system will be precisely repeated.

Thus, «slow» movements of the working point on sections da and bc periodically alternate with «quick» (stepwise) movements on sections ab and cd provoking oscillations $u_s(t)$ of relaxation type. Therefore, movement trajectory $a \rightarrow b \rightarrow c \rightarrow d \rightarrow a$ is a stable cycle indicating steady state self-oscillating mode in the considered system. Periodic change of $u_s(t)$ takes place from u_1 to u_2, i.e. in the limits of earlier set zone (and it, if necessary, can be pretty narrow).

Figure 4 shows that «relaxation» oscillations of voltage $u_s(t)$ have a saw-tooth nature. Period of self-oscillations T_k is determined by sum of two time intervals Δt_1 and Δt_2. Interval Δt_1 during which voltage $u_s(t)$ rises from u_1 to u_2 is determined according to equation (10) by relationship

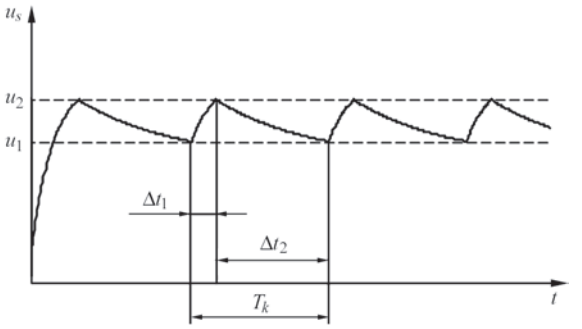

Figure 4. Diagram of change of $u_s(t)$ voltage at set threshold values u_1 and u_2 (see description in the text)

$$\Delta t_1 = T_1 \ln\left(\frac{u_1 - g_1}{u_2 - g_1}\right). \quad (11)$$

Similarly, a time interval Δt_2 during which voltage $u_s(t)$ reduces from u_2 to u_1, is determined in accordance with (9) by expression

$$\Delta t_2 = T_2 \ln\left(\frac{u_2 - g_2}{u_1 - g_2}\right). \quad (12)$$

Formulae (11) and (12) taking into account relationship (7) acquire the next form:

$$\Delta t_1 = T_1 \ln\left(\frac{\Delta g}{\xi} - 1\right), \quad \Delta t_2 = T_2 \ln\left(\frac{\Delta g}{\xi} - 1\right),$$

where $\Delta g = g_2 - g_1 = (S_2 - S_1)v_e M^{-1}$.

Respectively,

$$T_k = (T_1 + T_2) \ln\left(\frac{\Delta g}{\xi} - 1\right). \quad (13)$$

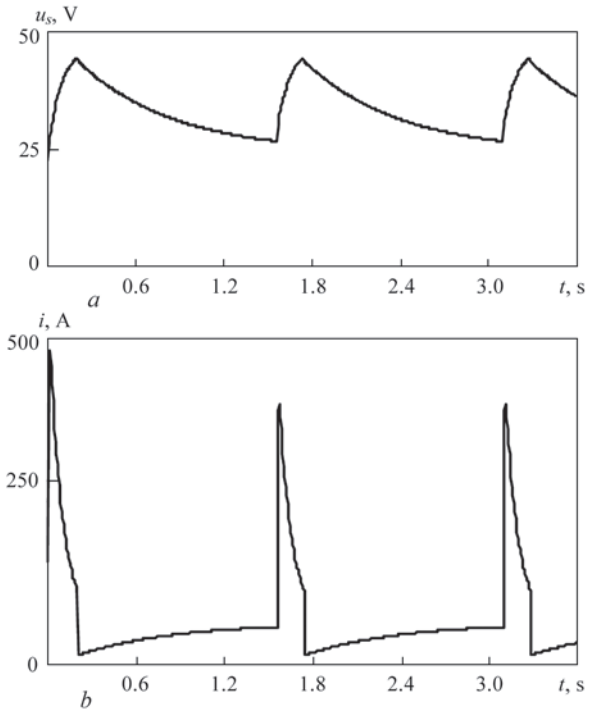

Figure 5. Diagrams at ξ = 2.5 V: *a* — $u_s(t)$; *b* — $i(t)$

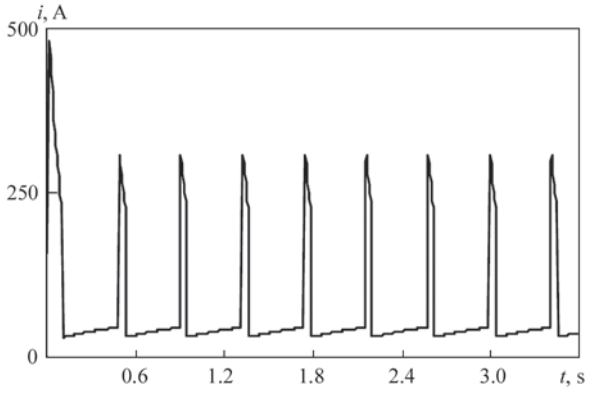

Figure 6. Diagram $i(t)$ at ξ = 8 V

A period of relaxation T_k (at earlier selected values of S_1 and S_2) depends only on value of parameter ξ, varying which it is possible to set desired frequency $f = 1/T_k$ of self-oscillating process of the considered system.

The results of computer modelling. Figures 5–7 present the results of modelling of the self-oscillating processes setting in the considered system at the next values of parameters of robotic arc welding: u_x = = 50 V; u_0 = 18 V; S_1 = 0.05 V/A; S_2 = 0.4 V/A; S_a = = 0.02 V/A; R = 0.01 Ohm; $L = 5 \cdot 10^{-4}$ H; E = 2 V/mm; v_e = 20 mm/s; M = 0.31 mm/(A·s); H = 17 mm.

Figure 5, in particular, shows that the output voltage of arc power source $u_s(t)$, as it should be expected, has a saw-tooth shape and welding current $i(t)$ has a pulsed nature. The current pulses appear in the moments of «spontaneous» transfer of current state of the considered system from point *c* to point *d* (Figure 3).

Diagram $i(t)$, presented in Figure 6, was obtained at ξ = 8 V. Comparing the diagrams, presented in Figures 5 and 6, it is possible to see that increase of ξ provokes rise of pulse repetition rate $f = 1/T_k$.

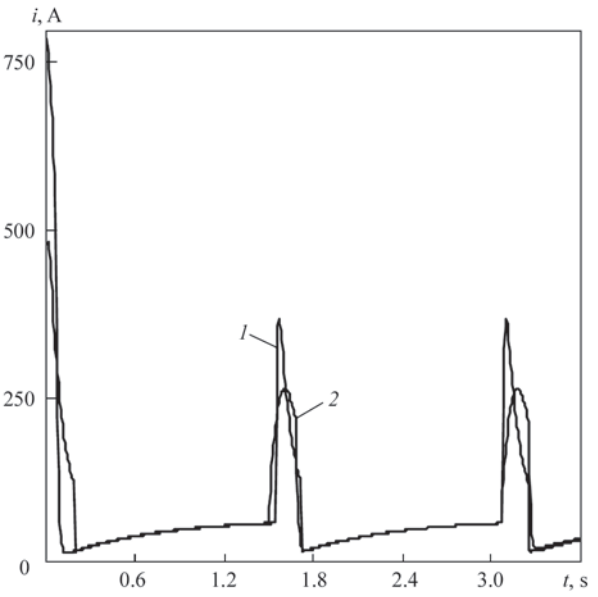

Figure 7. Diagrams $i(t)$ at ξ = 2.5 V: *1* — $L = 5 \cdot 10^{-4}$ H; *2* — L = = $5 \cdot 10^{-3}$

Let's come back to the issue of how significant is the effect on the self-oscillating process of a small parameter T_L not considered by us and depending according to (4) on system inductance L. To solve this problem, instead of simplified equation (6), initial equation (3) was used in computer modelling.

Figure 7 presents the results of modelling obtained at two different values of inductance: $L = 5 \cdot 10^{-4}$ H (curve *1*) and $L = 5 \cdot 10^{-3}$ H (curve *2*). Let's firstly compare current pulses $i = i(t)$ in Figure 7 (curve *1*) with current pulses in Figure 5, obtained at $L = 0$. They virtually do not differ from each other neither by shape no on height. Respectively, small inductances (i.e. when $L < 5 \cdot 10^{-4}$ H) do not have significant effect on dynamics of relaxation process $i = i(t)$.

Let's now compare curves *1* and *2* in Figure 7. Height of the pulses reduced only 1.5 times at significant (10 times) increase of inductance L. At that, shape of pulses is somewhat changed (pulse «tip» was smoothed), but nature of relaxation oscillations virtually remains without noticeable changes.

Conclusions

1. The results of theoretical consideration and computer modelling allow making a conclusion about the fact that a satisfactory mode of pulsed arc consumable electrode welding can be realized using the ideas of the system with variable structure.

2. Peculiarities of realizing the considered method of pulsed arc welding lie in the fact that switching of the volt-ampere characteristics is provided not forcedly, but automatically based on information about present state of arc welding process.

3. The main advantage of considered method is a simplicity, reliability and low cost of its realizing.

1. Voropaj, N.M., Ilyushenko, V.M., Lankin, Yu.N. (1999) Peculiarities of pulsed-arc welding with synergic control of mode parameters (Review). *Avtomatich. Svarka*, **6**, 26–32 [in Russian].
2. Zhernosekov, A.M., Andreev, V.V. (2007) Pulsed metal arc welding (Review). *The Paton Welding J.*, 10, 40–43.
3. Krampit, N.Yu., Burakova, E.M., Krampit, M.A. (2014) Short review of methods for control of shielded-gas arc welding process. In: *Modern problems of science and education, 1*. URL:http://www.science-education.ru/115-12069 [in Russian].
4. Dyurgerov, N.G., Lenivkin, V.A. (2015) Technological stability of consumable electrode pulsed-arc welding. *Svarochn. Proizvodstvo*, **4**, 14–18 [in Russian].
5. Shejko, P.P., Pavshuk, V.M. (1992) Power source for consumable electrode pulsed-arc welding with smooth control of parameters. *Avtomatich. Svarka*, **6**, 44–46 [in Russian].
6. *Jing* Nie, Xiao-Feng Meng, Yu Shi (2011) Study on evaluation method of aluminum alloy pulse MIG welding stability based on arc voltage probability density. *Signal and Information Processing*, **2**, 159–164.
7. Mathivanan, A., Senthilkumar, A., Devakumaran, K. (2015) Pulsed current and dual pulse gas metal arc welding of grade AISI. *Defense Technology*, 11(**3**), 269–274.
8. (1988) *Control theory. Terminology*. Ed. by B.G. Volik. Issue 107. Moscow, Nauka [in Russian].
9. Tsybulkin, G.A. (2014) *Adaptive control in arc welding*. Kiev, Stal [in Russian].

Received 02.04.2019

DOI: http://dx.doi.org/10.15407/tpwj2019.07.02

INFLUENCE OF TOOL SHAPE FOR FRICTION STIR WELDING ON PHYSICOMECHANICAL PROPERTIES OF ZONES OF WELDS OF ALUMINIUM ALLOY EN AW 6082-T6

K. KRASNOVSKY[1], **Yu.A. KHOKHLOVA**[2] and **M.A. KHOKHLOV**[2]
[1]Institute of Welding
16-18 Bl. Czeslava Str., Gliwice, 44-100, Poland. E-mail: is@is.gliwice.pl
[2]E.O. Paton Electric Welding Institute of the NAS of Ukraine
11 Kazimir Malevich Str., 03150, Kyiv, Ukraine. E-mail: office@paton.kiev.ua

The paper presents the results of studying the formation of macrostructure and distribution of mechanical properties in welded joints of flat specimens from aluminium alloy EN AW 6082-T6 of 8 mm thick, produced by the method of friction stir welding with application of three types of specially designed pins with collars: C — cylindrical threaded pin and collar with a spiral groove; T—cylindrical threaded pin with three grooves and collar with a spiral groove; S — smooth cylindrical pin without thread and flat collar. Friction stir welding was performed in the equipment of the Institute of Welding in Gliwice (Poland), and treatment and mechanical tests were conducted at the E.O. Paton Electric Welding Institute of the NAS of Ukraine. Mechanical testing by indentation was performed in Micron-gamma device, which allows experimental identification of structural state of metal after refinement and determination of the strain hardening presence by limiting values of ratio of hardness to Young's modulus of elasticity. It was found that for all three specimens the HAZ hardness decreases, and in the zone of thermomechanical effect the hardness increases. Maximum hardness values are inherent to the central part of welded joint nugget, as well as to light-coloured oval concentrated fragments of structure in the nugget upper and lower part. Judging by the presence of nanosized hardened structure and uniformity of its distribution in the nugget, as well as good dispersion of oxide films and absence of discontinuities, the friction stir welding with C-type tool can be regarded as the optimum variant. An assumption was made that formation of a uniform structure in welds can be achieved at three-four rotations of the tool in friction stir welding in one place. 21 Ref., 1 Table, 7 Figures.

Keywords: *friction stir welding, zone of thermomechanical effect, weld nugget, indentation, Berkovich indenter, Young's modulus, physicomechanical properties*

The technology of friction stir welding (FSW) is used to join different alloys of magnesium, copper, titanium, zinc and even steel, but the main industrial application of FSW is for butt joining of long-length parts of aluminium alloys (about 99 % of all joints). The characteristics of FSW technology and its advantages associated with a particular type of joints or application are the subject of numerous publications [1–11]. In general, during FSW, a rotating tool equipped with a pin and a collar, is slowly submerged between the edges of the elements being joined (touching each other) and moved along the welding line [5]. The heat, necessary for plasticizing the material, is generated by friction between the tool and the materials being joined, the rotational and translational movement of the pin provides an intense plastic deformation of the heated softened material to move from the tip of the pin to the collar, creating a permanent structure of a joint on both sides of materials being joined.

The basic technological parameters of the FSW process are the following: speed of tool rotation and rotation direction, rpm; linear welding speed, mm/min; inclination angle of the tool relative to the surface of elements to be welded, deg; type of tool and its dimensions: diameter of the pin and diameter of the collar, mm [10].

The key parameter, that determines the quality standard of FSW joints is the pin geometry for mixing, which determines different conditions of local heating and mutual mass transfer of the metal of elements, being joined. In addition to the pin, an important element of FSW tool is the collar, the main function of which is the heat generation due to friction between the collar and materials being welded, pressure transfer and formation of deformations in the weld surface area.

It is believed that after intense twisting plastic deformation in the nugget of FSW weld, a change in the nature of interatomic interactions and the formation of a structure, close to nanosized, occurs. Alongside with the formation of nanostructures, the formation of metastable states, supersaturated solid solutions and metastable phases can occur. Also, due to large deformations of the material of both edges of parts welded, the thermomechanical zone may contain a highly fragmented and disoriented structure of the recrystallized amorphous state. All this inevitably affects the physical and chemical properties of the joint zone.

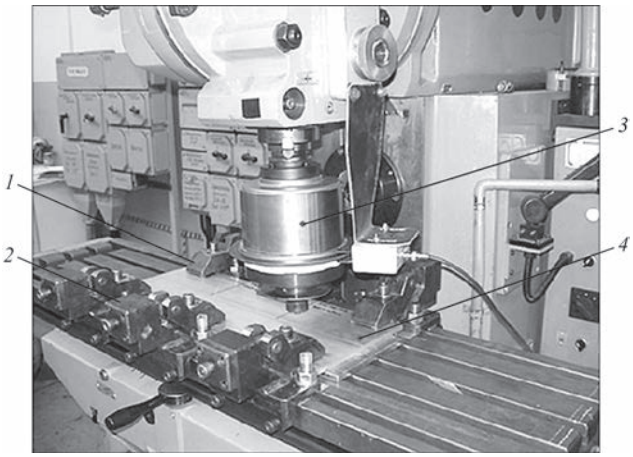

Figure 1. Type of installation for friction stir welding: *1* — tool; *2* — fastener; *3* — unit for tool fixation; *4* — parts to be welded

Therefore, it is of interest to study the dependence of the influence of the key parameter of the FSW: the welding tool geometry on the formation of nano-dispersed zones of welds with minimal defectiveness and uniform structure, which should positively affect the strength of welded joint as a whole.

The aim of this work is to determine the optimal shape of FSW tool based on the results of a local study of structure and physical and mechanical properties of zone of thermomechanical effect in welds, made using three types of specially designed pins with collars. In order to solve this aim, a joint investigation was carried out: FSW was carried out in the equipment of the Institute of Welding in Gliwice, and the treatment and mechanical tests of specimens were performed at the E.O. Paton Electric Welding Institute of the NAS of Ukraine. From the results of mechanical tests and the ratio of hardness to Young's elasticity modulus, the structural state of weld zones was experimentally identified.

Equipment, materials and investigation methods. FSW was carried out in a modified milling installation FYF32JU, equipped with a gripping system and a measuring head for control of welding process parameters (Figure 1).

For welding, specimens of aluminium alloy 6082-T6 (analogue of AD35) were selected in the form of flat hot-rolled rods of 10 cm long and 0.8 cm thick. Heat treatment of the alloy was carried out at a temperature of about 540 °C with the following artificial aging at 170 °C. The chemical composition is presented in Table.

FSW tools of three types (Figure 2) were specially made of high-speed, high-strength (for twisting) alloyed steel HS6-5-2 of increased wear resistance up to 600 °C. According to the type of geometric features, they are classified as follows:

- C is an ordinary tool of the «conventional» type, consisting of a body, a cylindrical threaded pin and a collar with a spiral groove;
- T is a tool of the «triflute» type, consisting of a body, a cylindrical threaded pin with three grooves and a collar with a spiral groove;
- S is a «simple» tool, consisting of a body, a smooth cylindrical pin without a thread and a flat collar.

The process of FSW was performed in the following mode: speed of tool rotation — 710 rpm; linear welding speed — 900 mm/min; tools of the type C, T and S with a pin length of 7.8 mm; inclination angle of the tool with respect to welded workpieces is 1.5°; direction of rotation of the tool is clockwise. The mentioned parameters provide the most economical process in terms of welding speed. After welding, each weld passed visual inspection for compliance with the standard with a positive result.

For optical examination of macrostructure of FSW joints, thin sections were prepared using a standard method for aluminium alloys: the surfaces of specimens were grinded in the machine-tool 3E88IM with an abrasive paper of different grain sizes (P120 — 100–125, P240 — 50–63, P600 — 20–28, P1200 — 10–14 μm), polished with paste GOI to a mirror shine, washed with water and alcohol, dried with a filter paper. Etching of a structure was performed with a reagent of 5 ml of HNO_3, 30 ml of CH_3COOH, 300 ml of H_2O.

For mechanical indentation tests, the device Micro-gamma was used (Figure 3, *a*), designed in the laboratory of nanotechnology of the Aerospace Institute of the National Aviation University of Ukraine. Indentation is the test based on the method of Oliver and Pharr [13–16] for determination of hardness H and elasticity modulus *E* according to indentation diagrams, which are

Chemical composition of aluminium alloy 6082, wt.% [12]

Alloy	Si	Fe	Cu	Mn	Mg	Cr	Zn	Ti	Al
6082	0.7–1.3	Up to 0.5	0.1	0.4–1.0	0.6–1.2	Up to 0.25	Up to 0.2	Up to до 0.1	Rest

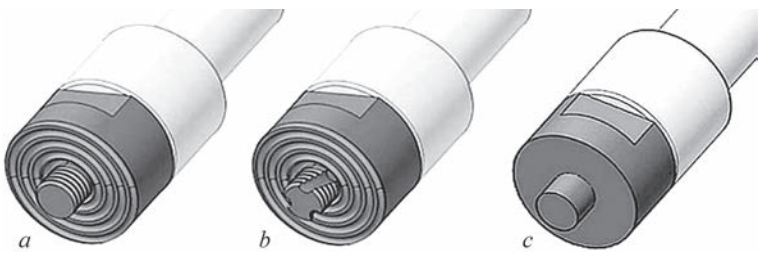

Figure 2. Tools for friction stir welding: *a* — type C; *b* — T; *c* — S

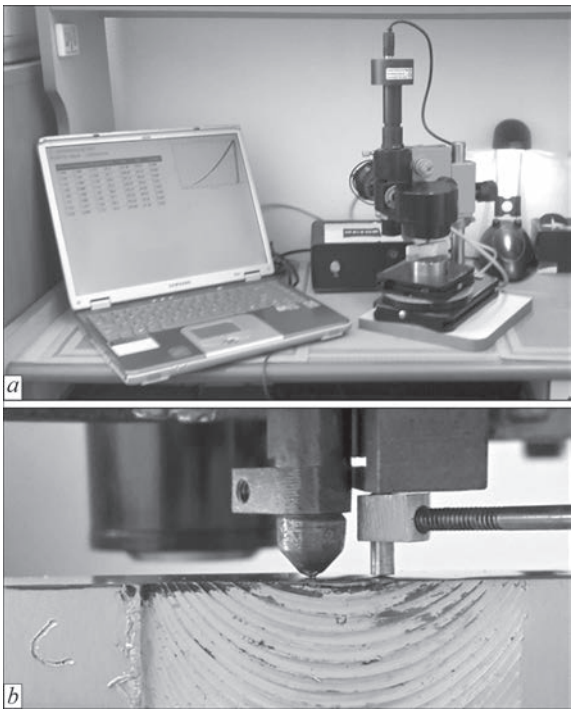

Figure 3. Device «Micron-gamma» (*a*) in the process of recording diagram of continuous indentation of the indenter into the material (*b*)

fixed at continuous pressing-in of a diamond trihedral pyramidal indenter of Berkovich [17, 18] in accordance with ISO/FDIS 14577-1:2015; Metallic materials — Instrumented indentation test for hardness and materials parameters — Part 1: Test method (ISO Central Secretariat, Geneva, Switzerland). The indentation was carried out on the polished surface of specimens without etching at 100 g loading of indenter (Figure 3, *b*).

Based on the ratio H/E, the structural state of metal was identified experimentally after grinding, and the presence of strain hardening was determined. It is known that all materials in a different structural state, depending on the ratio of hardness to elasticity modulus (H/E) can be placed in a row, including three groups [19–21]. The first group is coarse-crystalline ($H/E < 0.04$), the second is fine-crystalline and nanomaterials ($H/E \approx 0.05$–0.09) and the third group is materials in the amorphous and amorphous-crystalline states

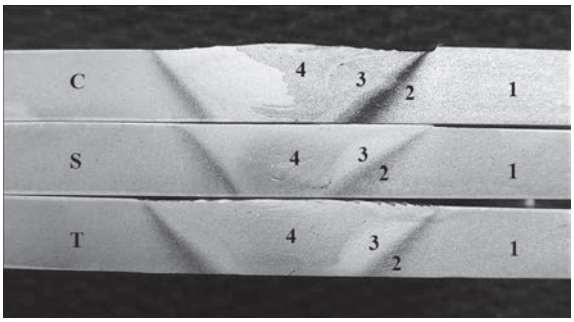

Figure 4. Macrostructure and zones of FSW joints of aluminium alloy EN AW 6082-T6 of 0.8 cm thickness (1–4, see description in the text)

($H/E \geq 0.1$). The establishment of limiting values for H/E for different structural states facilitates identification of a material with an unknown structural state.

Results and discussion. The asymmetrical sides of «running-on» (AS) and «running-out» (RS) observed in the FSW welds (Figure 4) are predetermined by the asymmetry of metal twisting deformation and are related to the asymmetry of finding the initial point of tool touching at increasing pressure, and consequently, with the difference in distribution of temperature fields of heating at intensive mechanical effect.

Typical for all three FSW specimens is the formation of a nugget zone in the centre of joints, which contains oval concentric fragments, differing in structure. The formation of oval rings is associated with the peculiar features of metal mixing with different tool tips. A complex profile adjoins the nugget, which forms the weld upper part. As a result of etching sections, defects of joints were distinguished in the form of local discontinuities and cavities along the line separating the nugget centre from its surrounding zone of thermomechanical effect. These bands of aluminium oxide are inherent to the surfaces of materials being welded, because they were not sufficiently mechanically distributed by the welding tool. This type of defect is typical for FSW welds and depends on linear welding speed, i.e., with an increase in the linear welding speed, the dispersion of oxides during mechanical mass transfer is increased and the number of defects is decreased.

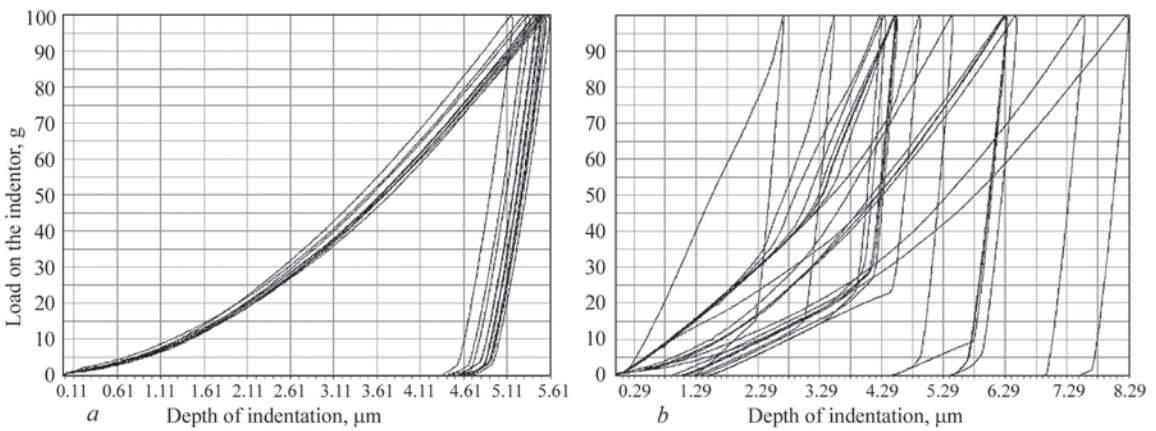

Figure 5. Difference in diagrams of base metal indentation (*a*) and different heat-affected zones of S-type specimen (*b*)

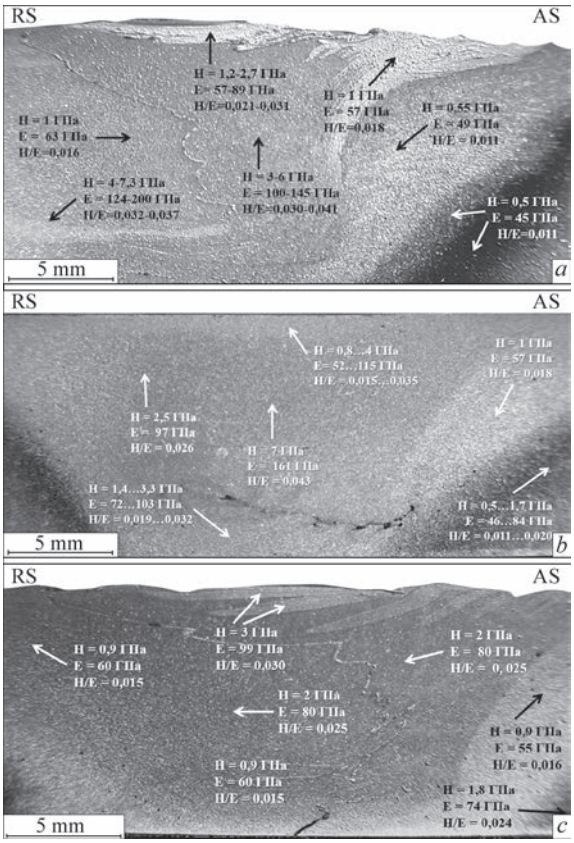

Figure 6. Distribution of hardness H, elasticity modulus E and resistance to deformation H/E in the microstructure of FSW weld of a tool of C-type (*a*); S-type (*b*); T-type (*c*)

Another typical horizontal defect, caused by insufficient mixing of materials, is observed in a specimen produced using a smooth tool of S-type without thread on the tool pin. The cause for such a defect is that the flat surfaces of tool during friction lead to local overheating of metal up to the melting temperature.

Thus, in the welded joint, four zones specific for FSW are formed: directly to the zone 1 (base metal — BM) the zone 2 is adjoined, where the metal of workpieces remains nondeformed and changes its structure only under the influence of heating (heat-affected zone — HAZ); zone 3, where the metal is subjected to significant plastic deformations and heating (zone of thermomechanical effect — ZTME) and zone 4 — is the joint nugget, where dynamic recrystallization occurs.

The mechanical test showed a fundamental difference for FSW welds in the diagrams of base metal indentation (Figure 5, *a*) and of different zones (Figure 5, *b*), which characterizes the presence of a modified structural state.

For all three specimens, the hardness of zone 2 (HAZ) is reduced. The maximum values of hardness are characteristic for the zone 4, the central part of the nugget (Figure 6), as well as for bright oval concentric fragments of the structure of the upper and lower parts of the nugget (Figure 6, *a*, *c*). The averaged values of physicomechanical properties of three types of FSW joints are as follows:

- zone 1 (BM) — H = 1.2 GPa, E = 70 GPa;
- zone 2 (HAZ) — H = 0.5–1.0 GPa, E = 45–57 GPa;
- zone 3 (ZTME) — H = 1.0–3.0 GPa, E = 63–103 GPa;
- zone 4 (nugget) — H = 2.0–7.0 GPa, E = 80–161 GPa.

Figure 6, *b* shows welded joint, produced by a tool of C-type with a cylindrical threaded pin and a collar with a spiral groove, which contains the maximum hardness value of 7.3 GPa for all three specimens (light oval fragment of the lower part of the nugget), also the maximum values of E to 200 GPa and the ratio of H/E to 0.041. Such values fix the presence of a nanodispersed multiphase structure formed at the highest degree of deformation. A similar structure is also characteristic for the 4th zone of nugget of FSW welds: for C-type H/E to 0.041; for S-type H/E to 0.043 at the initial polycrystalline structural state of the base metal H/E = 0.017. Such hardening during refinement of the structure grains is usually associated with a decrease in the density of dislocations and their braking.

Thus, if one considers the presence of a nanosized hardened structure in the weld produced by FSW and the uniformity of its distribution, good dissipation of oxide films and the absence of discontinuities as ad-

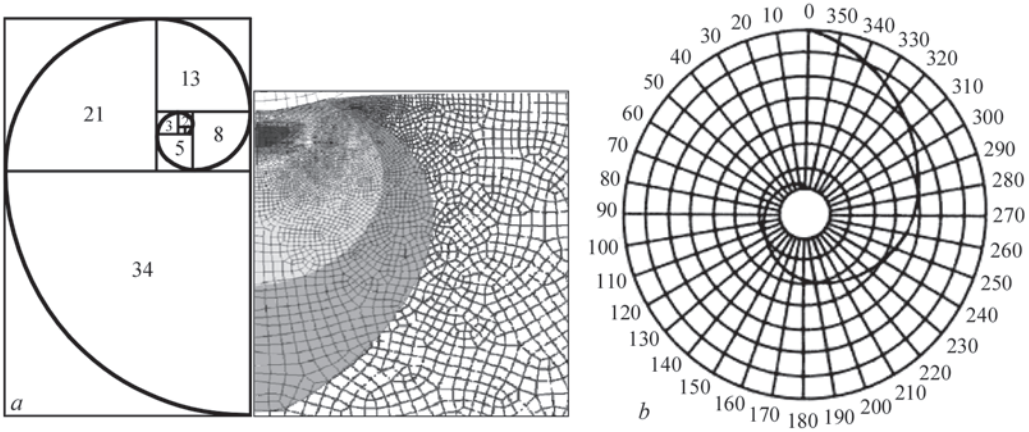

Figure 7. Fibonacci spiral and FSW model with a large-scale change in the structure fragments (*a*) and radial change in the structure segments during twisting (*b*)

vantageous, then a tool of C-type is optimal in this investigation.

In the course of the work, it was assumed that according to the degree of refinement of grains of the metal structure to nanosizes at a twisting deformation, it is possible to determine the number of tool rotations for FSW in one place. If the twisting deformation is considered in the form of a spiral mathematical Fibonacci proportion — 1, 2, 3, 5, 8, 13 ... (Figure 7, *a*), where a full revolution (unwinding) is a sequence of four values, then, in the opposite direction (twisting) of a spiral, a substantial structural refinement will take place already after deformation by a half-revolution of 0...180° (Figure 7, *b*), and to create a homogeneous nanostructure, deformation by several revolutions is required.

Taking the averaged grain diameter of the refined structure as 100 nm, and the averaged grain diameter of the initial polycrystalline aluminium: 100 000 nm (0.1 mm), this ratio will be 1:1000. Then, refinement of grain in such an inverse proportion will occur at three or four revolutions of the FSW tool in one place:

- 1st revolution — 1597, 987, 610, 377;
- 2nd revolution — 233, 144, 89, 55;
- 3rd revolution — 34, 21, 13, 8;
- 4th revolution — 5, 3, 2, 1.

Technologically, this can be controlled by changing the speed of revolutions and/or linear speed of the tool movement during welding, but usually the welding equipment has a fixed speed, which limits the control.

Conclusion

The physicomechanical properties of welds of joints from aluminium alloy EN AW 6082-T6, produced by friction stir welding with the use of three tools of different geometric shapes, were investigated. For all three specimens, the hardness of heat-affected zone decreases, and in the zone of thermomechanical effect the hardness increases. The maximum values of hardness are typical for the central part of the nugget of welded joints, as well as for light oval concentric fragments of structure of the upper and lower parts of the nugget. By the presence of a nanosized hardened structure and the uniformity of its distribution, as well as good dissipation of oxide films and the absence of discontinuities in the nugget of welds, the FSW tool of C-type is optimal. It was assumed that the formation of a uniform structure in welds can be obtained at three or four revolutions of the FSW tool in one place.

1. Thomas, W.M., Nicholas, E.D., Needham, J.C. et al. (1991) *Friction stir butt welding*. European Patent Specification 06 15 480 B1.
2. Dawes, C.J. (1995) An introduction of friction stir welding and its development. *Welding & Metal Fabrication*, **63**, 13–16.
3. Mishra, R.S., Ma, Z.Y. (2005) Friction Stir Welding and Processing. *Mater. Sci. Eng.*, **50A**, 1–78.
4. Uday, M.B., Ahmad Fauzi, M.N., Zuhailawati, H., Ismail, A.B. (2010) Advances in friction welding process: *A Review. Sci. Technol. Weld. Join*., **15**, 534–558.
5. Krasnowski, K., Sędek, P., Łomozik, M., Pietras, A. (2011) Impact of selected FSW parameters on mechanical properties of 6082-T6 aluminium alloy butt joints. *Archives of Metallurgy and Materials*, 56, **4**, 965–973.
6. Threagill, P.L., Leonard, A.J., Shercliff, H.R., Withers, P.J. (2009) Friction stir welding of aluminium alloys. *Int. Mater. Rev.*, 54(**2**), 49–93.
7. Nandan, R., DebRoy, T., Bhadeshia, H.K.D.H. (2008) Recent advances in friction-stir welding: process, weldment structure and properties. *Prog. Mater Sci*., **53**, 980–1023.
8. Krasnowski, K., Dymek, S. (2013) A comparative analysis of the impact of tool design to fatigue behavior of single-sided and double-sided welded butt joints of EN AW 6082-T6 Alloy. *J. of Mater. Eng. and Performance*, 22(**12**), 3818–3824.
9. Krasnowski, K. (2014) Fatigue and static properties of friction stir welded aluminium alloy 6082 lap joints using Triflute-type and smooth tool. *Archives of Metallurgy and Materials*, 59(**1**), 157–162.
10. Kalemba, I., Kopyscianski, M., Dymek, S. (2010) Investigation of friction stir welded Al–Zn–Mg–Cu aluminum alloys. *Steel Research Int.*, 81(**9**), 1088–1096.
11. Mustafa, B., Adem, K. (2004) The influence of stirrer geometry on bonding and mechanical properties in friction stir welding process. *Materials and Design*, **25**, 343–347.
12. *Standard DIN EN 573-3:2009*: Aluminium and aluminium alloys. Pt 3: Chemical composition and form of wrought products. Chemical composition and form of products.
13. Oliver, W.C., Pharr, G.M. (1992) An improved technique for determining the hardness and elastic modulus using load displacement sensing indentation experiments. *J. Mater. Res*., **7**, 1564–1583.
14. Oliver, W.C., Pharr, G.M. (2004) Measurement of hardness and elastic modulus by instrumented indentation: Advances in understanding and refinements to methodology. *Ibid.*, 19(**1**), 3–21.
15. Khokhlova, Yu.A., Klochkov, I.N., Grinyuk, A.A., Khokhlov, M.A. (2009) Verification of Young's modulus determination using «Micron-gamma» microprobe system. *Tekh. Diagnost. i Nerazrush. Kontrol*, **1**, 30–32 [in Russian].
16. Khokhlova, Yu.A., Ishchenko, D.A., Khokhlov, M.A. (2017) Indentation from macro- to nanometer level and examples of investigation of properties of materials with a special structure. *Ibid.*, **1**, 30–36 [in Russian].
17. *Nano indenters from micro star technologies*. Revision 2.3. http://www.microstartech.com
18. Kazuhisa Miyoshi (2002) *Surface characterization techniques*: An Overview NASA/TM-2002-211497, 12–22.
19. Doener, M.F., Nix, W.D. (1986) Indentation problems. *J. Mater. Res*., **1**, 601–614.
20. Gorban, V.F., Mameka, N.A., Pechkovsky, E.P., Firstov, S.A. (2007) Identification of structural state of materials by automatic indentation method. In: *Proc. of Kharkov Nanotechnological Assembly (Ukraine, Kharkov, 23–27 April 2007)*. Ed. by I.M. Neklyudov et al. Vol. 1: Nanostructural materials, 52–55 [in Russian].
21. Firstov, S.A., Gorban, V.F., Pechkovsky, E.P., Mameka, N.A. (2007) Relationship of strength characteristic with indexes of automatic indentation. *Materialovedenie*, **11**, 26–31 [in Russian].

Received 06.03.2019

DOI: http://dx.doi.org/10.15407/tpwj2019.07.03

MODELLING OF TEMPERATURE FIELDS, STRESSES AND DEFORMATIONS IN CYLINDER SHELLS PRODUCED BY ADDITIVE MANUFACTURING METHOD*

V.A. KOSTIN and **G.M. GRIGORENKO**
E.O. Paton Electric Welding Institute of the NAS of Ukraine
11 Kazimir Malevich Str., 03150, Kyiv, Ukraine. E-mail: office_22@ukr.net

The paper presents the results of modelling of temperature fields, stresses and deformations in formation of additive multilayer structure of aluminum alloy 1561, low-alloy structural steel of 09G2S grade and titanium alloy of Grade 2 grade. Based on the experimental results obtained earlier at the E.O. Paton Electric Welding Institute during application of additive deposits of these materials the computer modelling was carried out for improvement of technology of additive process. In course of calculations there was analyzed an effect of algorithm of sequence of additive layers deposition, namely deposition of cylinder shell on circle and on spiral, on distribution of temperatures in deposition and its resistance to external loads. It is determined that for formation of cylinder shells by additive method it is reasonable to use the spiral deposition technology and apply less heat-conducting structural materials, i.e. structural steels and titanium alloys. 10 Ref., 7 Figures.

Keywords: *additive manufacturing, modelling, spiral deposition, cylinder shells, resistance, residual stresses*

In modern construction, aircraft and space engineering as well as in a series of other branches of commercial manufacturing the large importance is given to application of thin-wall shells of different materials [1]. Such shells can be used as bodies of rocket solid-fuel engines, construction domes, tanks for storage of active and cryogenic liquids, i.e. structures operating under high inner pressures at axisymmetric external loading.

Different structural steels, titanium and aluminum alloys, composite materials based on titanium, aluminum and ceramics are often used as raw materials for their production.

Application of thin-wall shells allows significantly reducing weight of structure at keeping the maximum volume, providing its necessary strength and rigidity, using various complex shapes in design of products of different types.

Traditionally, such shells are obtained by method of tool or magneto-pulse stamping, electrohydraulic stamping or explosion stamping, rotary drawing, bending of roll sheet material and next joining of its edges by welding [2].

In the case of application of shells of variable thickness there is a problem of removal of excess of material. It is realized by means of mechanical milling or chemical etching that significantly increases duration of a process of its manufacture and considerably rises fabrication cost. The mechanical defects, appearing in course of these operations, make it useless for repair restoration.

Renewed interest to investigation of thin-wall structures is caused by appearance of new materials and alloys, rapid development of computer technologies as well as possibility of application of new methods for manufacture of parts and their components using additive manufacturing [3, 4].

Today, many world companies in manufacture of their products started to use additive manufacturing for 3D printing. In the beginning of 2018 the famous American Aerospace Corporation Lockheed Martin presented [5] the first 3D-printed rocket-propellant tank of titanium alloy (Figure 1).

Selection of titanium was caused by its high specific strength, heat and corrosion resistance. When using the traditional technologies of manufacture of cylinder fuel tanks as a rule up to 70–80 % of valuable material is sent in recyclable wastes. A new method of printing from Lockheed Martin allows considerably saving on manufacture of these tanks (on Companies' data up to 87 %).

Cylinder fuel tanks are not a single product of Lockheed Martin being 3D printed. The Company has already used this technology for creation of satellite communication system and components for interplanetary station NASA Juno. The Company also plans to produce external shell for spaceship Orion using 3D-printing technology.

*Based on presentation made at International Conference «Consumables for Welding, Surfacing, Coating Deposition and 3D-Technologies», June 04–05, 2019, Kyiv.

Figure 1. Rocket fuel tank (*a*) and electron beam chamber for 3D printing (*b*) [5]

Additive manufacturing is a new highly-efficient method of development of products and structures based on addition of small portions of material. The products and materials are developed by melting of metallic powder [4], solid wire or flux-cored wire [6] with concentrated heat sources.

Application of metallic wire instead of powder in additive process allows rising efficiency of metallurgical processes, providing higher energy efficiency, increasing material utilization rate, decreasing residual stresses and deformations, providing necessary level of properties. Application of additive method in repair of thin-wall shells can allow restoration of their structural integrity and bearing capacity. At the same time, development of working thin-wall structure requires preliminary laboratory investigations and computer modelling.

Aim of the present work was improvement of the technologies for development of thin-wall shells by additive method based on selection of geometry of their deposition.

Experiment procedure. Due to the fact that thin-wall structures are widely used in aerospace engineering, shipbuilding and commercial construction, initially, for investigations two types of materials, namely titanium alloy Grade 2 and structural low-alloy steels of 09G2S grade, were selected.

The peculiarities of formation of structures of titanium alloys (high power of heat source, presence of high vacuum in deposition chamber) required application of a special system of additive manufacturing xBeam 3D Metal Printing [7]. The system is based on application of a hollow conical electron beam as a heat source and application of wire as a consumable. This creates favorable conditions for melting of consumable material and its layer-by-layer controlled deposition.

Arc system for development of additive structures was used [8] to deposit the products of structural steel. It is based on application of welding robot ABB IRB-1600.

E.O. Paton Electric Welding Institute has developed a software for creation of 3D model based on scanning of additive coating, planning the trajectory of welding torch movement considering correction of data of laser-TV and videopyrometric probes.

Thin-wall products from researched materials are shown in Figure 2. Welding wires of corresponding composition and thickness were used as a consumable for additive manufacturing of 3D products.

Computer modelling was carried out in order to improve a technology of development of thin-wall shells by additive method and increase their mechanical properties.

Titanium alloy of Grade 2 grade (VT1-0), containing wt.%: 0.03 N; 0.1 C; 0.25 O; 0.3 Fe was used for modelling. A yield limit of alloy made 275 MPa, strength limit was 345 MPa. Steel of 09G2S grade, used for welded structures and containing, wt.%: 0.12 C; 0.6 Si; 1.5 Mn; 0.3 Cu; 0.04 S; 0.003 P was selected as low-alloy steel. Steel yield limit made 345 MPa, strength limit was 490 MPa, relative elongation 21 %.

Application of high-strength aluminum alloys is wide spread in practice of development of cylinder shells for aero- and rocket-space engineering. Therefore, it was reasonable to use developed approaches to analysis of development of additive shells for these alloys.

Due to limitation of access to experimental results in this branch, a modelling of electric arc wire surfacing of thin-wall product of wrought aluminum alloy of 1561 (AMg61) grade in shielding argon medium was carried out as a predicted variant. Alloy of 1561 grade contains, wt.%: 6.1 Mg; 0.9 Mn; 0.4 Si; 0.4 Fe; 0.003 Be, 0.12 Zr. This alloy is widely used in manufacture of thin-wall elements of aerospace engineering. Aluminum alloy has a yield limit not less than 250 MPa and strength limit not less than 360 MPa.

Calculated cylinder shells are the layers of material of 2 mm width and 2 mm thickness in sequence deposited on a substrate by circle with 20 mm radius. Number of deposited layers shall satisfy the condition of thin wall, i.e. shell is supposed as thin, if $h/R \leq 1/10–1/20$. Following from selected parameters this condition was fulfilled when number of layers exceeds 10.

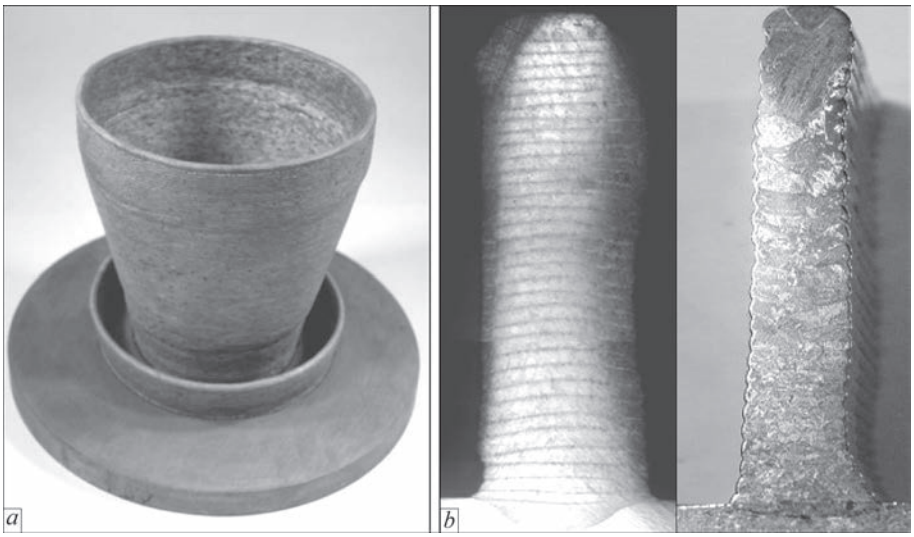

Figure 2. Deposits of investigated materials produced by additive method: *a* — low-alloy steel of 09G2S grade; *b* — titanium alloy Grade 2

Technological parameters of additive manufacturing

Power of heat source (Al/Fe/Ti), kW	0.6/1/5
Plate thickness, mm	5
Thickness of deposited layer, mm	2
Deposition width, mm	2
Deposition radius, mm	20
Deposition height , mm	40
Number of layers	20
Arc movement rate, rps	0.1; 0.2; 1
Number of deposited layers	20–30

Selection of power of arc heat source was determined by typical modes of welding for this type of material, namely electron beam welding of titanium alloys (5 kW), gas-shielded arc welding of low-alloy steels (1 kW) and consumable electrode arc welding of aluminum alloy (0.6 kW).

Two methods of deposition of additive layers were investigated, i.e. on circle and on spiral. Angular rate of deposition of one layer was determined by technological possibilities of units and made 0.1; 0.5 and 1 rps.

Computational model. To model the effect of deposit application on its properties the temperature fields and stress-strain state of cylinder products in process of their formation were calculated. Computational package COMSOL Multiphysics® was used for calculations. A mathematical model of additive process was presented in works [9, 10]. It was assumed based on experimental results that in the initial moment of time the precipitated material was in a solid-liquid state between temperatures of liquid and solid body. Therefore, the liquid phase can be neglected in the calculations.

For numerical analysis of the kinetics of temperature field change in the deposited shell a 3D nonstationary heat-conduction equation was solved:

$$\rho C_p\left(\frac{\partial T}{\partial t}+u\nabla T\right)=\nabla\left[k(T)\nabla T\right], \qquad (1)$$

where ρC_p is the specific heat capacity; k is the coefficient of heat conduction of the material.

Boundary conditions, necessary for solution of equation (1), are determined by a balance of heat input and heat sink from the surface of part being precipitated. Heat transfer in the area of contact of deposited product with a substrate can be described by Newton's law, whereas a heat radiation on a free surface is regulated by Stefan–Boltzmann law. The boundary conditions for solution of heat-conduction equation (1) have the following form (2):

$$-k(T)\frac{\partial T}{\partial n}=\begin{cases}h(T-T_{ext}),\\ \text{in contact area}\\ h(T-T_{ext})+\varepsilon\sigma_0(T^4-T_{ext}^4)-q_{arc}-q_{wire},\\ \text{on free surface}\end{cases} \qquad (2)$$

where n is the normal line to surface; h = 10 (W/m^{2}K) is the coefficient of convective heat conduction; ε = = 0.8 is the coefficient of material radiation; σ_0 is the Stefan–Boltzmann constant ($5.6\cdot10^{-8}$ J·s^{-1}m^{-2}·K^{-4}); T_{ext} = 293 K is the environment temperature; q_{arc} is the density of heat flux developed by arc heat source (W/m^2); q_{wire} is the density of heat flux developed by molten wire (W/m^2).

The work used the model of joint energy transfer from two simultaneously operating heat sources, namely from arc source and molten wire. The arc coordinates, moving on the surface, are set by equation (3):

$$X=X_g+R\cos(2\pi\omega t);\ Y=Y_g+R\sin(2\pi\omega t) \qquad (3)$$

where X_g, Y_g are the initial arc position; ω is the angular rate; R is the trajectory radius; t is the time.

Distribution of density of heat flux of moving arc $q_{arc}(X, Y, t)$ was set by equation (4):

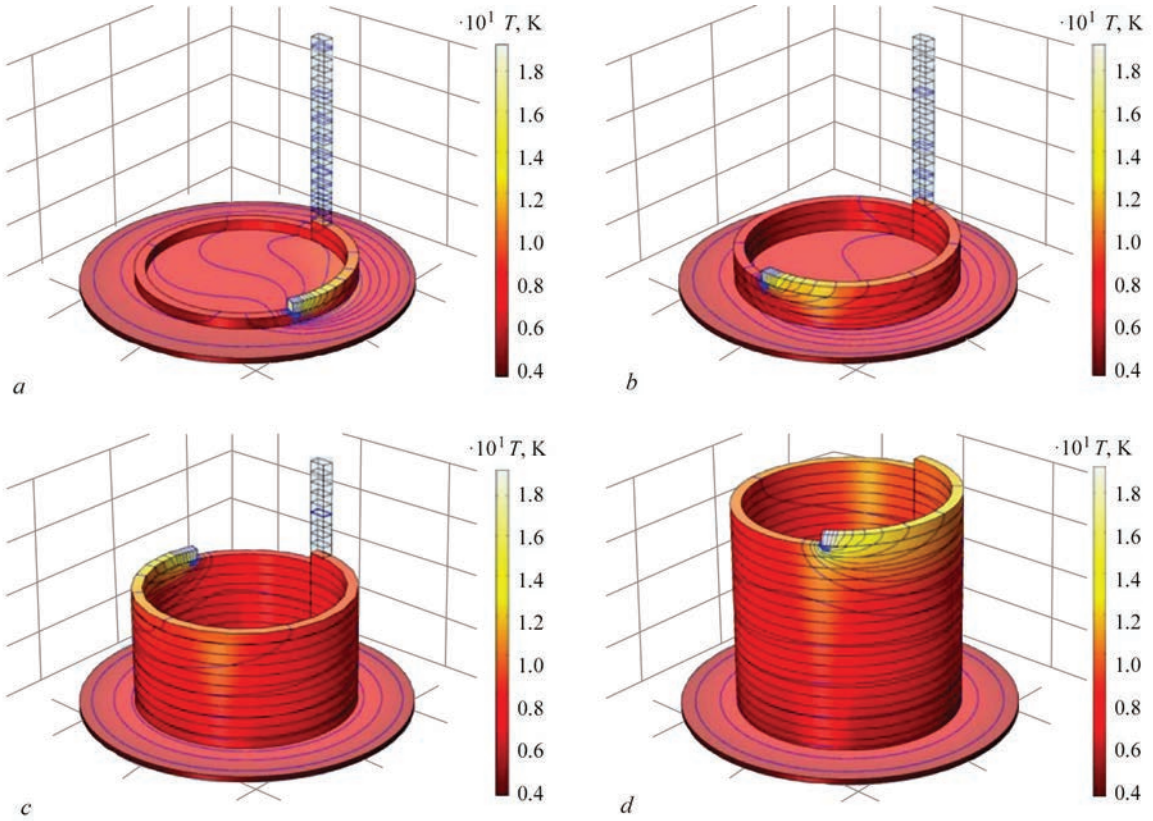

Figure 3. Distribution of temperature in cylinder shell of titanium alloy Grade 2 obtained at 0.1 rps rate by time: *a* — 13; *b* — 35; *c* — 108; *d* — 194 s

$$q_{arc}(x,y,t) = \\ = q_{\max} \exp\left[-K_x\left(\frac{X-X_g}{R}\right)^2 - K_y\left(\frac{Y-Y_g}{R}\right)^2\right], \quad (4)$$

where X, Y are the coordinates of heat source; $q_{max} = \eta U_a I_w$ is the arc power; η is the coefficient of efficiency (0.9–0.95) of source; U_a is the arc voltage; I_w is the arc current; K_x, K_y are the coefficients of concentration of specific heat source.

Distribution of density of heat flux from molten wire q_{wire} (X, Y, t) was set by movement of edge of forming layer with angular rate omega at constant temperature $T_{wire} = T_{melt}$. In researched materials T_{melt} made 625, 1504 and 1716 °C for aluminum alloy 1561, steel grade 09G2S and titanium Grade 2, respectively.

Modelling results. The fields of temperatures, stresses, deformations and displacements in formation of cylinder shells by additive method were calculated as a result of modelling.

Figure 3 shows the temperature fields of titanium alloy Grade 2 in time. The analysis demonstrated virtually uniform distribution of temperature over the thickness of deposited layer. Temperature distribution on shell height showed that it does not change in process of deposition of 9–10 layers. Substrate temperature does not exceed 200–230 °C, and, respectively, its structural-phase state does not change.

The calculations show that the quickest stabilizing of shell temperature is observed in welding with wire

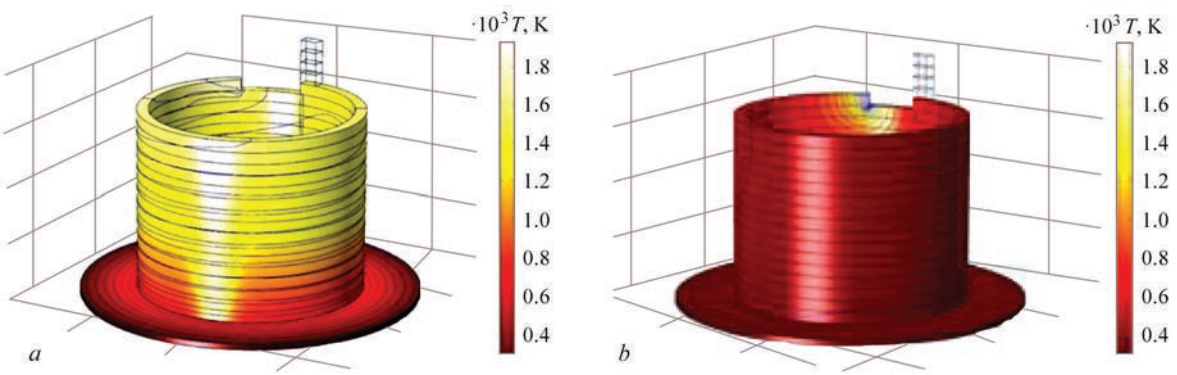

Figure 4. Effect of deposition material on temperature field in shell: *a* — alloy 1561; *b* — Grade 2

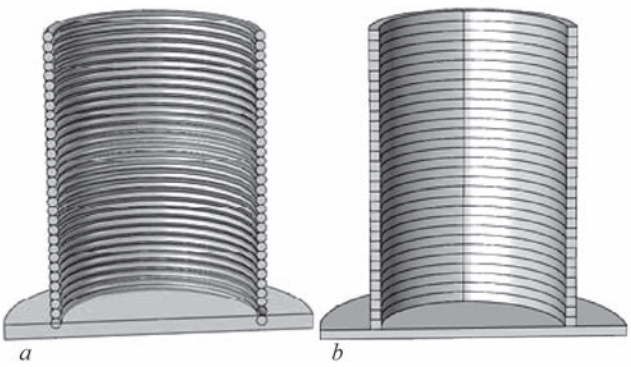

Figure 5. Nature of deposition of additive layers: *a* — on spiral; *b* — on circle

of 09G2S steel after 35–40 s. For aluminum alloy 1561 this time makes 65–70 s, whereas for titanium alloy Grade 2 there is no stabilizing.

The calculations show that depending on composition of used wire the maximum temperature of deposition exceeded the melting temperature of given alloy by 50–75 °C(for aluminum alloy 1561), by 100–150 °C (for steel 09G2S) and by 200 °C (for titanium alloy Grade 2).

The analysis of temperature distribution on deposit height shows (Figure 4) that depending on type of used material there is different effect of molten wire on already deposited layers. Thus, the most significant effect as a result of effect of previous layers is achieved in deposition of aluminum alloy 1561, which propagates on underlying 8–10 layers (Figure 4, *a*). In deposition of molten wire of steel 09G2S or titanium alloy Grade 2 this effect is considerably lower. For steel it makes 3–4 layers, for titanium alloy 1–2 layers (Figure 4, *b*). Obtained results can be explained by noticeably higher heat conduction of aluminum alloy (100–150 W/(m·K)) in comparison with steel (23–28 W/(m·K)) or titanium alloy (17–25 W/(m·K)).

A cylinder structure of aluminum alloy 1561 cools down visibly quicker and reheating reaches deeper layers that results in grain growth and decrease of mechanical properties of these alloys. Application of 09G2S steel and titanium alloy Grade 2 in the additive process results in formation of more homogeneous structure of the deposit and reduces residual stresses, forming in cylinder shell formation.

Effect of algorithm of performance of additive cylinder deposit, namely deposition on circle or spiral, on temperature of deposition and parameters of stability of additive shell to external loads (Figure 5) was analyzed in course of calculations.

Majority of works on modelling of additive manufacturing do not consider effect of deposit shape. This is related with the fact that in this case it is necessary to take into account drop hydrodynamics, solidification processes, interaction of drops between themselves, etc. In order to eliminate these difficulties and approach to real deposit geometry a shape of deposited layer on section was set in advance. In the most cases a view of side surface of the shell has wavelike «ribbed» nature, moreover it depends on layer thickness and deposition rate.

In course of work it was accepted that the spiral deposition forms wavelike geometry of side wall, whereas in deposition on circle it is flat. This assumption grounds on the fact that a real deposition is carried out continuously over the whole height of products and this provokes formation of «ribbed» surface, whereas deposition on circle is more idealized variant, which is used for calculations.

The analysis of obtained data showed that spiral deposit is heated to higher temperatures in comparison with circular one. This, apparently, is related with reduced heat transfer between the layers. At that, a deposited layer cools down quicker, that is determined by larger area of cooled surface.

The parameters of cooling of cylinder shell of less heat-conducting titanium alloy Grade 2 in comparison with shell of steel 09G2S provide higher temperature levels. As a consequence, rise of overheating of liquid pool and coming out of range of temperatures of solid-liquid state for this alloy (T_{sol}/T_{liq}) is possible. Thus,

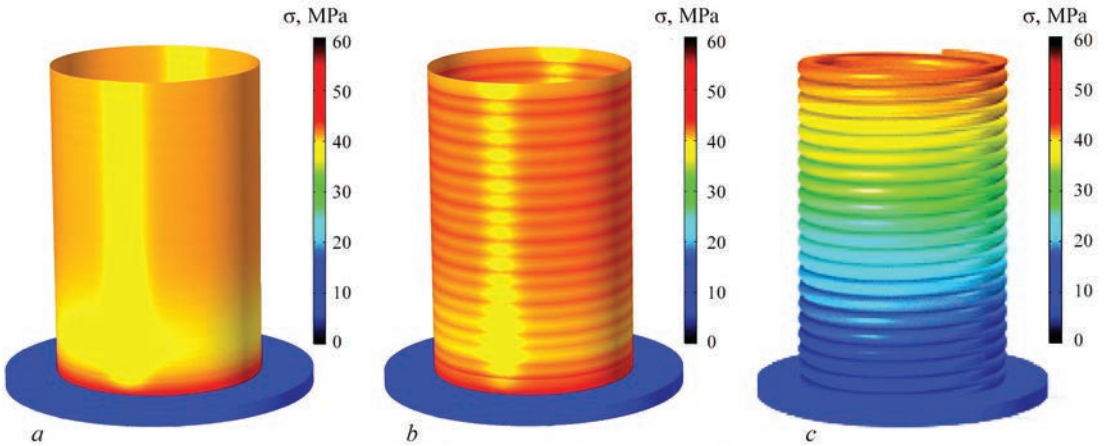

Figure 6. Distribution of equivalent stresses in cylinder shells of titanium alloy Grade 2 under effect of axial loading P = 50 MPa produced by different methods: *a* — traditional from sheet; *b* — multilayer deposition on circle; *c* — multilayer deposition on spiral

there is increase of a risk of «leaking» of liquid melt on side surface of the cylinder shell.

Difference in mechanical stability of cylinder additive shells produced by different methods was analyzed in the work.

Analyzing the stability of cylinder shells, produced by additive method, it is necessary to take into account presence of residual stresses, which are formed on a boundary of deposited layers. In the case of deposition of layers on circle the residual stresses on the boundaries make 40–50 MPa, at the same time in deposition of layers on spiral the residual stresses are somewhat lower and make 10–30 MPa. At that, as it was shown by previous investigations [10] the highest level of stresses was observed on a boundary of the additive layers and substrate. In this case the level of stresses makes 100–150 MPa.

A nature of distribution of stresses in the cylinder shells, produced by different methods, under effect of axial compressive load P = 50 MPa is given in Figure 6. As can be seen from given results, presence of stresses, forming in process of additive manufacturing, changes in whole nature of distribution of stresses in shells under effect of axial compression load.

Analysis of obtained results (Figure 6) shows that a nature of forming stresses significantly depends on method of shell formation. The differences, first of all, lie in a level of stresses forming in them. The highest stresses (55–60 MPa) are formed in a shell produced by circular layers, whereas the lowest (35–40 MPa) are formed in a multilayer deposit made on spiral. This result is, probably, explained by some damping of external axisymmetric loads by layers of deposited on spiral.

Analysis of shell stability, produced by different methods, to effect of axial compressive load is presented in Figure 7. Loss of shape structure under effect of external forces was meant under stability loss. The van Mises yield criterion (5) was used for determination of start of plastic deformations:

$$g(\sigma) = \sqrt{\frac{1}{2}\left(\frac{(\sigma_1-\sigma_2)^2+(\sigma_2-\sigma_2)^2+(\sigma_1-\sigma_3)^2}{\sigma_y^2}\right)}-1\geq 0, \quad (5)$$

where σ_1, σ_2, σ_3 are the main normal stresses; σ_y is the yield limit.

Investigation of cylinder shells, produced by different methods, showed that multilayer deposition on spiral provides the highest level of critical stresses (180–200 MPa), at which it loses stability in comparison with shells produced from solid sheet (150–165 MPa) and multilayer deposition on circle (145–150 MPa).

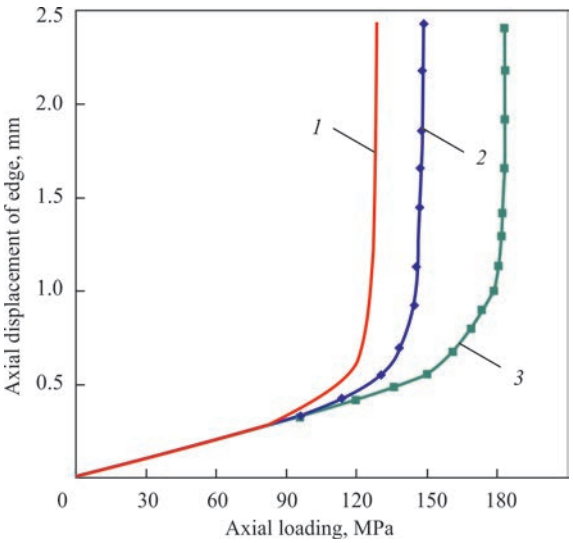

Figure 7. Stability of cylinder shells produced by different methods to effect of axial compression loads: *1* — from solid sheet; *2* — from multilayer circle deposit; *3* — from multilayer spiral deposit

Thus, it can be concluded based on carried work that formation of the cylinder shells by additive method is reasonable using technology of additive manufacturing on spiral.

1. Krivoshapko, S.N. (2013) On possibilities of shell constructions in modern architecture and building. *Stroit. Mekhanika Inzhen. Konstruktsij i Sooruzhenij*, **1**, 51–56 [in Russian].
2. Barvinok, V.A., Kirilin, A.N., Komarov, A.D. (2002) *Higheffficient technological processes of manufacture of piping and fuel systems of aircrafts*. Moscow, Nauka i Tekhnologii [in Russian].
3. Zhukov, V.V., Grigorenko, G.M., Shapovalov, V.A. (2016) Additive manufacturing of metal products (Review). *The Paton Welding J.*, **5–6**, 137–142.
4. Kaufui, V.Wong, Aldo Hernandez (2012) A review of additive manufacturing. *Ont. Scholarly Res. Network – Mechanical Engineering*, Art. ID 208760, Doi: 10.5402/2012/208760.
5. US NAVY printed the underwater apparatus ready to immersion. https://hi-news.ru/technology/vms-sshanapechatali-gotovyj-k-pogrusheniyu-podvodnyi-apparat.html
6. Jandric, Z., Labudovic, M., Kovacevic, R. (2004) Effect of heat sink on microstructure of three-dimensional parts build by welding-based deposition. *Int. J. of Machine Tools and Manufacture*, 44(**7–8**), 785–796.
7. Kovalchuk, D.V., Melnik, V.I., Melnik, I.V., Tugaj, B.A. (2017) New possibilities of additive manufacturing using xBeam 3D Metal Printing technology (Review). *The Paton Welding J.*, **12**, 16–22.
8. Shapovalov, E.V., Dolinenko, V.V., Kolyada, V.A. et al. (2016) Application of robotic and mechanized welding under disturbing factor conditions. *Ibid*., **7**, 42–46.
9. Kostin, V.A., Grigorenko, G.M. (2017) Peculiarities of formation of 3D structure of S460M steel product in additive metallurgical technology. *Sovrem. Elektrometall*., **3**, 33–42 [in Russian].
10. Grigorenko, G.M., Kostin, V.A., Zhukov, V.V. (2017) Modeling of metallurgical additive process of manufacture of 09G2S steel structures. *Ibid*., **2**, 35–44 [in Russian].

Received 08.04.2019

DOI: http://dx.doi.org/10.15407/tpwj2019.07.04

EFFICIENCY OF APPLICATION OF FILLER METAL CORED WIRE IN TIG WELDING OF COPPER*

V.M. ILYUSHENKO, A.N. BONDARENKO, E.P. LUKIYANCHENKO and **T.B. MAJDANCHUK**
E.O. Paton Electric Welding Institute of the NAS of Ukraine
11 Kazimir Malevich Str., 03150, Kyiv, Ukraine. E-mail: office@paton.kiev.ua

The experience of the E.O. Paton Electric Welding Institute in creating a metal cored wire for helium arc TIG welding of copper and its alloys was described. The deposited metal of the wire contains not more than 0.35 wt.% of alloying additives and is characterized by a high electrical and heat conductivity. Examples of the effective use of the developed wire in welding rotors of electric machines and in repair of gas-oxygen copper chambers of arc steel melting furnaces are given. 2 Ref., 4 Figures.

Keywords: *TIG welding, helium shielding, copper and copper alloys, metal cored wire, electrical and heat conductivity, efficiency of application*

Welding in shielding gases is one of the main technological processes of joining non-ferrous metals. This is largely predetermined by the simplest solution to the problem of protecting weld pool metal from the surrounding atmosphere, the possibility of visual observation of welding process, and the simplicity and reliability of the process automation. Welding of copper abroad is mainly performed using this method.

In domestic practice, especially, for metal of small and medium thicknesses (up to 10 mm), welding with a nonconsumable electrode, TIG process, becomes widely used. In a much smaller volume, mainly due to the lack of special welding wires, a consumable electrode welding, MIG/MAG-process, is used.

Welding of copper in shielding gases together with the noted advantages encounters also serious difficulties, namely, the need to apply preheating and also concurrent heating in case of large thicknesses, which significantly complicates the welding process. Copper is also prone to the formation of pores in the welds, which occur during the weld pool crystallization as a result of gases evolution.

As shielding gases for welding copper, argon, helium, nitrogen and their mixtures are used. Taking into account the special thermophysical properties of copper, when selecting the optimal protective environment, the preference should be given to helium and nitrogen, providing a higher efficiency factor of the process. However, it is still necessary to take into account the negative effect of nitrogen on the porosity of welds when welding copper and some of its alloys. The earlier opinion about nitrogen inertness with respect to copper is erroneous. Recent studies have established that under the conditions of welding heating, nitrogen is absorbed by liquid copper and during the weld pool crystallization it can lead to the formation of gas porosity. Producing dense welds in nitrogen-arc welding is possible with the use of filler materials containing elements that bind nitrogen to stable nitrides.

Taking into account the fact that the main cause of porosity in copper welding is the formation and evolution of water vapors from weld pool metal as a result of interaction of hydrogen with oxygen, the main measure for prevention of porosity is the active deoxidation of the weld pool metal. Therefore, the required quality of welds during welding in shielding gases is achieved primarily by the correct selection of filler material [1]. The analysis of application of wires for welding copper, which are produced by industry according to GOST 16130-90 (MNZhKT 5-1-0.2-0.2; BrKMts3-1; BrKh0.7; BrKhNT, etc.) shows that the presence of such active deoxidizers and nitride-forming elements like titanium, silicon, manganese, etc. in the wires, provides metallurgical treatment of the pool and producing dense defect-free welds. However, despite the satisfactory welding and technological properties, these wires do not provide the necessary thermophysical properties of welded joints: their thermal and electrical conductivity is at the level of

*Based on presentation made at International Conference «Consumables for Welding, Surfacing, Coating Deposition and 3D-Technologies», June 04–05, 2019, Kyiv.

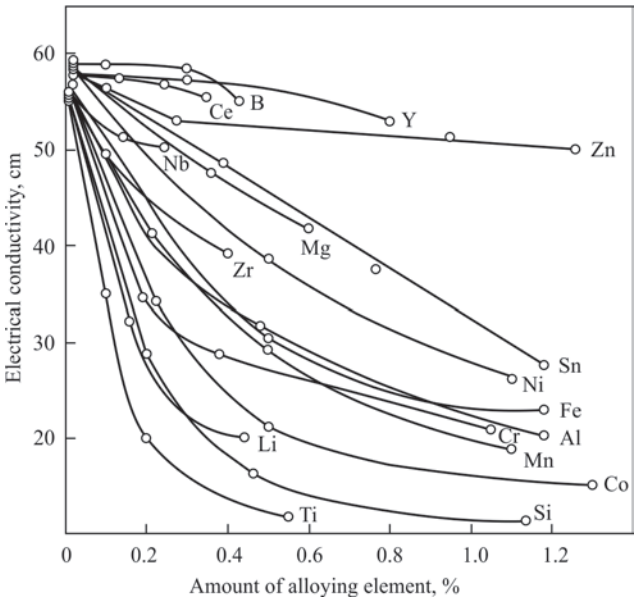

Figure 1. Effect of additives on the electrical conductivity of copper (according to the «Tsvetmetobrabotka» Institute)

20–30 % of the level of those for metal being welded. In practice, these materials are unsuitable for welding products that require high electrical and thermal conductivity of welds.

As experience shows, the same low values of thermophysical properties are also provided by the wire OK Autrod19.12 (ERCu/AWSA5.7) produced abroad, which has the following typical chemical composition of the deposited metal, wt.%: 0.2 Si, 0.2 Mn and 0.8 Sn.

For many years, E.O. Paton Electric Welding Institute, together with the «Tsvetmetobrabotka» Institute, developed welding wires of optimal chemical compositions for welding of copper and its low-alloyed alloys, which meet the complex requirements of welding-technological properties in welding with both consumable and nonconsumable electrode, and also providing the necessary thermophysical properties of welded joints. The wires of grades Sv.ML0.2; Sv.MBMg, Sv.MLMgB; Sv.MLKhMg were developed, containing not more than 0.1–0.4 % of effective deoxidizers and nitride-forming elements (lithium,

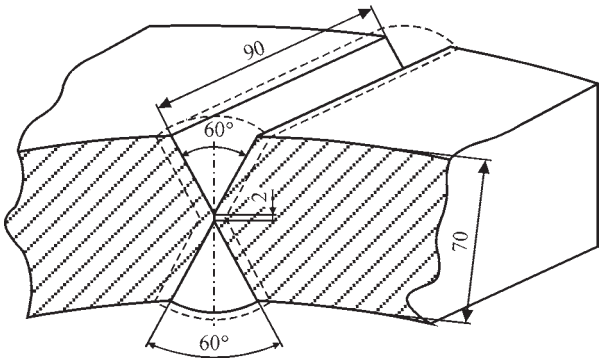

Figure 2. Preparation of butt for double-sided welding of rings

magnesium, boron). As is seen from Figure 1, such small additives provide high electrical conductivity of copper (75–85 % of that for pure copper). However, the technology for manufacturing these wires is quite complicated: melting in vacuum furnaces using master alloys, pressing of rods under high heating, annealing and drawing to the required diameter, therefore their production is set up only in an experimental manner [2].

It is simpler and economically more rational to develop electrode material of the flux-cored wire type, applying copper strip as a sheath. Using a strip with a thickness of 0.8–1.0 mm and a width of 12–15 mm, and a copper powder as the main filler of a core, we can produce a metal flux-cored wire as a result, into the composition of which a dosed amount of deoxidizers and, if necessary, slag-forming components are easily introduced. As a result of experimental studies, a metal cored wire of the grade PP-ANM1 was developed, which provides the deposited metal with a content of not more than 0.35 % of alloying additives. Such a deposited metal has an electrical and thermal conductivity, which is 2.5–3.0 times higher than that during welding with the standard wires.

The most effective was the use of filler metal flux-cored wire in helium-arc welding. This technology was successfully applied in the production of rotors of large electric machines.

The basic design of rotors represents two copper rings made of rectangular section copper bars. The di-

Figure 3. Typical defects of copper chambers after operation

Figure 4. Appearance of restored gas-oxygen chamber

ameter of the rings, depending on the type of motor is in the range of 600–1000 mm. The cross-section of workpieces is min 60×20 mm; max is 90×70 mm. The rings are made on rolling units, and then, depending on the diameter, they are welded with one or two butt welds. Figure 2 shows the shape of the butt edge preparation of the workpiece with a section of 90×70 mm.

Helium-arc welding is performed with the use of filler metal cored wires of the grade PP-ANM1, which provides a minimum reduction of the electrical conductivity in the welded joint. The butt joint of the section, shown in Figure 2, is made with a double-sided weld in 5–6 passes on each side. The electrical conductivity of the weld metal is not less than 60–70 % of the electrical conductivity of copper. The developed welding technology was mastered at the Large Electric Machines Plant (Novaya Kakhovka).

The use of this cored wire in the repair of copper gas-oxygen chambers of arc steel melting furnaces (ASF) is highly effective. These parts are worn out during operation as a result of extremely complex operating conditions (thermal, chemical and mechanical effect). At the end part of the chambers, deep cracks are initiated, a local burning-out of copper occurs up through burn-outs of walls of water-cooling channels (Figure 3), which leads to the appearance of leaks. In the presence of leaks, the chambers are rejected and subjected to replacement by new ones. Taking into account the high cost and scarcity of these products (supplied by import), the task of extending their service life is very urgent.

The studies on the selection of a rational technology for repairing gas-oxygen chambers showed that for these purposes the helium-arc welding with the use of filler metal cored wire PP-ANM1 is preferable. Providing a dense metal in multilayer surfacing, the process allows restoring the edge surface of the chamber to the desired size in height. Here, the thickness of the deposited layer can amount up to 20 mm. The presence of a very small amount of slag-forming additives in the filler wire, as a rule, does not require the removal of slag between the passes, which is a significant advantage over welding with coated electrodes.

Figure 4 shows the appearance of the restored ASF chamber. As was shown by the industrial tests of the restored chambers at the Metallurgical Plant «Dneprosteel LLC», their service life increased by 60–80 %. At the same time, an experience of already two-time repair of gas-oxygen chambers is available.

It should also be emphasized that this technology, providing high electrical and thermal conductivity of welded joints, is very promising for welding of busbars and electrical networks of different purposes.

1. Ilyushenko, V.M., Lukiyanchenko, E.P. (2013) *Welding and surfacing of copper and alloys on its base*. Kiev, IAW [in Russian].
2. Nikolaev, A.K., Kostin, S.A. (2012) *Copper and heat resistant alloys. Encyclopedic and terminological dictionary:* Fundamental Refer. Book. Moscow [in Russian].

Received 24.04.2019

DOI: http://dx.doi.org/10.15407/tpwj2019.07.05

PLASMA-ARC BRAZING OF STEEL 08kp (rimmed) BY USING BRAZING FILLER METALS OF Cu–Mn–Ni–Si SYSTEM

S.V. MAKSYMOVA and **I.V. ZVOLINSKYY**
E.O. Paton Electric Welding Institute of the NAS of Ukraine
11 Kazimir Malevich Str., 03150, Kyiv, Ukraine. E-mail: office@paton.kiev.ua

The paper presents the results of high-temperature differential thermal analysis of brazing filler metals based on Cu–Mn–Ni–Si system, metallographic examination of brazed joints of 08kp steel, made with application of plasma-arc heating. It is shown that at silicon alloying of Cu–Mn–Ni system the alloy melting temperature decreases and its wetting ability increases. X-Ray microanalysis revealed that brazed weld of 08kp steel joints consists of copper-based solid solution and dispersed precipitates of a silicon-enriched phase. An iron-based phase with higher concentration of silicon and manganese is formed on brazing filler metal–base metal interphase as a thin band (along the brazed weld), that is indicative of appearance of silicides of a complex composition. Brazed joint strength becomes higher with increase in nickel concentration in the alloy and is equal to 367 MPa (average value). 9 Ref., 2 Tables, 6 Figures.

Keywords: *plasma-arc brazing, brazing filler metal, microstructure, spreading, solidus and liquidus temperature, strength*

Brazing together with welding is one of the most widespread methods for producing permanent joints. The most important advantage of brazing is the formation of a brazed weld at a temperature below the point of autonomous melting of materials being joined. During brazing, different sources of heating are used, including concentrated ones like arc, plasma, etc. At present, the technological process of brazing by plasma-arc heating is used in the manufacture of different parts and components in the instrument-making industry, automotive industry, electrical engineering, aircraft industry, etc. [1–3].

This paper presents the results of high-temperature differential thermal analysis and the initial structure of brazing filler metals of the Cu–Mn–Ni–Si system. It shows the peculiar features of microstructure formation of brazed joints of structural carbon steel 08kp using plasma-arc heating.

Experimental alloys were produced by casting on a «cold» substrate using arc heating. The solidus and liquidus temperatures were determined using high-temperature differential analysis (HTDA) in helium environment. Plasma-arc brazing of butt joints of the sheet carbon steel 08kp was carried out at a special laboratory bench. As a heating source, the installation KEMPPI Master TIG MLS 2300 AC/DC, applied for argon-arc welding, and the unit for ignition of pilot arc were used. The spreading of brazing filler metals on the base metal substrate in a shielding medium of argon, as well as in a mixture of argon + 10 % hydrogen was carried out.

Specimens were cut out of the produced brazed joints for manufacture of microsections and carrying out metallographic and micro X-ray spectral analysis using a scanning electron microscope TescanMira 3 LMU, equipped with an energy-dispersed spectrometer Oxford Instruments X-max of 80 mm^2 under the control of software package INCA. The locality of measurements was up to 1 μm. The distribution of elements and filming of microstructures were carried out in back-scattered electrons (BSE), which allow examination of microsections without chemical etching.

As the basic brazing filler metal Cu–23.5Mn–9Ni [4] was used, which has a solidus temperature of 920 °C and a liquidus temperature of 955 °C. However, when studying spreading on carbon steel 08kp under the conditions of arc heating, it showed unsatisfactory result. In order to improve spreading of brazing filler metal, alloying with silicon was used (1–3 wt.%), which is a universal depressant for many brazing filler metals [5–8].

The analysis of the results of high-temperature differential thermal analysis of experimental brazing filler metals, containing a high concentration of nickel, showed that the introduction of 3 wt.% of silicon reduces the solidus temperature to 903 °C and the liquidus temperature to 949 °C. A further decrease in the liquidus temperature by about 56 °C (899 °C) became possible at the lower nickel content.

The structure of brazing filler metals of the system Cu–Mn–Ni–3Si is two-phase: solid solution dendrites, along the boundaries of which the phase,

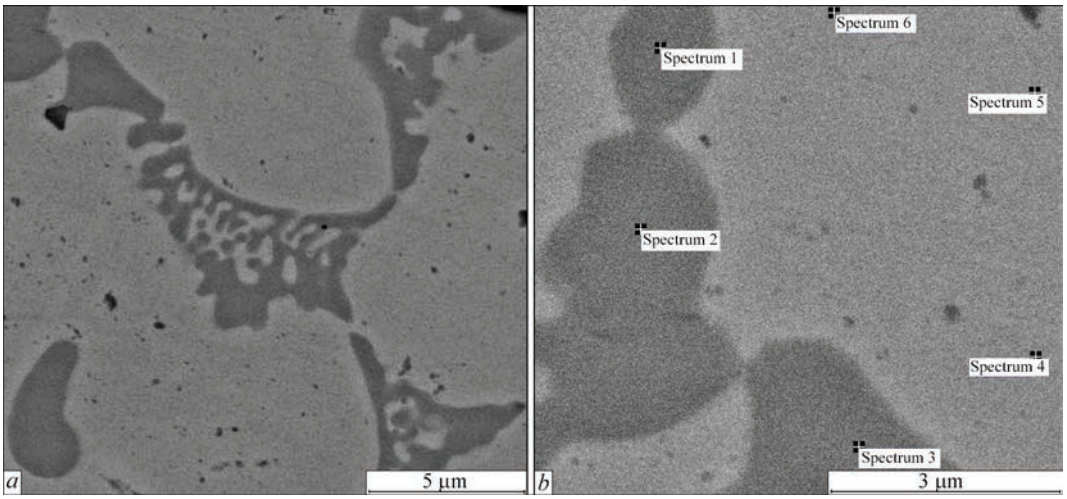

Figure 1. Microstructure (*a*) and investigated areas (*b*) of brazing filler metal of Cu–Mn–Ni–3Si system in the initial cast state

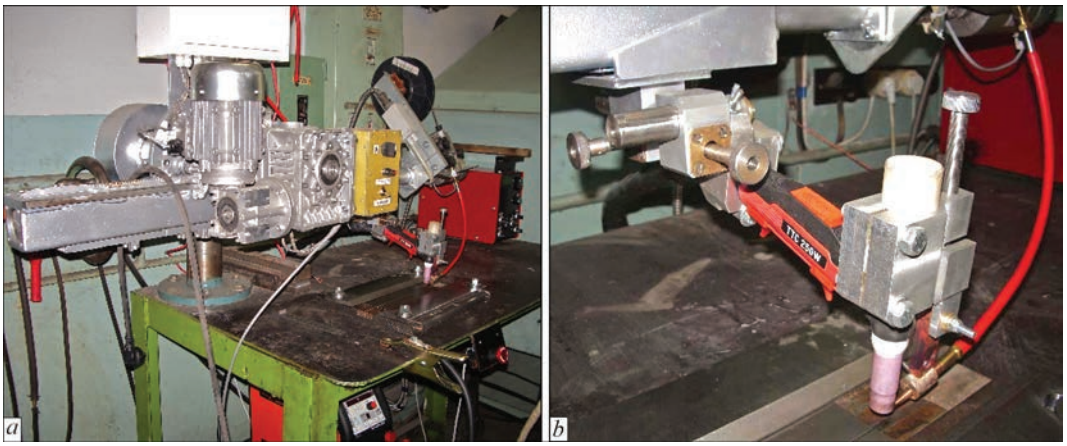

Figure 2. Special bench for plasma-arc brazing (*a*) and unit for torch displacement (*b*)

enriched with silicon, crystallizes (Figure 1, *a*, *b*, Table 1).

The local X-ray spectral microanalysis determined the discrete concentration of silicon in the solid solution and showed that it does not exceed 1.95 wt.%, while in the phase that precipitates along the grain boundaries, its concentration rises to 7.9 wt.% (Figure 1, *b*, Table 1).

In study of the brazing filler metals spreading, a special laboratory bench was used (Figure 2, *a*), which allows moving and fixing the torch, as well as the base metal substrate (Figure 2, *b*).

Brazing filler metals were applied in a cast state, the amount of brazing filler metal, distance from the electrode end to brazing filler metal and temperature were controlled. The thermocouple was fixed on the back side of the substrate. The brazing filler metal was heated at a direct current in a shielding argon medium and in a mixture of argon with hydrogen. The

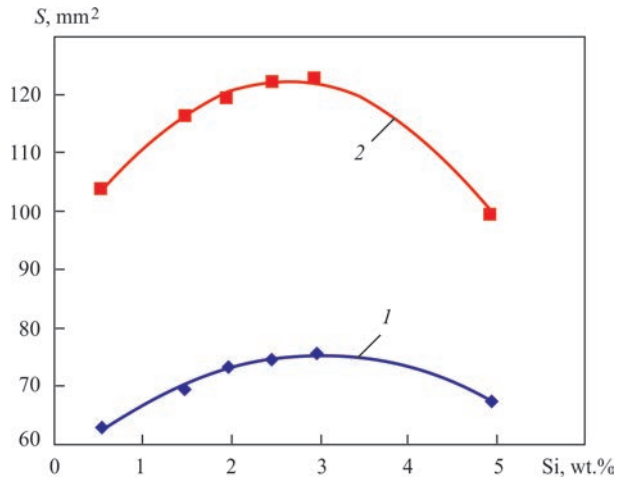

Figure 3. Dependence of area of brazing filler metal spreading on the content of Si at arc heating in argon (*1*) and a mixture of argon with hydrogen (*2*)

Table 1. Distribution of chemical elements in separate phases in brazing filler metal Cu–Mn–Ni–3Si

Spectrum number	Chemical elements, wt.%			
	Si	Mn	Ni	Cu
1	7.40	28.68	3.52	60.40
2	7.90	30.30	3.36	58.44
3	7.55	29.83	4.06	58.56
4	1.95	12.61	0.38	85.06
5	1.72	12.22	0.46	85.61
6	1.91	12.28	0.59	85.22

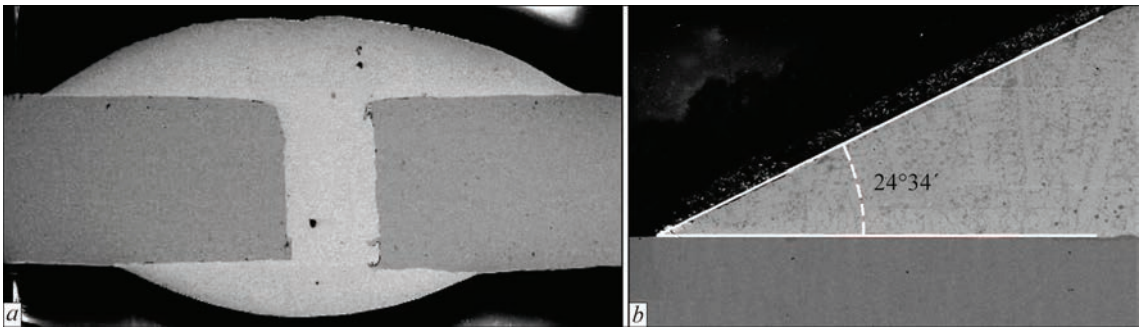

Figure 4. General view of brazed joint (*a*), wetting angle (*b*) of carbon steel 08kp produced by brazing filler metal Cu–Mn–Ni–3Si in the conditions of plasma-arc heating

experiments on spreading of brazing filler metal under arc heating (TIG) in argon showed that the adding of silicon into the alloy of the Cu–Mn–Ni system significantly increases the area of brazing filler metal spreading. Its most intensive effect is observed when the content of silicon is 2–3 wt.% (Figure 3). The further increase in the silicon content to 5 wt.% leads to a decrease in spreading area.

A similar dependence is observed during the study of brazing filler metal spreading in the shielding mixture of argon with 10 % hydrogen, but spreading area increases significantly (Figure 3, curve *2*). This dependence can be explained by the fact that hydrogen is an active reducing agent.

On the basis of experimental alloys the brazing filler metals in the form of flux-cored wires of 2.9 and 3 mm diameter, respectively, were manufactured, which were used to carry out plasma-arc brazing of specimens of steel 08kp (in argon). The feeding of brazing filler metal in the form of a wire was carried out manually.

During optimizing the technological process of plasma-arc brazing, the optimal modes (I = 50 A, U = = 14 V) were established, which provide a good formation of bead of a brazing filler metal, wetting of base metal and the value of a contact angle of 24°34′ (Figure 4, *a*, *b*).

The formation of direct and reverse fillets is observed. Examinations of the weld microstructure in brazed joints, produced using two brazing filler metals, did not reveal any significant differences. Most of the section is occupied by the grains of a solid solution based on copper, containing a small amount of silicon (1.38 wt.%). Along the grain boundaries of the solid solution, the copper-based phase, enriched in silicon (up to 7.93–8.45 wt.%) is precipitated, which confirms the presence of silicides (Figure 5, Table 2).

In both cases, on the boundary interface brazing filler metal–base metal, a diffusion layer based on iron enriched with silicon (up to 10.23–13.08 wt.%) and manganese (13.58–15.92 %) solidifies, which indicates the formation of iron silicides of a complex composition (Figure 4, Table 2) and well correlated with the state diagrams of metallic systems. Thus, in accordance with the binary diagrams of state of the iron-silicon system state, the limiting solubility of silicon in γ-iron at 1150 °C is 3.84 at.%. With the temperature drop, it decreases, which leads to the formation of silicide phases [9]. The solubility of copper in iron is limited and also decreases with the drop in temperature. Such structural features of the diagrams of state of iron-silicon and copper-silicon metallic systems contribute to the fact, that during brazing the iron silicides are formed at the interface.

Table 2. Chemical composition of the structural components of the brazed weld

Spectrum	Chemical composition, wt.%				
	Si	Mn	Fe	Ni	Cu
1	1.38	13.05	0.64	0.62	84.31
2	7.93	31.16	1.02	2.11	57.77
3	8.45	31.44	1.73	4.76	53.61
4	12.68	15.70	66.73	2.20	2.69
5	12.20	15.35	62.80	2.08	7.57
6	10.32	13.58	54.98	1.95	19.16
7	13.08	15.92	67.06	2.15	1.80

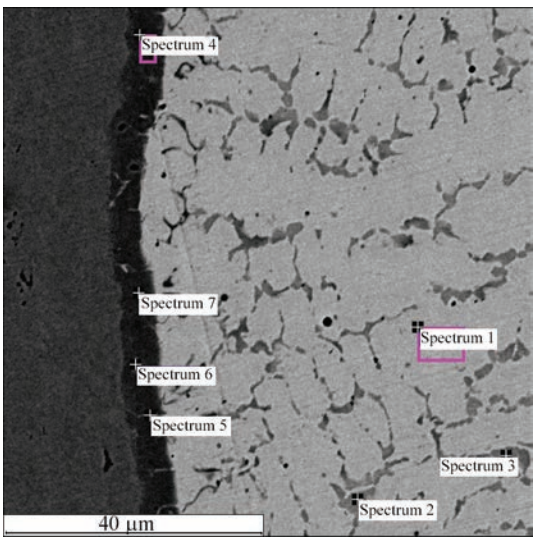

Figure 5. Boundary interface of the joint made by brazing filler metal of the Cu–Mn–Ni–3Si system using plasma-arc heating

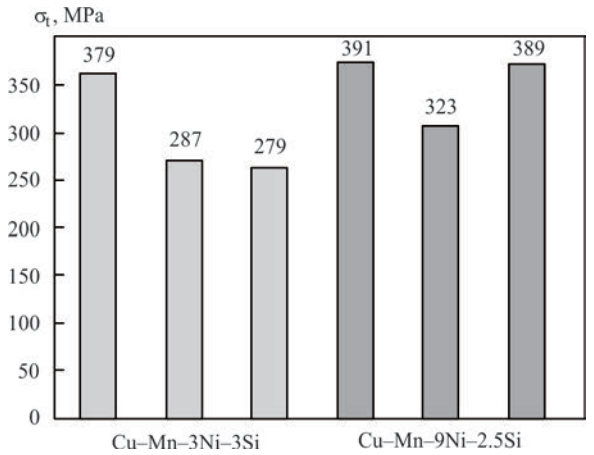

Figure 6. Rupture strength of brazed butt specimens of carbon steel 08kp

As is evidenced by the results of mechanical rupture tests of butt flat brazed specimens, produced using plasma-arc brazing and the brazing filler metal Cu–Mn–Ni–3Si, the fracture occurs along the weld. A large scattering in strength values from 279 to 379 MPa is observed (Figure 6), the average values of strength are approximately 93 % of the base metal strength (315 MPa). The increase in nickel content in brazing filler metal to 9 wt.% provides higher and more stable strength values (Figure 6). Specimens are fractured in base metal in the heat-affected zone, the average values of rupture strength increase to 367 MPa.

Based on the obtained results, a choice can be made in favor of the second brazing filler metal, which provides higher strength values and a degree of data stability.

Conclusions

Alloys of the system Cu–Mn–Ni–Si with different content of nickel and silicon were studied, melting intervals were determined, and it was shown that decrease in the liquidus temperature by about 56 °C (899 °C) provides a reduction in the nickel concentration to 3 %.

It was found that when alloying the brazing filler metals of the Cu–Mn–Ni system with silicon, the area of spreading increases. The optimum concentration of silicon does not exceed 3 wt.% In the structure of a brazed weld the dendrites of a solid solution based on copper and manganese are predominated, at the boundaries of which a phase with a higher mass fraction of manganese (31 %) and silicon (about 8 %) is located. An iron-based silicide containing manganese and silicon is formed along the brazing filler metal–base metal interface, with the content of the latter being 10.32–13.08 wt.%

It was established that an increase in the nickel content in brazing filler metal (up to 9 %) contributes to increase in strength values and their stability. Moreover, the fracture occurs in the base metal in the heat-affected zone, the average values of the rupture strength of brazed joints are 367 MPa, which is at the level of the base metal strength.

1. Knopp, N., Killing R. (2003) Hartlöten verzinkter Feinbleche mit dem Lichtbogen — sicher und wirtschaftlich (Teil 1). Solingen. *Der Praktiker*, **12**, 366–371 [in German].
2. Füssel, U., Schetzsche, V., Sziesb, U., Husner, J. (2002) Plasmalöten mit stromführendem Zusatzwerkstoff. *Ibid.*, **10**, 336–340 [in German].
3. Kallabis, M., Schwankhart, G. (2002) Plazmatron-technologie im Karosseriebau. *Blech Rohre Profile*, **4**, 42–45 [in German].
4. Pugh, C. (1970) *Die Verwendung von Ni–Mn–Lotes fur Plattierlotungen sowie das Verfahren zum Herstellen eines solchen Lotes*. FRG, Pat. 1284262 [in German].
5. Zhang, Q.K., Pei Yinyin, Weimin Long (2013) Investigations on formation mechanisms of brazing cracks at the austenitic stainless steel/filler metal brazing joint interfaces. *Acta Metallurgica Sinica — Chinese Edition*, 49(**10**), 1177–1184, October 2013, DOI: 10.3724/SP.J.1037.2013.00219
6. Davis, J.R. (Ed.) *ASM Specialty Handbook. Copper and Copper Alloys*, 276–302, DOI: 10.1361/caca P276.
7. Sejč, P., Kubíček, R. (2015) *MIG brazing of 304L type stainless steel using CuSi3 and CuSi3MnAl brazing wire*. Kovove Mater., **53**, 365–375, DOI: 10.4149/km 2015 5 365.
8. Jyrki Miettinen. (2003) *Thermodynamic description of the Cu–Mn–Ni system at the Cu–Ni side.* Calphad 27(**2**), 147–152, June 2003, DOI: 10.1016/j.calphad.2003.08.003.
9. (1997) *State diagrams of binary metallic systems*. Ed. by N.P. Lyakishev. In: Refer. Book, 3 Vol., Vol. 2. Moscow, Mashinostroenie [in Russian].

Received 22.04.2019

DOI: http://dx.doi.org/10.15407/tpwj2019.07.06

INFLUENCE OF THE COMPOSITION OF ELECTRODE COATING BINDER ON TOXICITY OF WELDING FUMES

O.G. LEVCHENKO[1], **A.O. LUKYANENKO**[2] and **O.V. DEMETSKAYA**[3]
[1]National Technical University of Ukraine «Igor Sikorsky KPI»
37 Pobedy Ave., 03056, Kyiv, Ukraine. E-mail: levchenko.opcb@ukr.net
[2]E.O. Paton Electric Welding Institute of the NAS of Ukraine
11 Kazimir Malevich Str., 03150, Kyiv, Ukraine. E-mail: office@paton.kiev.ua
[3]Kyiv International University
49 Lvivska Str., 03179, Kyiv, Ukraine

Results of sanitary-hygienic evaluation of coated electrodes for welding high-alloyed chromium-nickel steels were used to study the influence of the composition of electrode coating binder on the toxicity of fumes, which form at application of these electrodes. Express-method of determination of cytotoxicity, levels of evolution and chemical composition of welding fumes, as well as their calculated hygienic indices in accordance with international standard DSTU ISO 15011-4:2008 were applied for this purpose. It is shown that in order to develop new grades of welding electrodes with improved hygienic characteristics, it is reasonable to have not only the data of primary sanitary-hygienic evaluation, but also the results of biological studies of the toxicity of welding fumes. It is found that application in electrode coating of a binder based on pure lithium or lithium-sodium-potassium liquid glass instead of potassium-sodium one, enables reducing the level of welding fume evolution into the air, its content of highly toxic hexavalent chromium, and lowering its general toxicity due to that. 14 Ref., 3 Tables, 4 Figures.

Keywords: *coated electrodes, welding fumes, hexavalent chromium, cytotoxicity index*

Electric arc welding is characterized by evolution of fumes harmful for the human body into the working zone air, the toxic action of which is determined by the chemical composition of welding electrodes [1]. Therefore, development of new grades of welding consumables must be accompanied by their primary sanitary-hygienic evaluation, in keeping with the international standards DSTU ISO 15011-1:2008 [2] and DSTU ISO 15011-4:2008 [3]. These standards allow obtaining the necessary information on the chemical composition of welding fumes (WF) and performing tentative calculation of the risk of their harmful effect on the body of the welder. In order to create new grades of welding electrodes with improved hygienic characteristics, it is worthwhile to have not only the data of primary sanitary-hygienic evaluation, but also the results of biological studies of WF toxicity. Such investigations, particularly using experimental animals, are realized during a rather long time and require considerable expenses.

In order to assess the toxic action of poorly soluble industrial aerosols, including welding fumes, the most important is such key property as cytotoxicity that determines the risk of development of occupational illness — pneumoconiosis [4]. Cytotoxicity, as a property of dust particles (aerosol) is the determinant factor for assessment of the extent of its action on the human body and mathematical prediction of comparative risk of pneumoconiosis development. Cytotoxicity determines the kinetics of dust accumulation and retention in human lungs and lymph nodes, as well as the intensity of harmful effect on the tissues of these organs. This characteristic is assessed in different short-term tests, that is related to the prevailing ideas of the key role of dust particles damaging the macrophages in pathogenesis of silicosis and other kinds of pneumoconiosis. Also used are tests, based on recording the phenomena of macrophage activation or on some kind of combination of these phenomena. However, interpretation of test results and their application for prediction of the effect of fumes on the human body are often performed without allowing for the role of the processes of activation and damaging of the macrophage, either in mechanisms which are at the basis of the test, or in the pathogenesis of pneumoconiosis [5].

Application of the so-called alternative toxicological models (cell cultures, express-tests, etc.) provides data on the toxicity and hazardousness of chemical compounds and materials using less costly ways and approaches in shorter terms and more humanely from the viewpoint of bioethics, compared to the traditional methods of experimental studies on laboratory animals in vivo. In its turn, the data, obtained in vitro experiments can be used for screening the welding consumables as a «vector» for conducting in-depth experimental studies in vivo. In particular, express-assessment of WF toxicity, using short-term suspension

Table 1. WF evolution indices and chemical composition

Kind of liquid glass (coating binder)	Evolution intensity V_f, g/min	Specific evolution G_f, g/kg	Weight fraction, % in WF					
			Cr^{6+}	Cr^{3+}	Mn	Ni	F_p	$F_{??}$
K–Na (0 %)	0.51	11.58	1.96	2.62	4.81	1.47	11.68	1.30
Li–Na–K (0.7 %)	0.45	10.10	1.77	2.67	5.27	1.38	10.24	1.69
Li–Na–K (1.8 %)	0.35	7.28	1.44	2.82	5.69	1.29	10.35	1.88
Li–Na (2.7 %)	0.26	5.52	0.89	3.04	5.73	1.62	11.65	1.34
Li (3.2 %)	0.20	4.52	Not found	3.91	5.20	1.39	5.76	1.56
Note. Li_2O mass fraction in liquid glass is shown in brackets.								

culture of bull sperm as a test object markedly lowers the labour consumption and cost of testing. The method allows assessment of the cumulative effect from the impact of the totality of toxicants present in WF on the culture by the biological effect of its extract on the test object during time not longer than 3 hours [5].

Applicability of the above procedure of express-assessment for comparative hygienic evaluation of welding electrodes was confirmed in reference [6]. Here, it was verified that the toxicity of WF, forming during welding of high-alloyed steels, is much higher than that in welding carbon and low-alloyed steels, and it is predominantly determined by the content of carcinogenic hexavalent chromium (Cr^{6+}) and nickel in electrode coating [7]. At the same time, as shown in work [8], WF toxicity essentially depends on the ratio of lithium, sodium and potassium (Li–Na–K) in the composition of electrode coating binder (liquid glass), that is exactly what determines presence of carcinogenic hexavalent chromium (Cr^{6+}) in WF composition.

The objective of this work was determination of the influence of chemical composition of Li–Na–K binder of electrode coating for welding high-alloyed chromium-nickel steels on cytotoxicity of WF forming at their application.

WF sampling for determination of their sanitary-hygienic characteristics was performed in keeping with the standard [2] by the method of complete trapping of fumes that form during welding, using a special stand with FPP filter, mounted in the path of WF movement from the welding zone enclosure. The following characteristics of WF formation were determined: evolution intensity, V_f, g/min; specific evolution G_f (mass of WF forming at melting of a kilogram of welding electrodes), g/kg; WF chemical composition, wt.%).

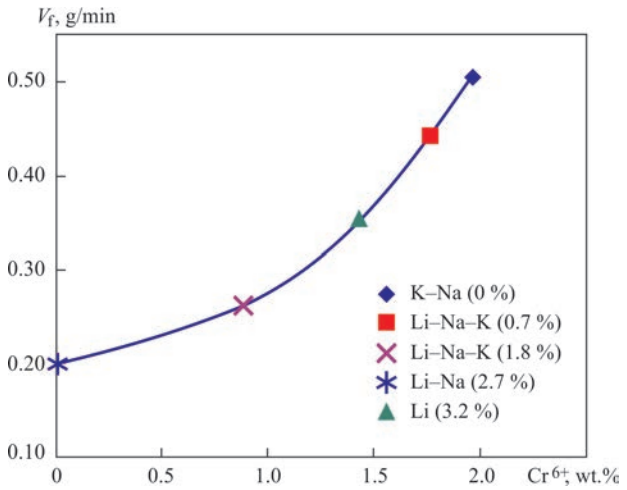

Figure 1. Dependence of WF evolution intensity V_f on the content of hexavalent chromium Cr^{6+} in it (Li_2O mass fraction in liquid glass is shown in brackets)

Toxicity assessment was performed on the basis of experimentally determined cytotoxicity index I_t by the procedure [5] of express-assessment of WF toxicity in vitro in serial analyzer AT-05 and (for comparison) by the calculated hygienic indices — limit value and class of WF in keeping with DSTU ISO 15011-4:2008 [3]. The above-given values of WF evolution intensity, V_f, mg/s and their chemical composition were used for this purpose, in keeping with the procedures of [2, 9].

Test grades of welding electrodes of E-08Kh20N9G2B type with different composition of liquid glass-binder in the coating were used for taking WF samples (Table 1). Surfacing was performed on a plate from 12Kh18N10T steel at direct current (150 A) of reverse polarity using VDU-504 rectifier. Minimum three experiments were performed for each variant. Obtained investigation results (Table 1) show that application of Li–Na–K liquid glass instead of K–Na as binder in the electrode coating allows (depending on its Li content) lowering the values of WF evolution approximately 1.2–1.5 times and reducing its content of highly toxic hexavalent chromium (Cr^{6+}) up to 1.4 times, whereas application of Li–Na binder allows lowering WF evolution 2 times and reducing its Cr^{6+} content 2.2 times (Figure 1). Application of Li-liquid glass in the coating allows lowering WF evolution 2.5 times and preventing Cr^{6+} formation in it (Figure 2).

Absence of Cr^{6+} in WF composition in this case is attributable to chemical properties of rare-earth elements. It is known that during melting and WF formation, presence of K and Na in the electrode coating usually leads to formation of their chromates and bichromates, as a result of interaction of these substances with chromium:

$$Cr + K_2O, Na_2O \rightarrow K_2CrO_4, Na_2CrO_4,$$
$$Cr + K_2O. Na_2O \rightarrow K_2Cr_2O_7, Na_2Cr_2O_7.$$

Table 2. Classification of welding consumables, depending on evolution level and calculated WF limit value [3]

WF limit value $LV_{WF(A)}$, mg/m^3	WF evolution intensity V_f, mg/s	< 3	3–8	8–15	15–25	> 25
	Welding consumable class	A	B	C	D	E
> 4.5	5	5a	5b	5c	5d	5e
3.5–4.5	4	4a	4b	4c	4d	4e
2.5–3.5	3	3a	3b	3c	3d	3e
1.5–2.5	2	2a	2b	2c	2d	2e
0.5–1.5	1	1a	1b	1c	1d	1e
< 0.5	0	0a	0b	0c	0d	0e

These are exactly the chemical compounds, that are extremely hazardous (carcinogenic) substances, which is this case determine the value of WF toxicity. Now application of Li_2O in the electrode coating, owing to the peculiarities of its chemical properties, does not lead to formation of similar chromates [8, 10–12]. Formation of other extremely hazardous compounds of hexavalent chromium CrO_3 was not confirmed, either, except for moderately toxic trivalent Cr_2O_3 [13]. The next stage of this work was determination of the effect of liquid glass composition on the value of WF toxicity [14]. For this purpose the following calculated toxicity indices [3] were determined and analyzed: WF limit value $LV_{WF(A)}$ and hygienic class of electrodes, which, in its turn, is determined by this limit value and intensity of WF evolution (Table 2), as well as experimentally determined cytotoxicity index.

Investigation results (Table 3) showed that WF limit value $LV_{WF(A)}$ decreases with increase of hexavalent chromium content in the electrode coating: it is minimum (0.31 mg/m^3) in the case of welding with electrodes with K–Na binder, increases with increase of lithium content in it and has maximum value (0.97 mg/m^3) at application of liquid glass based on pure lithium in the coating. Minimum value of $LV_{WF(A)}$ is indicative of WF maximum relative toxicity (for comparison WF are of the same mass) and, accordingly, maximum value points to smaller toxicity, characteristic for WF, generated in welding by electrodes containing lithium in their coating. Determined value $LV_{WF(A)}$ leads to the conclusion that toxicity of

Table 3. WF hygienic characteristics

Kind of liquid glass (coating binder)	WF evolution intensity V_f, mg/s	WF limit value $LV_{WF(A)}$, mg/m^3	Electrode class	Cytotoxicity I_t, %
K–Na (0 %)	8.3	0.31	0C	22.3
Li–Na–K (0.7 %)	7.5	0.33	0B	12.5
Li–Na–K (1.8 %)	5.8	0.37	0B	18.8
Li–Na (2.7 %)	4.3	0.44	0B	29.0
Li (3.2 %)	3.3	0.97	1B	66.2
Note. Li_2O mass fraction in liquid glass is shown in brackets.				

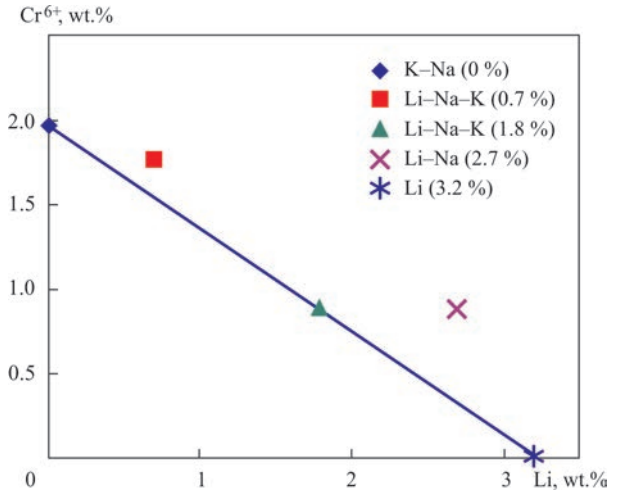

Figure 2. Dependence of hexavalent chromium Cr^{6+} on lithium content in liquid glass

WF generated in welding by electrodes with lithium-containing binder, is approximately three times smaller than that of WF, generated at application of Na–K liquid glass, that is attributable to absence of hexavalent chromium in WF (Figure 3).

As regards hygienic class of electrodes as a general (practically absolute) characteristic of toxicity, it has zero «0» value for all electrodes, except for electrodes with lithium binder in the coating, which belongs to class 1 and is indicative of lower WF toxicity. Thus, electrodes with Na–K and Li–Na–K binder belong to the worst hygienic class, as hexavalent chromium is present in the composition of WF, which form in welding with them, while electrodes with lithium binder belong to less hazardous class «1».

At the same time, taking into account the index of WF evolution intensity, we determine more precisely to which generalizing class of electrodes they belong. So, electrodes with Na–K binder of the coating belong to the worst hygienic class — «0C» with maximum intensity of WF evolution (V_f = 8.3 mg/s), and

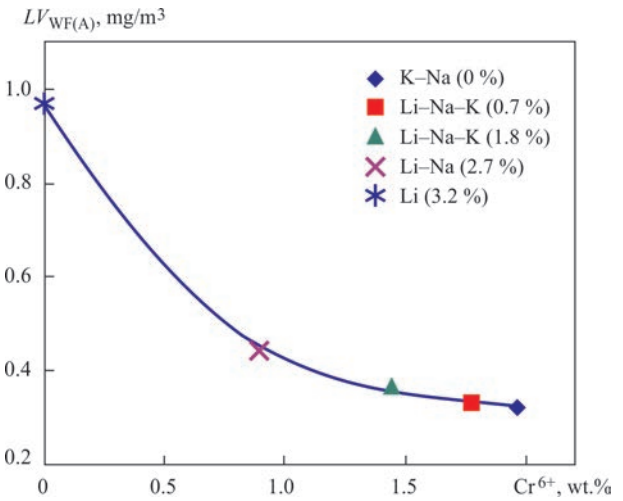

Figure 3. Dependence of WF limit value on the content of hexavalent chromium Cr^{6+} (Li_2O mass fraction in liquid glass is shown in brackets)

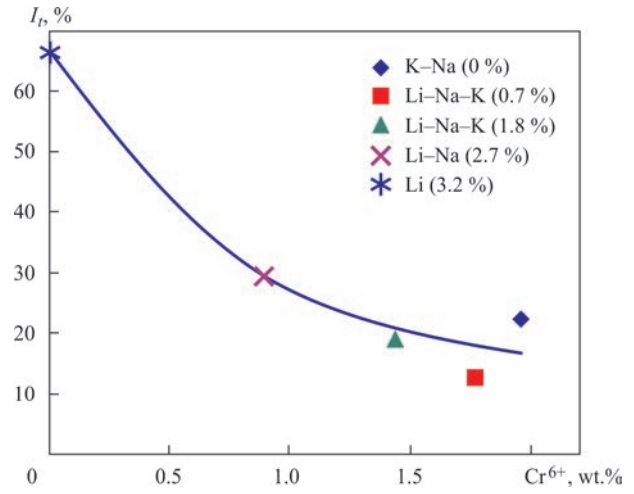

Figure 4. Dependence of cytotoxicity index I_t on the content of hexavalent chromium Cr^{6+} in WF (Li_2O mass fraction in liquid glass is shown in brackets)

electrodes with lithium binder are in the best class in this case (V_f = 3.3 mg/s). Here, it should be noted that practically all the electrodes for welding high-alloyed chromium-nickel steels belong to class «0», limit value $LV_{WF(A)}$ of which should not exceed the most stringent threshold of 0.5 mg/m^3 (see Table 2), according to standard DSTU ISO 15011-4:2008 [3]. Thus, for welding high-alloyed chromium-nickel steels it is desirable to use electrodes with binder based on pure lithium liquid glass. This allows going beyond the limits of the most toxic hygienic class «0», i.e. improving the hygienic characteristics of the electrodes.

And, finally, the index of WF cytotoxicity allowed determination of numerical values of their toxicity I_t (see Table 3). So, at application of lithium binder in electrode coating it has the maximum value (I_t = = 62.1 %), that is indicative of minimum WF toxicity (as at values I_t = 70–120 % the test material is considered non-toxic). In welding by electrodes with other binders, it changes from 12.5 up to 29.0 %, depending on binder composition, that is indicative of the tendency of increase of WF toxicity at lowering of lithium content in liquid glass composition. Certainly, this, in its turn, is accounted for by hexavalent chromium content in WF: with increase of its concentration in WF composition, the cytotoxicity index decreases, i.e. WF toxicity rises (Figure 4).

It should be noted that application of this screening method [5] in practice at sanitary-hygienic evaluation of welding electrodes does not allow making an unambiguous conclusion on WF toxicity dependence on Li, Na, K and hexavalent chromium content in the coating, as WF toxicity is also affected by other components of electrode coating, such as nickel, manganese, dissolved fluorides, etc.

Conclusions

Application of known international standardized methods of sanitary-hygienic evaluation of welding consumables together with the method of determination of cytotoxicity index of welding fumes showed that use of a binder based on pure lithium or lithium-sodium-potassium liquid glass, instead of potassium-sodium one, in the coating of electrodes for welding high-alloyed chromium-nickel steels, allows reducing the level of welding fume evolution into the air, its content of highly toxic hexavalent chromium, and, due to that lowering its general toxicity.

1. Levchenko, O.G. (2015) *Welding aerosols and gases: Processes of formation, methods of neutralization and security protection means*. Kiev, Naukova Dumka [in Russian].
2. (2011) *DSTU ISO 15011-1:2008*: Occupational health and safety in welding and allied processes. Laboratory method of aerosol and gas extraction formed in arc welding. Pt 1: Determination of emission level and sampling for analysis of aerosol microparticles. Valid from 2008-8-15. Kyiv: Derzhspozhyvstandart Ukrainy [in Ukrainian].
3. (2011) *DSTU ISO 15011-1:2008*: Occupational health and safety in welding and allied processes. Laboratory method of aerosol and gas extraction. Pt 4: Fume data sheets. Valid from 2008-8-15. Kyiv: Derzhspozhyvstandart Ukrainy [in Ukrainian].
4. Kundiev, Yu.I., Korda, M.M., Kashuba, M.O., Demetska, O.V. (2015) *Toxicology of fume*s. Ternopil, TDMU Ukrmedknyga [in Ukrainian].
5. Demetska, O.V., Leonenko, N.S., Movchan, V.O. et al. (2016) *Method of express-evaluation of toxicity of welding fumes in vitro*. Pat. 110801, Ukraine, Int. Cl. G 01 N 33/48 (2006/01) [in Ukrainian].
6. Levchenko, O.G., Demetska, O.V., Lukyanenko, A.O. (2016) Cytotoxicity of welding fumes formed in arc welding with coated electrodes. *Ukrainsky Zh. z Problem Medytsyny Pratsi*, 48(**3**), 30–36 [in Ukrainian].
7. Yushchenko, K.A., Bulat, A.V., Levchenko, O.G. et al. (2009) Effect of composition of base metal and electrode covering on hygienic properties of welding fumes. *The Paton Welding J.*, **7**, 44–48.
8. Yushchenko, K.A., Bulat, A.V., Skorina, N.V. et al. (2017) Effect of binder type on manufacturability and properties of E-08Kh20N9G2B type coated electrodes. *Ibid*., **1**, 2–9.
9. (1990) *4945–88*: Procedural guidelines on determination of harmful substances in welding fumes (solid phase and gases). Moscow, Minzdrav SSSR.
10. Kimura, I., Kobayashi, M., Godai, T. et al. (1979) Investigations on chromium in stainless steel welding fumes. *Welding J.*, Res. Suppl., **8**, 195–204.
11. Astrom, H. (1993) Advanced development techniques for coated electrodes. *Welding Review. Int*., 12(**2**), 72, 74, 76.
12. Griffiths, T., Stevenson, A. (1989) Binder developments for stainless electrodes. *Welding Review*, 8(**3**), 192, 194, 196.
13. Levchenko, O.G., Bezushko, O.N. (2015) Thermodynamics of formation of chromium compounds in welding aerosols. *The Paton Welding J*., **7**, 22–25.
14. Levchenko, O.G., Lukianenko, A.O., Demetska, O.V., Arlamov, O.Y. (2018) Influence of composition of binder of electrodes coating on citotoxicity of welding aerosols. *Mater. Sci. Forum*, **927**, 86–92.

Received 22. 01.2019

DOI: http://dx.doi.org/10.15407/tpwj2019.07.07

EVALUATION OF SHORT-TERM MECHANICAL PROPERTIES OF A JOINT OF DIFFICULT-TO-WELD NICKEL HIGH-TEMPERATURE ALLOYS OF ZhS6 TYPE

K.A. YUSHCHENKO, A.V. YAROVITSYN, N.O. CHERVYAKOV, A.V. ZVYAGINTSEVA, I.R. VOLOSATOV and **G.D. KHRUSHCHOV**
E.O. Paton Electric Welding Institute of the NAS of Ukraine
11 Kazimir Malevich Str., 03150, Kyiv, Ukraine. E-mail: office@paton.kiev.ua

A procedure was developed for evaluation of short-term mechanical properties of «base–deposited metal» welded joint of difficult-to-weld nickel high-temperature alloys of ZhS6 type at high-temperatures, simulating restoration of edges of blades of aircraft gas-turbine engines at their serial repair. The need of limiting reduction in comparison with acting reference documents of sizes of the welded billets and samples for mechanical tests was shown following the condition of providing the technological strength of such welded joint. The developed procedure was tested on servohydraulic machine MTS-810 during samples' testing. It allowed making the grounds for selection of the modes of preliminary heat treatment in order to get optimum strength properties of deposited metal ZhS6K. 19 Ref., 4 Tables, 7 Figures.

Keywords: *microplasma powder surfacing, GTE blades, repair of flange platforms, difficult-to-weld nickel alloy, welded joint, technological strength, sample preparation, mechanical properties, high temperature*

For more than 10 years microplasma powder surfacing is used for serial repair of parts of aircraft gas-turbine engines (GTE) of difficult-to-weld nickel high-temperature alloys [1–4], in particular, restoration of edges of blades of high-pressure turbine of 1.0–3.5 mm thickness. Application under manufacturing conditions of this process of one-layer arc surfacing is characterized by the next field of energy parameters, where a tendency of given materials to formation of cracks in process of fusion welding and further heat treatment [5–7] is not revealed, namely welding current intensity 2–35 A; effective arc heat power 50–600 W, heat input considering heating efficiency of part 400–2000 J/mm.

Short-term mechanical properties of «base–deposited metal» welded joint at operation temperature of part of aircraft GTE, including the values of yield limit σ_y, ultimate strength σ_t and relative elongation δ of material, are the primary indices of reliability of developed technology. It is believed that the level of short-term strength properties of welded joint not less than 0.6 relatively to base metal shall be provided in a temperature range of flange platforms' operation to fulfill the conditions of restoration of flange platforms of HPT blades. An important role for meeting the given requirements, in particular, in the case of surfacing of more than one layer, plays rational selection of composition and modes of further heat treatments of the deposited metal.

Aim of the present work was development of a procedure for determination of high-temperature properties of «base–deposited metal» welded joint of ZhS6U–ZhS6K system (Table 1) from difficult-to-weld nickel high-temperature alloys applicable to the problem of restoration of flange platform of a Z-profile blade of one of the modern GTE (Figure 1). Absence of cracks in a surfacing zone was preliminary determined using the penetrant and metallographic testing methods (Figure 2).

To fulfill the set goal it was necessary to solve the next problems:

- analyze known and acting reference documents (RD), regulating an order of preparation of welded joint samples for next determination of their short-term mechanical properties;
- argue the selection of shape and sizes of static tension sample at 1000 °C temperature and, respectively, initial welded billet;
- at 1000 °C test temperature investigate the regularities of change of indices of short-term mechanical

Table 1. Composition (wt.%) on main alloying elements of nickel high-temperature alloys ZhS6U-VI and ZhS6K-VI according to OST1 90126–85

Alloy	C	Cr	Ni	Co	Al	Ti	Mo	W	Nb	Fe	Mn	Si	B
ZhS6U-VI	0.13–0.20	8.0–9.5	Base	9.5–10.5	5.1–6.0	2.0–2.9	1.2–1.4	9.5–11.0	0.8–1.2	<1.0	<0.4	<0.4	<0.035
ZhS6K-VI	0.13–0.2	9.5–12.0	Same	4.0–5.5	5.0–6.0	2.5–3.2	3.5–4.8	4.5–5.5	1.4–1.8	<2.0	<0.4	<0.4	<0.02

Figure 1. Appearance of pilot turbine blade of nickel high-temperature alloy ZhS6U restored by microplasma powder surfacing of ZhS6K alloy: *a* — characteristics of repair zone; *b* — appearance of deposited flange platform with Z-profile; *c* — appearance of restored flange platform after machining and penetrant testing

properties of typical zones of «base–deposited metal» welded joint of ZhS6U-ZhS6K system at different modes of their heat treatment.

It is determined that new national harmonized [9–12] and international [13] standards for evaluation of short-term properties of welded joints at elevated temperatures propose to use:

- for deposited weld metal at longitudinal tension the cylinder samples with test portion diameter 8 mm and more; major diameter of their gripping part 12 mm and more and total length of the sample more than 77 mm;
- for welded joints at their transverse tension except for mentioned above cylinder samples — flat samples of thickness from 3.0–8.3 mm with gripping part width 35 mm and total sample length 190–215 mm.

Earlier acting in our country GOST 6996 [8] (till 01.01.2019) for evaluation of short-term mechanical properties of deposited metal in comparison with new national harmonized standards [9–12] additionally proposed to use cylinder samples with diameter of test portion 3 and 6 mm; major diameter of their gripping part 6 and 12 mm and total length of samples 30–86 mm.

Also analyzed RDs [9–13] for evaluation of short-term mechanical properties of deposited metal require using welded billets of significant thickness, i.e. butt welds with thickness of base metal 12 mm [9, 10]; with total width and height of bead 20 and more than 30 mm, respectively [8].

Adequacy of the requirements, mentioned above in RDs [8–13], applicable to deposited metal of difficult-to-weld nickel high-temperature alloy ZhS6K, was checked on a series of technological probes due to presence of limitations on level of heat input in part and volume of deposited metal [7, 14, 15] for welded joints of nickel high-temperature alloys with high content of strengthening γ′-phase. Verification of technological probes on presence of cracks in base and deposited metal was carried out visually (with up to ×10 magnification) as well as penetrant testing. Obtained and expected results of such verification are presented in Table 2, scheme of surfacing of technological probe on narrow substrate and example of its external view in form of deposit on narrow substrate in Figure 3.

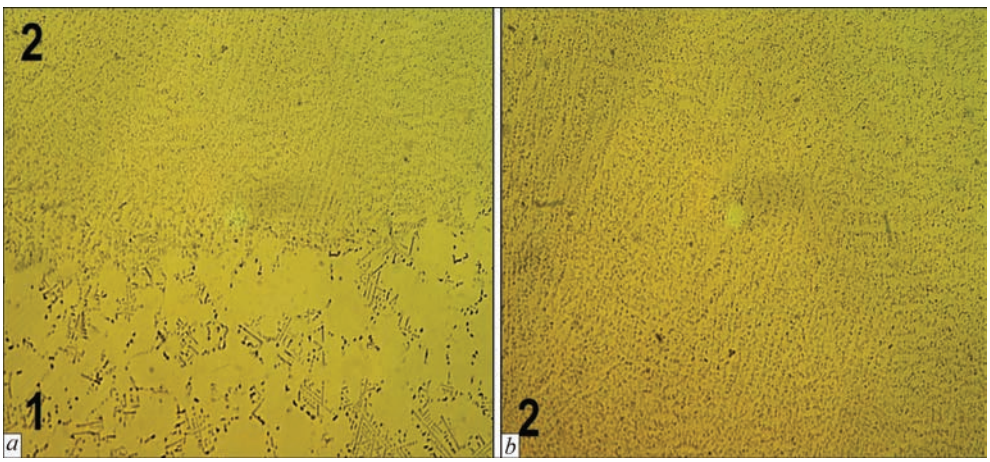

Figure 2. Microstructure (×100) of «base–deposited metal» joint of restored flange platform (ZhS6U–ZhS6K system): *a* — fusion line; *b* — deposited metal ZhS6K

Table 2. Peculiarities of technological strength in welded joints with the involvement of deposited metal of difficult-to-weld nickel high-temperature alloy ZhS6K

Number of probe	Type of surfacing/ welding	δ, mm	BM type	*B*, mm	*H*, mm	*L*, mm	V_d, cm^3	Providing technological strength in the process	
								Surfacing/ welding	Next h/t
1	NS	2.0	ZhS6U	3–5	5	40–45	0.60–1.13	+	+
2	NS	2.5–3.0	ZhS6U	4–6	12–15	40–45	1.92–4.50	+	+
3	NS	5.0	ZhS6U	7–8	5–7	50	1.75–2.80	+	+
4	NS	1.8–2.5	ZhS6U, ZhS6K	4–6	10–14	140–210	5.60–17.60	–	–
5	NS	2.0–3.0	Aust. stain. steel	5–7	25–30	50–70	6.25–14.70	+	+
6	NS	2.0–3.0	Aust. stain. steel	5–7	35–40	50–70	8.75–19.6	+	–
7	Pl	2.0	ZhS6K	5–7	2–3	50–70	0.50–1.47	–	–
8	W	1.5–2.0	ZhS3DK	5–7	2–3	50–70	0.40–1.31	–	–
Expected results									
9	NS	12–20	ZhS6, aust. stain. steel	14–20	≥30	≥80	≥3.6	–	–
10	W	12–16	ZhS6U	12–16	2…3	≥150	≥26.8	–	–

Note. NS, Pl, W — surfacing on narrow substrate, plate and weld, respectively; δ — thickness (width) of base metal (BM); *B*, *H*, *L* — width, height and length of deposited bead (in case of weld — bead reinforcement); V_d — volume of deposited metal.

It is determined that after exceeding some volume of deposited bead of difficult-to-weld high-temperature alloy ZhS6K (first of all characterized with height *H* of more than 35 mm at deposited bead length *L* = = 50–70 mm and *H* > 5 mm at *L* ≥ 140 mm) there is appearance the reheat cracking in it. Respectively, due to presence of cracks the bead of ZhS6K deposited metal of such volume can not have acceptable level of mechanical properties, including at high temperatures. Similar situation is possible in the case of performance of welds or surfacing on plate.

At the same time it is shown that with limitation of length of deposited bead less than 50–70 mm it is possible to get multilayer surfacing of alloy ZhS6K without violation of technological strength of corresponding welded joint in the next cases:

- at ZhS6U base metal thickness δ = 2.5–3.0 mm on height not less than 12 mm;
- at ZhS6U base metal thickness δ = 5.0 mm on height not less than 5 mm;
- at base metal thickness of austenite stainless steel on height up to 30 mm.

The determined zone, which provides technological strength in «base–deposited metal» welded joint with the involvement of deposited metal ZhS6K, on deposit volume exceeds the necessary volume of deposited metal on real part, namely aircraft GTE turbine blade, in 2.5–13 times.

Following from mentioned above the next conclusions can be made. Realization of RD requirements [9–12] applicable to static tension tests at 1000 °C temperature of the joints with involvement of difficult-to-weld nickel high-temperature alloy ZhS6K can result in unjustified increase of technical requirements to power of tearing machine; dimensions of special grips for high-temperature tests; consumption of expensive material of nickel high-temperature alloy on welded billets; laboriousness of direct manufacture of samples for machining. However, the main reason of irrationality of RD requirements [9–12] is the fact that process of preparation and performance of butt welded joint from difficult-to-weld nickel high-temperature alloy of ZhS6 type of 12–16 mm thickness will result in considerable increase of the

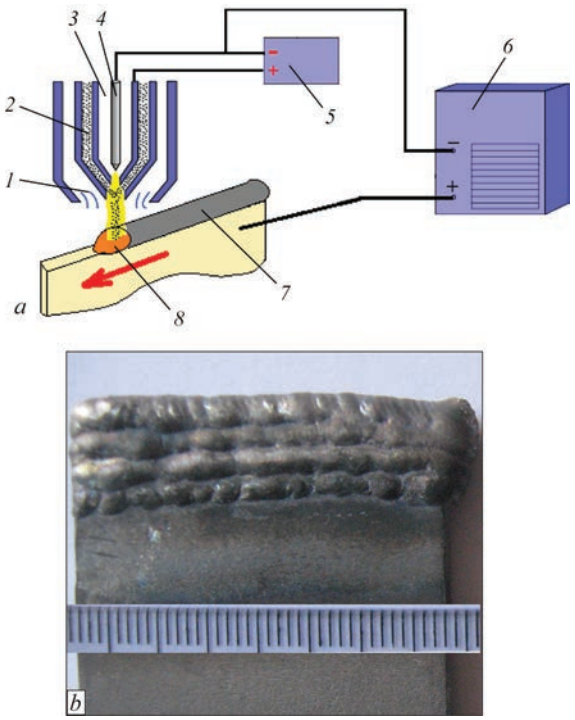

Figure 3. Scheme of microplasma powder surfacing on narrow substrate (*a*) and appearance of corresponding technological probe in multilayer surfacing (*b*) (*1* — shielding gas; *2* — carrier gas and powder; *3* — plasma gas; *4* — W-electrode; *5* — power source of pilot arc; *6* — power source of microplasma arc; *7* — deposited bead; *8* — weld pool

necessary power of microplasma arc and multiple rise of level of acting tensile stresses and deformations in process of welding thermal deformation cycle. According to preliminary estimations it will be necessary to increase the intensity of welding current not less than 5–10 times in comparison with real mode of restoration surfacing of the considered blade. This in most of the cases leads to violation of thermal mode of operation of used plasmatron and requires, as a minimum, development of new model for increased power of microplasma arc. At the same time under given conditions it is high probability of violation of technological strength of such joint with formation of cracks in its zone in process of fusion welding or next heat treatment.

Thus, the main provisions of developed procedure of evaluation of short-term mechanical properties at high temperatures (1000 °C) for «base-deposited metal» joint of difficult-to-weld nickel high-temperature alloy with high content of γ′-phase can be stated in the following way.

1. Geometry of initial welded billet and range of values of energy indices of modes for its preparation should correspond to possibility of fulfillment in corresponding joint of the conditions providing technological strength (no cracks) in process of fusion welding and next heat treatment.

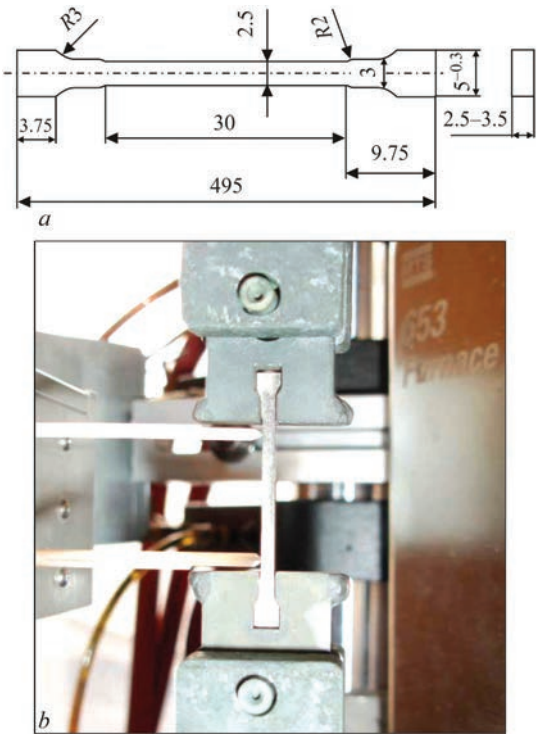

Figure 4. Shape and dimensions of flat proportional sample for evaluation of short-term mechanical properties of difficult-to-weld deposited metal ZhS6K at high temperatures (*a*) and appearance of special adaptors to grips of testing servohydraulic machine MTS-810 (*b*)

2. Range of values of energy indices of modes for preparation of welded billet characterizing power of microplasma arc and total heat input in the part should be close to the maximum to real surfacing modes and, respectively, values of indices of heat input into the part using planned technology of restoration of edge of aircraft GTE blade.

3. Geometry and shape of sample for mechanical tests were selected in such a way that it was possible to make one or several such samples from initial welded billet of specific size, where difficult-to-weld nickel high-temperature alloy shows no tendency to crack formation.

4. Geometry and shape of separate sample for mechanical tests are selected in such a way as to provide the minimum consumption of expensive material, technical capability and acceptable laboriousness of its manufacture; reasonable application of power of test machine and fulfillment of the conditions of long-term life of testing machine grips.

To fulfill the requirements mentioned above a flat sample with optimized section of test portion (Figure 4, *a*) made by electroerosion cutting was proposed. In order to reduce the dimensions of gripping part of the sample there was introduced a system of intermediate adapters to grips (Figure 4, *b*) of test servohydraulic machine MTS-810 (maximum tearing force 3 t). The new sample, in contrast to regulated in RDs [8–12], allowed eliminating the critical excess of thickness and length, typical to cylinder and flat samples, respectively. Thus, volume of deposited metal was brought into correspondence to preliminary set on technological probes requirements for providing technological strength for «base–deposited metal» welded joint with involvement of nickel high-temperature alloy ZhS6K. Table 3 contains generalized analysis of correspondence of shape and dimensions of proposed in Figure 4 sample to the basic requirements of flat proportional samples in RDs [13, 16, 17]. Calculation evaluation of sum amount of heat inputs into the part for welded billet of new pattern in comparison with cylinder samples (Figure 5) according to RDs [13] demonstrates their decrease in approximately 7–10 times. In comparison with butt welded joint the expected effect of decrease of sum heat inputs in preparation of welded billet of new pattern make roughly 11–15 times.

Short-term mechanical properties of «base–deposited metal» joint of difficult-to-weld nickel high-temperature alloy simulating restoration of blade edge are evaluated by means of static tension testing of two types of samples, namely 50 % base + 50 % deposited metal simulating area of fusion line; 100 % of deposited metal. Appearance of initial welded billets of sys-

Table 3. Comparison of fulfillment of main requirements for sample according to Figure 4 as for its shape and dimensions in international [13] and domestic RDs [16, 17]

GOST 1497–84 [16]	Condition fulfillment	DSTU EN 10002-1:2006 [17]	Condition fulfillment	ISO 6892-1:2016 (E) [13]	Condition fulfillment
Requirements to initial calculation length of sample test portion $l_0 = 11.3\sqrt{F_0} \approx 30$ mm (c. 1.8)	+	Requirements to initial calculation length of sample test portion $L_0 = 11.3\sqrt{S_0} \approx$ 30 mm (c. 6.1)	+	Requirements to initial calculation length of sample test portion $L_0 = 11.3\sqrt{S_0} \approx 30$ mm (c. 6.1)	+
–	–	Requirements to minimum initial calculation length of sample test portion $L_0 > 20$ mm (c. 6.1)	+	Requirements to minimum initial calculation length of sample test portion $L_0 > 15$ mm (c. 6.1)	+
–	–	–	+	Requirements to dimensions of base section for installation of extensometer $0.9L_0 > L_e > 0.5L_0, L_e = 25$ mm (c. 8.3)	+
Requirements to total length of sample test portion $l = l_0 + (1.5–2.5)\sqrt{F_0} = 30 +$ + (4.11–6.84) ≈ 34–41 (c. 1.12)	+	Requirements to total length of sample test portion $L = L_0 + (1.5)\sqrt{S_0} = 30 +$ + (4.11–6.84) ≈ 34–37 (Addition D 2.1)	+	Requirements to total length of sample test portion $L - L_0 + (1.5)\sqrt{S_0} = 30 +$ + (4.11–6.84) ≈ 34–37 (Annex D 2.1)	+

tem ZhS6U6(BM)–ZhS6K(DM) and ZhS6K(DM), for which technological strength of corresponding joints is provided in process of multilayer surfacing and next heat treatments, with scheme of sample cutting for high-temperature mechanical tests is presented in Figure 6.

Static tensile tests of the samples at 1000 °C temperature were carried out on servohydraulic machine MTS-810 (Figure 7) at different modes of preliminary heat treatment: 1050 °C — 2.5 h [2]; homogenization at 1220 °C temperature (according to OST1 90126–85), duration 2 and 4 h; homogenization at 1220 °C temperature (according to OST1 90126–85), duration 4 h and next aging at 950 °C temperature, duration 4 h [18]. Figure 4 provides the averaged based on two tests values of indices of short-term mechanical properties for three types of samples (base, 50 % of base metal ZhS6U + 50 % of deposited metal ZhS6K; 100 % of deposited metal ZhS6K) as well as table data on base metal ZhS6U and ZhS6K [19].

It is determined that in order to get the optimum level of properties at 1000 °C of deposited metal ZhS6K and transition zone BM ZhS6U–DM ZhS6K it is necessary to carry out heat treatment in form of homogenization at 1220 ° C temperature during 4 h. Further aging on mode 950 °C — 4 h, which is often used in practice for diffusion annealing of redeposited protective coatings without significant change of strength characteristics of deposited metal ZhS6K limits its ductility, approaching it to corresponding value of base metal ZhS6U. At that in the transition zone BM ZhS6U–DM ZhS6K there is somewhat decrease of values of yield limit and increase of ductility.

It is shown that sufficiently high level of strength properties in comparison with base metal ZhS6U and ZhS6K is reached in the samples after homogenization during 4 h as well as after next aging on 950 °C — 4 h mode in testing at 1000 °C. The next level of full-strength in comparison with base metal ZhS6U is reached on the samples 50 % BM ZhS6U + + 50 % DM ZhS6K simulating the zone of fusion line in restoration of flange platform of blade, namely for

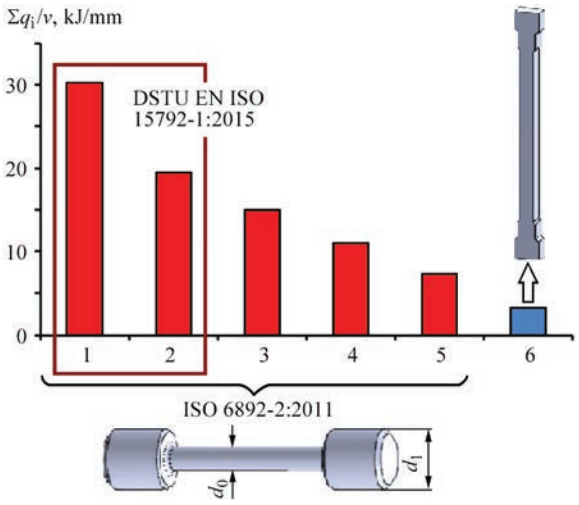

Figure 5. Calculation evaluation of sum amount of heat inputs into part in producing the billets of samples by multilayer surfacing of ZhS6K alloy on plate edge for a series of cylinder samples according to RD ISO 6892-2:2011 [13] (Nos 1–5) and new flat proportional sample (No.6) (1 — d_0 = 10 mm, d_1 = M16; 2 — d_0 = = 8 mm, d_1 = M12; 3 — d_0 = 6 mm, d_1 = M10; 4 — d_0 = 5 mm, d_1 = M8; 5 — d_0 = 4 mm, d_1 = M6; 6 — according to Figure 4

Table 4. Values of indices of short term strength of static tension samples at 1000 °C

Type of sample	Mode of heat treatment	σ_y, MPa	σ_t, MPa	δ, %
100 % DM ZhS6K	1050 °C — 2.5 h	322.5	380.5	0.35
	1220 °C — 2 h	256.3	300.9	5.80
	1220 °C — 4 h	307.2	415.3	7.20
	1220 °C — 4 h + 950 °C — 4 h	315.0	406.0	2.60
50 % BM ZhS6U +50 % DM ZhS6K	1220 °C — 2 h	403.9	496.2	3.14
	1220 °C — 4 h	427.0	516.1	1.60
	1220 °C — 4 h + 950 °C — 4 h	372.0	509.0	3.70
ZhS6U BM	1220 °C — 4 h	428.4	504.8	5.5
ZhS6K BM [19]	1220 °C — 4 h	300–320	500-570	4.5
ZhS6U BM [19]	1220 °C — 4 h	460–500	520	1.0–2.0

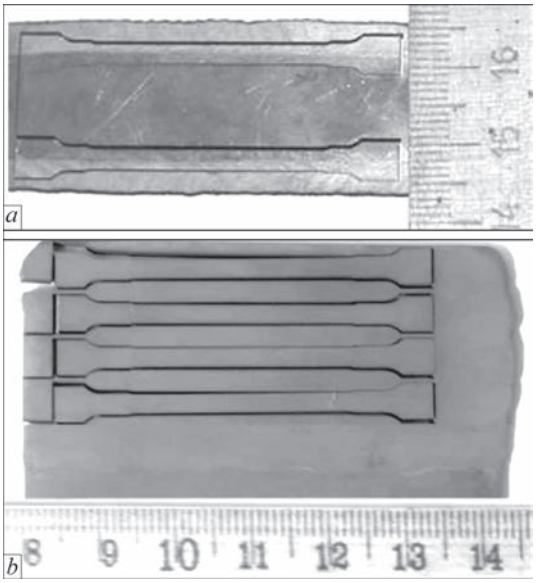

Figure 6. Appearance of initial welded billets with scheme of sample cutting for high-temperature mechanical tests: *a* — 50 % ZhS6U (BM) + 50 % ZhS6K (DM); *b* — ZhS6K (DM)

values of yield limit σ_y — not less than 0.78; ultimate strength σ_t — approximately 1.0. On the samples of 100 % DM ZhS6K simulating restored part of flange platform of blade the following level of full strength is achieved in comparison with base metal ZhS6U, i.e. on values of yield limit σ_y not less than 0.65; ultimate strength σ_t not less than 0.80.

Thus, it is determined that «base–deposited metal» joint of difficult-to-weld nickel high-temperature alloys of ZhS6U–ZhS6K system, made by microplasma powder surfacing, provides at 1000 °C the level of high-temperature strength not less than 0.65–0.80 relatively to base metal ZhS6U that corresponds to primary recommendations on working capacity of material of restored flange platform of turbine blade.

Conclusions

In order to get the objective evaluation of strength properties of «base–deposited metal» joints of difficult-to-weld nickel high-temperature alloys with content of strengthening γ′-phase more than 50 vol.%, it is necessary preliminary to choose geometry of initial

Figure 7. Appearance of servohydraulic machine MTS-810 for high-temperature tests of difficult-to-weld nickel high-temperature alloys

billet and sample for mechanical tests with the purpose to provide their technological strength in process of fusion welding as well as in process of next heat treatment.

Analysis of the procedures for evaluation of strength properties of deposited metal, regulated by acting RDs (GOST, DSTU, ISO) showed that given above condition for corresponding joints of nickel high-temperature alloys of ZhS6 type can not be fulfilled due to the requirements of artificial increase of rigidity of welded joint (butt weld), increased dimensions of gripping part of cylinder samples (diameter not less than 12 mm) or total length of flat samples (not less than 190 mm).

A need in development of special procedure has appeared due to irrelevance of the requirements of acting RDs applicable to evaluation of strength properties of such joints from difficult-to-weld nickel high-temperature alloys.

Based on reference recommendations of acting RDs there was proposed a practical form of a flat proportional sample with working section 6–10 mm^2. Dimensions of the gripping part of such sample are

reduced to the maximum due to application of intermediate adaptors to grips of MTS-810 test machine.

It is determined that obtaining of the optimum at 1000 °C level of properties of deposited metal ZhS6K and its transition zone in the area of fusion line with base metal ZhS6U requires heat treatment in form of homogenization at 1220 °C temperature during 4 h and next aging at 950 °C temperature for 4 h.

1. Pejchev, G.I. (2005) Repair of worn out during operation structure components of flange platforms of turbine cast blades from alloys of ZhS type. Aviats.-Kosmich. *Tekhnika i Tekhnologiya*, 9(**25**), 221–223 [in Russian].
2. Yushchenko, K.A., Savchenko, V.S., Yarovitsyn, A.V. et al. (2010) Development of the technology for repair microplasma power cladding of flange platform faces of aircraft engine high-pressure turbine blades. *The Paton Welding J.*, **8**, 21–24.
3. Zhemanyuk, P.D., Petrik, I.A., Chigilejchik, S.L. (2015) Experience of introduction of the technology of reconditioning microplasma powder surfacing at repair of high-pressure turbine blades in batch production. *Ibid*., **8**, 39–42.
4. Yushchenko, K.A., Yarovitsyn, A.V. (2012) Improvement of technology of repair of upper flange platform of aircraft gas turbine engine blades. In: *Special-purpose program of NASU of Ukraine: Problems of life and safety of constructions and Machines: Collect. of the results of 2010–2012. Kyiv, PWI, 506–509* [in Russian].
5. Yushchenko, K.A., Yarovitsyn, A.V., Chervyakov, N.O. (2016) Dependencies of discrete-additive formation of microvolumes of metal being solidified in multilayer microplasma powder surfacing of nickel alloys. *The Paton Welding J*., **5–6**, 143–149.
6. Zhemanyuk, P.D., Petrik, I.A., Chigilejchik, S.L. (2016) Peculiarities of bead shape regulation in single-layer microplasma surfacing on edges of aircraft gas turbine engine blades. *Ibid*., **11**, 23–40.
7. Yushchenko, K.A., Yarovitsyn, A.V., Chervyakov, N.O. (2017) Effect of energy parameters of microplasma powder surfacing modes on susceptibility of nickel alloy ZhS32 to crack formation. *Ibid*., **2**, 2–6.
8. GOST 6996–66 (ISO 4136–89, ISO 5173–81, ISO 5177–81): Welded joints. Methods of mechanical properties determination (with modifications 1, 2, 3, 4) [in Russian].
9. (2015) *DSTU EN ISO 15792-1:2015*: Welding consumables. Pt 1. Tests methods for all-weld metal test specimens in steel, nickel and nickel alloys [in Ukrainian].
10. (2015) *DSTU EN ISO 15792-2:2015*: Welding consumables. Pt 2. Preparation of single-run and two-run technique test specimens in steel [in Ukrainian].
11. (2015) *DSTU EN ISO 5178:2015*: Destructive tests on welds in metallic materials. Longitudinal tensile test on weld metal in fusion welded joints [in Ukrainian].
12. (2015) *DSTU EN ISO 4136-1:2015*: Destructive tests on welds in metallic materials. Transverse tensile test [in Ukrainian].
13. (2011) *ISO 6892-2:2011*: Metallic materials. Pt 2. Method of test at elevated temperature.
14. DuPont, J.N., Lippold, J.C., Kisser, S.D. (2009) *Welding metallurgy and weldability of nickel-base alloys*. John Wiley & Sons, Inc. Hoboken, New Jersey.
15. Yarovitsyn, A.V. (2015) *Energy approach in analysis of microplasma powder surfacing modes*. *The Paton Welding J*., **5–6**, 14–21.
16. (1984) *GOST 1497–84*: Metals. Tensile testing methods (valid to 01.01.2021) [in Russian].
17. (2006) *DSTU EN 10002-1:2006*: Metallic materials. Tensile tests. Pt 1. Testing method at room temperature [in Ukrainian].
18. Koval, A.D., Andrienko, A.G., Gajduk, S.V., Kononov, V.V. (2012) Optimization of heat treatment mode for alloy ZhS3LS doped with hafnium and tantalum. *Novi Materialy v Metalurgii ta Mashynobuduvanni*, **2**, 15–19 [in Russian].
19. Kishkin, S.T. (2006) *Development, investigation and application of high-temperature alloys*. Moscow, Nauka [in Russian].

Received 17.04.2019

DOI: http://dx.doi.org/10.15407/tpwj2019.07.08

FLUX-CORED WIRE FOR RESTORATION SURFACING OF WORN SURFACES OF RAILWAY WHEELS*

V.D. POZNYAKOV, A.A. GAJVORONSKY, A.V. KLAPATYUK, A.S. SHISHKEVICH and **V.A. YASHCHUK**
E.O. Paton Electric Welding Institute of the NAS of Ukraine
11 Kazimir Malevich Str., 03150, Kyiv, Ukraine. E-mail: office@paton.kiev.ua

Research was performed and flux-cored wire of PP-AN180MN/98 grade was developed for restoration surfacing of worn areas of advanced higher-strength railway wheels. A set of physicomechanical properties of the deposited metal was determined. It is found that at application of PP-AN180MN/98 wire for surfacing higher-strength wheels, irrespective of preheating temperature and number of deposited layers, deposited metal hardness is optimum (0.94–1.0 of rail hardness). Here, a comparatively homogeneous bainite-martensite structure forms in all the joint areas (in the deposited metal, fusion zone and overheating area of HAZ metal). The deposited metal features a high level of resistance to brittle fracture and wear at sliding friction in contact with rail steel. Obtained research results lead to the conclusion that at application of flux-cored wire PP-AN180MN/98 for surfacing, the restored wheels will have a high reliability, and traffic safety will be ensured under the conditions of increasing operating loads. 17 Ref., 5 Tables, 4 Figures.

Keywords: *electric arc surfacing, railway wheel, flux-cored wire, structure, mechanical properties, brittle fracture, wear*

At present freight car wheels are made in Ukraine from high-strength steel of grade 2, with carbon content of 0.55–0.65 %. This steel ensures quite high values of mechanical properties of wheel metal — ultimate strength σ_t = 930–1130 MPa, wheel rim hardness *HB* ≥ 2500 MPa [1, 2]. Wheels made from such steel have quite high reliability in operation at a relatively low cost. The level of load on the axle of freight car wheel pair in operation in the railways of Ukraine and CIS countries is up to 23.5 t.

During operation the wheels wear on rolling profile. Because of the features of work of «wheel–rail» friction-rolling pair, the working surface of the wheel flange wears more intensively, and defects of the type of «nicks» often form on the wheel rolling surface. Flange wear occurs as a result of mechanical friction, and at development of «nicks» the thermomechanical nature of defect initiation is realized as a result of quenching structure formation in subsurface layer of wheel metal [3–5].

Surfacing technologies are traditionally applied at restoration of worn wheel flanges, which is cost-effective. Restoration of flange wear by surfacing allows reducing the rim metal wastes at mechanical turning along the wheel rolling profile, as well as lowering the flange wear due to deposition of metal with specified properties on its surface [6, 7]. Nowadays the wheels with «nicks» are not restored by surfacing, but they are treated by turning up to complete removal of the defects.

At present application of solid wires of Sv-08KhM, Sv-08KhMF and Sv-10KhN2GSMFTYu types, as well as flux-cored wire of PP-AN180MN/90 grade (10KhNMGSFT alloying system), is recommended for surfacing the railway wheel flanges. Surfacing with solid wires is performed as submerged-arc process, and surfacing with flux-cored wire is conducted both using flux and in shielding gas atmosphere. Metal, deposited with application of these welding consumables, matches the level of strength and hardness of railway wheels, made from wheel steel of grade 2, and also features higher wear resistance.

Modern tendencies in development of domestic main railway transport are aimed at increasing the axle load up to 27.5 t and freight train speed up to 150 km/h that requires application of higher strength wheels, the metal of which would have sufficiently high level of crack and wear resistance. In this connection, today in Ukraine, new wheel steels are developed on the base of wheel steel of grade 2, in which improvement of physicomechanical properties is achieved by their microalloying by carbide- and nitride-forming elements [8–10].

It is obvious that the recommended welding consumables cannot be used for restoration surfacing of the developed higher strength wheels. Therefore, the

*Based on presentation made at International Conference «Consumables for Welding, Surfacing, Coating Deposition and 3D-Technologies», June 04–05, 2019, Kyiv.

Table 1. Chemical composition of deposited metal of test flux-cored wires, wt.%

PP-AN180MN/90 wire	C	Si	Mn	Cr	Ni	Ti	V	S	P
I	0.07	0.42	0.8	0.8	0.5	0.018	0.08	0.01	0.025
II	0.14	0.62	1.3	1.1	0.7	0.028	0.10	0.02	0.025
III (PP-AN180MN/98)	0.12	0.48	1.15	0.96	0.7	0.022	0.10	0.02	0.03
IV	0.067	0.45	1.02	0.32	0.4	0.016	0.10	0.01	0.01

objective of this work was development of the new welding consumable, with application of which the deposited metal would correspond to the set of properties of higher strength wheel metal. This will allow an essential extension of the operating life of new wheels and ensuring traffic safety at increase of operating loads.

Experimental procedures. The new welding consumable was developed with application of physical testing methods for evaluation of strength, ductile and impact toughness properties of the deposited metal according to GOST 1497 and GOST 9454. Wear resistance was determined in keeping with the accepted methods of wear testing at «friction-sliding» of the contacting surfaces of metal products [11, 12]. Deposited metal resistance to brittle fracture was assessed at three-point bending using fracture mechanics criteria [13, 14]. Traditional optical microscopy methods were used to study structural changes in the metal.

The object of study was metal deposited with PP-AN-180MN/90 wire and with the new developed welding consumable. In some experiments, wires of Sv-08KhM and Sv-10KhN2GSMFTYu grades were used for comparison.

Development of welding consumable. Flux-cored wire of PP-AN180MH/90 (10KhNMGSFT) grade was taken as the base for development of the new consumable. $CaO–MgO–CaF_2–SiO_2$ system, which is traditionally used in a number of wires of PP-AN180MN type, was selected as the slag system for the new flux-cored wire. Test compositions of deposited metal obtained during development of the new wire are shown in Table 1.

Hardness is one of the main indices of mechanical characteristics of the deposited metal, which is responsible for its operating properties. In order to determine the hardness values of the deposited metal, comparative single-, two- and three-layer deposits in shielding gases at energy input of 8.5–10 kJ/cm^2 were made on 200×100×20 mm samples of wheel steel of grade 2 (0.58 % C) at the first stage of wire development. Preheating temperature was equal to 150 °C, as in surfacing the railway wheel flanges. Hardness was determined on the deposit surface with application of hardness meter of TK grade in *HRC* units with subsequent conversion to *HB* units. Hardness measurement results are given in Table 2.

As one can see, hardness of the 1st, 2nd and 3rd layers of the metal, deposited with test flux-cored wire II, is higher than that of rail steel (*HB* ≥ 3200 MPa). Optimized alloying and slag systems of test flux-cored wire III ensure stable values of hardness of the 2nd and 3rd layers of the deposited metal (on the level of 3000–3200 MPa). Molybdenum was removed from the alloying system of the flux-cored wire without lowering of the mechanical and technological characteristics. Test sample of flux-cored wire PP-AN180MN/90 (III) was taken as the base and was assigned the working grade PP-AN180MN/98.

Deposited metal structure at application of PP-AN180MN/90 and PP-AN180MN/98 wires is characterized as bainite-martensite. At deposition with PP-AN180MN/90 wire without preheating the ratio of bainite and martensite structural components is equal to 55/45, at 100 °C preheating it is 70/30. At deposition under similar conditions with PP-AN180MN/98 wire, the ratio of bainite and martensite is equal to 50/50 and 65/35, respectively. Microhardness of bainite structural component changes, depending on preheating temperature, in the range from 2820 up to 3090 MPa, that of martensite — from 3290 up to 3660 MPa. In the fusion zone and in coarse-grain area in the HAZ, the fraction of bainite rises up to 75 %. Characteristic structures of the joint metal at surfacing with PP-AN180MN/98 wire are shown in Figure 1.

At the second stage, the level of deposited metal hardness at surfacing a wheel pair from steel 2 with preheating to 250 °C was evaluated. Such a tempera-

Table 2. Deposited metal hardness, depending on composition and number of deposit layers (T_{pr} = 150 °C)

PP-AN180MN/90 wire	Number of deposited layers	*HB*, MPa
I	1	2500–2700
	2	2300–2500
	3	2000–2300
II	1	3200–3700
	2	3500–3600
	3	3400–3500
III (AN180MN /98)	1	3200–3500
	2	3000–3200
	3	2800–3100
IV	1	2400–2700
	2	2200–2400
	3	2000–2200

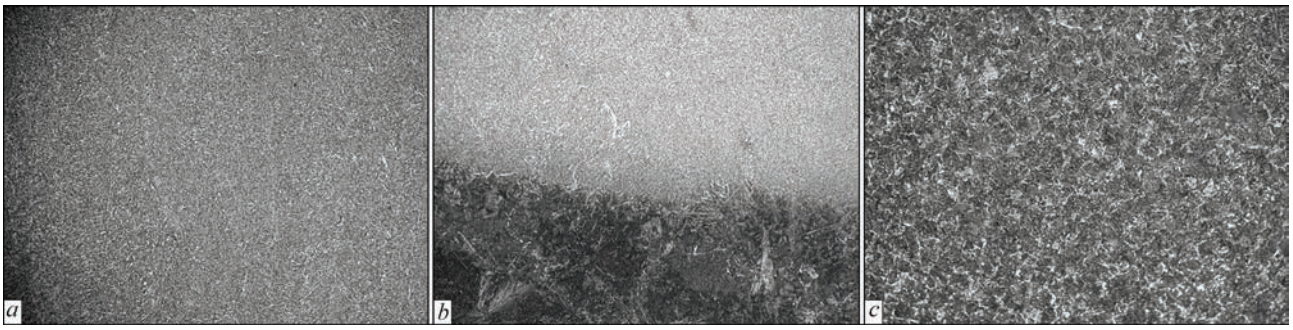

Figure 1. Microstructure (×200) of single-layer deposit made with PP-AN180MN/98 wire at energy input of 8.9 kJ/cm at T_{pr} = 100 °C: *a* — deposited metal; *b* — fusion zone; *c* — HAZ overheating zone

ture of metal is characteristic for the wheel rim after the 5th pass at continuous process of flange surfacing. Investigation results are given in Figure 2. For comparison the Figure also gives the data on hardness values of the metal deposited with other materials. The dash-dotted line marks the hardness level of higher strength wheels. As one can see, flux-cored wire PP-AN180MN/98 provides stable high results on deposited metal hardness even at such a temperature.

Flux-cored wire PP-AN180MN/98 belongs to wires with low-slag base (less than 6 % of slag-forming components), that allows elimination of the negative effect of charge component separation in wire manufacture on its welding-technological properties and ensuring stability of deposited metal properties. The ratio of components, making up the slag base, guarantees high parameters of welding-technological properties in terms of slag crust separation, deposited metal spreading, bead surface formation and smooth transitions between the beads and base metal. The slag base of the wire ensures high resistance to porosity at low consumption of shielding gas (8–10 l/min) and low level of diffusible hydrogen in the deposited metal (0.3–0.5 cm^3/100 g), that is indicative of high resistance of the deposited metal to cold cracking.

The alloying base of the welding wire includes such components as chromium, nickel, manganese and titanium, ensuring high enough hardness of the deposited metal (Table 3) at the required level of mechanical characteristics. Mechanical properties of the metal deposited with PP-AN180MN/98 wire are given in Table 4.

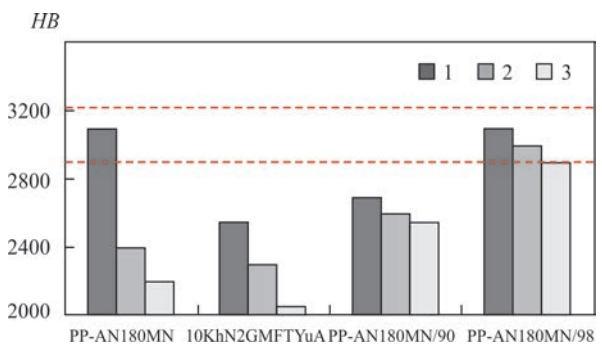

Figure 2. Deposited metal hardness at T_{pr} = 250 °C: *1* — 1st layer; *2* — 2nd layer; *3* — 3rd layer

Thus, the optimized alloying system of flux-cored wire PP-AN180MN/98 provides higher and more stable indices of deposited metal hardness (on the level of 3000–3200 MPa), than in deposition with other consumables. These values are optimum both at single-layer, and at multilayer surfacing of railway wheels. As shown by further studies, the metal deposited with flux-cored wire PP-AN180MN/98 also has higher brittle fracture resistance.

Brittle fracture resistance of deposited metal. It is known that deposited metal resistance to cracking under the impact of external loading, depends on its structural condition, which is determined by its chemical composition and cooling rate. Presence of diffusible hydrogen in the deposited metal also significantly affects crack initiation and propagation. Amount of diffusible hydrogen in the deposited metal is determined by welding method and modes, and the degree of its diffusion — by the metal chemical composition and temperature.

Deposited metal samples for testing were cut out of multilayer joints, which were made in the groove of a butt joint with 10 mm gap in the root. Deposits were

Table 3. Metal hardness at surfacing with PP-AN180MN/98 wire (T_{pr} = 50 °C)

Surfacing method	Surfacing energy input, kJ/cm	Number of deposited layers, pcs	*HB*, MPa
In CO_2	8.5–10	1	3200–3500
		2	3100–3150
		3	3000–3200
Under a layer of AN-60 flux	9–11	1	3200–3500
		2	3000–3200
		3	2800–3100

Table 4. Mechanical properties of metal at surfacing with PP-AN180MN/98 wire (T_{pr} = 150 °C, CO_2 surfacing method)

$\sigma_{0.2}$, MPa	σ_t, MPa	δ_5, %	ψ, %	*KCU*, J/cm²			*HB*, MPa
				+20	–40	–60	
800	890	10.7	54.3	96.0	76.8	66.5	3000–3200

Table 5. Brittle fracture resistance of deposited metal

Welding consumable	T_{pr}, °C	Deposited metal structure	K_{1c}, MPa√m	
			20 °C	–40 °C
Sv-08KhM	–	Bainite	97.9	88.5
	100	Bainite-pearlite	86.4	69.8
PP-AN180MN/90	–	Bainite-martensite 55/45	105.6	92.2
	100	Bainite-martensite 70/30	110.3	97.7
PP-AN180MN/98	–	Bainite-martensite 50/50	104.2	90.6
	100	Bainite-martensite 65/35	109.8	96.2

made by submerged-arc process using AN-60 flux. The following welding consumables were used: 3 mm solid wire Sv-08KhM and 2 mm flux-cored wires PP-AN180MN/90 and PP-AN180MN/98. Surfacing energy input was in the range of 9–11 kJ/cm. Surfacing was performed with and without metal preheating to temperature T_{pr} = 100 °C. Diffusible hydrogen content in the deposited metal, which was determined by pencil test, was equal to 3.5–3.8 ml/100 g in surfacing with Sv-08KhM wire and 2.2–2.4 ml/100 g at application of PP-AN180MN/90 and PP-AN180MN/98 wires.

A fatigue crack 3.0 mm deep was pre-grown in the samples. Then the samples were tested by three-point bending. The criterion for evaluation of deposited metal brittle fracture resistance was the critical stress intensity factor K_{1c}, at fracture of samples, which was calculated according to standard procedures of fracture mechanics [15]. Results of deposited metal testing for brittle fracture are generalized in Table 5.

It is found that without preheating brittle fracture resistance of the deposited metal at application of flux-cored wires PP-AN180MN/90 and PP-AN180MN/98 is approximately 10 % higher, than at surfacing with Sv-08KhM wire. This difference becomes greater at preheating up to the temperature of 100 °C. Increase of the critical stress intensity factor is already equal to 22 % at testing temperature of 20 °C and to 40 % at –40 °C. Here, deposited metal fracture, irrespective of the surfacing method and preheating temperature, occurs in the brittle mode at development of the main crack.

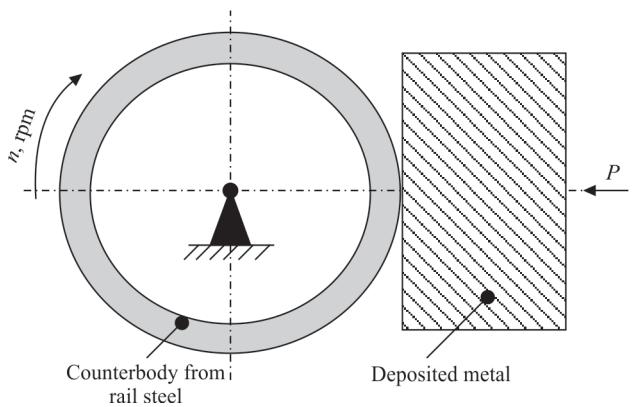

Figure 3. Schematic diagram at testing deposited metal samples at «friction–sliding»

It should be also noted that brittle fracture resistance of the metal deposited with Sv-08KhM wire, decreases by 12 % with preheating at testing temperature of 20 °C and by 21 % at –40 °C. At surfacing with flux-cored wires, contrarily, brittle fracture resistance of weld metal rises by approximately 4 % at application of preheating up to the temperature of 100 °C.

Established changes in brittle fracture resistance of the deposited metal, depending on alloying system of the welding consumable and preheating temperature, are attributable to joint action of two factors. First, diffusible hydrogen content in the metal deposited with flux-cored wires is almost 1.5 times lower than at surfacing with Sv-08KhM wire (2.3 compared to 3.65 ml/100 g). Secondly, this is a structural factor. Quenched metal, which has a mixed bainite-martensite structure, has higher resistance to brittle fracture than metal with just the bainite structure, or with the structure having a fraction of pearlite component [14, 16].

Deposited metal wear resistance. Wear resistance is one of the main indices of operational strength of railway wheels restored by surfacing. Wear resistance of deposited metal was assessed at «friction-sliding» of model samples. Testing was performed in keeping with the accepted research methods [12, 17]. According to this method, the deposited metal sample of 25×15×3 mm dimensions was pressed to the counterbody from rail steel of M-76 grade, which rotated at a constant speed (Figure 3). The sample pressing force

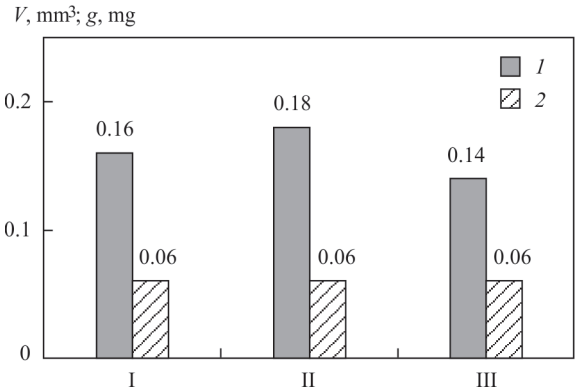

Figure 4. Wear of metal deposited with PP-AN180MN/90 (I, II) and PP-AN180MN/98 (III) wires at T_{pr} = 150 °C: I, III — submerged-arc surfacing; II — in CO_2 atmosphere (*1* — *V*, wheel steel); *2* — *q*, rail steel)

was equal to 81.3 N, counterbody rotation speed was 30 rpm, and testing time was equal to 30 min.

Contact of deposited metal sample and counterbody from rail steel resulted in wear of metals — a pit of constant depth formed on the sample, and a ring-shaped groove appeared on the counterbody surface. The extent of counterbody wear by weight (g, mg) was determined by weighing before and after loading in analytical scales (accuracy of 0.0005 g), and sample wear was determined by pit volume (V, mm^3). Generalized testing results of deposited metal of different alloying systems are given in Figure 4.

As is seen from the given data, at gas-shielded surfacing with PP-AN180MN/90 wire, unlike submerged-arc surfacing, deposited metal wear resistance decreases by approximately 11 % (pos. 1 and 2). This is related to the features of running of metallurgical processes at different surfacing methods. At CO_2 surfacing, partial burnout of titanium from the metal runs more intensively. At submerged-arc surfacing with PP-AN180MN/98 wire (pos. 3) deposited metal wear resistance rises by approximately 12.5 %.

Conclusions

1. New flux-cored wire PP-AN180MN/98 (12GSKhNFT) was developed on the base of flux-cored wire PP-AN180MN/90, due to optimization of alloying system (10GSKhNFT) and low-slag base (CaF_2–$CaCO_3$–MgO–SiO_2), which is not prone to separation.

2. At application of PP-AN180MN/98 wire for surfacing higher strength wheels, irrespective of preheating temperature and number of deposited layers, deposited metal hardness is optimum and equal to *HB* 3000–3200 MPa (rail hardness *HB* ≥ 3200 MPa). Here, comparatively homogeneous bainite-martensite structure forms in all the joint areas (in the deposited metal, fusion zone and in the overheating area of the HAZ metal).

3. Metal deposited with PP-AN180MN/98 wire has a high wear resistance at «friction-sliding» at contact with the rail. Wear resistance of metal, deposited with PP-AN180MN/98 wire, is 12.5 % higher than in surfacing with PP-AN180MN/90 wire. Here, rail wear is not increased.

4. Deposited metal has a high level of brittle fracture resistance that allows recommending PP-AN180MN/98 wire for application for surfacing higher strength wheels. Restored wheels will have a high reliability, and traffic safety will be ensured under the conditions of increasing operating loads.

1. Uzlov, I.G. (2003) Advanced processes of production and quality of railway wheels. *Stal*, **5**, 69–72 [in Russian].
2. *Railway wheels and tires KLW. Interpipe NTZ Ukraine*, www.interpipe.biz [in Russian].
3. Vakulenko, I.O., Anofriev, V.G., Gryshchenko, M.A., Perkov, O.M. (2009) *Defects of railway wheels*. Dnipropetrovsk, Makovetsky [in Ukrainian].
4. Babachenko, A.I., Kononenko, A.A., Dementieva, Zh.A. et al. (2010) Examination of causes of defect formation on roll surface of high-strength wheels in operation. *Zaliznychny Transport Ukrainy*, **5**, 35–38 [in Russian].
5. Ostash, O.P.,Andrejko, I.M., Kulyk, V.V., Prokopets, V.I. (2011) Contact-fatigue damage of roll surface of railway wheels of KP-2 and KP-T type. *Visnyk DNUZT*, **39**, 118–122 [in Ukrainian].
6. (1998) *Resource-saving technologies of repair of railway engineering using welding, surfacing and spraying. Trudy VNIIZhT*. Ed. by V.N. Lozinsky. Moscow, Intellect [in Russian].
7. Gajvoronsky, A.A., Poznyakov, V.D., Markashova, L.I. et al. (2012) Influence of deposited metal composition on structure and mechanical properties of reconditioned railway wheels. *The Paton Welding J*., **8**, 16–22.
8. Uzlov, I.G., Babachenko, A.I., Dementieva, Zh.A. (2005) Influence of microalloying of steel on fracture toughness of railway wheels. *Metallurgiya i Gornorudnaya Promyshlennost*, **5**, 46–47 [in Russian].
9. Babachenko, A.I., Litvinenko, P.L., Knysh, A.V. et al. (2011) Improvement of chemical composition of steel for railway wheels providing increase of their resistance to defect formation on roll surface. In: *Fundamentals and Applied Problems of Ferrous Metallurgy: Transact. of IFM*, **23**, 226–233 [in Russian].
10. Ivanov, B.S., Filipov, G.A., Demin, K.Yu. et al. (2007) Modification of wheel steel by nitrogen. *Stal*, **9**, 22–25 [in Russian].
11. Rybakova, L.M., Kuksenova, L.I. (1982) *Structure and wear resistance of metal*. Moscow, Mashinostroenie [in Russian].
12. Artemov, I.I., Savitsky, V.L., Sorokin, S.A. (2004) *Modeling of wear and prediction of tribosystem life*. Penza, PSU [in Russian].
13. (1972) *New methods of evaluation of metal resistance to brittle fracture*. Ed. by Yu.N. Robotnov. Moscow, Mir [in Russian].
14. Panasyuk, V.V. (1991) *Mechanics of quasibrittle fracture of materials*. Kiev, Naukova Dumka [in Russian].
15. *GOST 25.506*: Methods of mechanical tests of metals. Determination of characteristics of crack resistance (fracture toughness) at static loading.
16. Efimenko, M.G., Radzivilova, N.O. (2003) *Physical metallurgy and heat treatment of welded joints*. Kharkiv, NTU KhPI [in Ukrainian].
17. Ryabtsev, I.I., Chernyak, Ya.P., Osin, V.V. (2004) Block-module installation for tests of deposited metal. *Svarshchik*, **1**, 18–20 [in Russian].

Received 31.05.2019

DOI: http://dx.doi.org/10.15407/tpwj2019.07.09

RISK FACTORS AND CRITERIA OF FIRE AND EXPLOSION HAZARD AT FERROALLOYS GRINDING*

A.E. MARCHENKO
E.O. Paton Electric Welding Institute of the NAS of Ukraine
11 Kazimir Malevich Str., 03150, Kyiv, Ukraine. E-mail: office@paton.kiev.ua

Considered are the main indices, characterizing the fire and explosion hazard of products of grinding of ferroallys, applied in electrode technology. The effect of grinder type on behaviour of ferroalloy powders is noted, and comparative evaluation of industrial installations used in electrode production, is given. A conclusion is made about the need for regular certification of each specific technology of ferroalloys grinding. 11 Ref., 4 Tables, 3 Figures.

Keywords: *welding production, fire and explosion hazard, electrode technology, ferroalloys grinding, manufacturing quality, technology certification*

General information about explosion hazard of metallic powders. Grinding, screening and transportation of grinding products is accompanied by the formation of explosive aerosol suspensions and combustible deposits. Their inflammation and explosions inside the grinding and mixing equipment, in the pneumatic conveyor and aspiration systems, fans and bag filters repeatedly resulted in destructions, injuries and death of personnel. The inflammations and explosions were caused by thermal sources, as well as by local fires, provoked by warming up from a mechanical effect or by sparking of triboelectric nature.

In the process of explosion development, as a rule, dust participates, swirled from the surface of the equipment and building structures, as well as inside the ventilation systems.

Pieces of material in the initial stage of grinding are destroyed under the combined action of crushing and impact, and at the stage of fine grinding, under the impact combined with abrasion. The total energy of grinding E_{gr} is spent for elastic and plastic deformation of grains $a_{def}\Delta V$, for heating Q, as well as for destruction of particles with the formation of a new surface $s\Delta S$:

$$E_{gr} = a_{def}\Delta V + s\Delta S + Q,$$

where a_{def} is the energy of elastic and plastic deformation per a unit of volume of a solid body; s is the specific surface energy; ΔV is the deformed part of the volume of the material being grinded; ΔS is the increment of the material surface as a result of the grinding process.

The surface increment during a coarse grinding is negligible and the energy consumption for destruction is considered to be proportional to the volume of the body being destroyed. During fine grinding, the consumption of energy for the growth of a newly formed surface prevails. The ratio of the components of power consumption for grinding depends on the type of milling equipment, as well as on the mill set.

The potential fire and explosion hazard of the process of ferroalloy grinding depends on its physical

Table 1. Values of temperature of beginning of the exothermic reaction $T_{s.e}$ of powders of ferroalloys fraction of 0–40 μm [1]

Ferroalloy	Grinding method	$T_{s.e}$, °C
Ferromanganese	Grinding	200
	Vibration milling	140
Ferrotitanium	Grinding	220
	Vibration milling	180
Ferrosilicium	Grinding	450
	Vibration milling	450

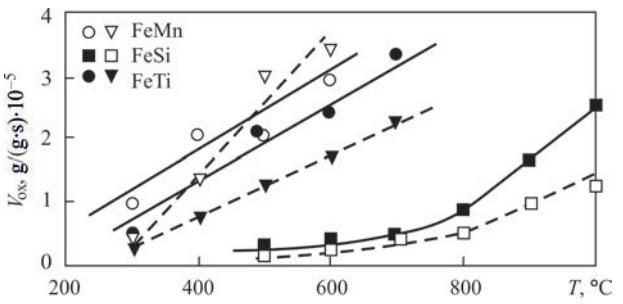

Figure 1. Effect of temperature on oxidation rate in the air environment of particles of ferroalloys with a size of 0–40 μm, sieved from powders produced by vibrating milling (solid curve) and grinding (dashed) [1]

*Retrospective review on the materials published in small editions and sources of non-welding profile.

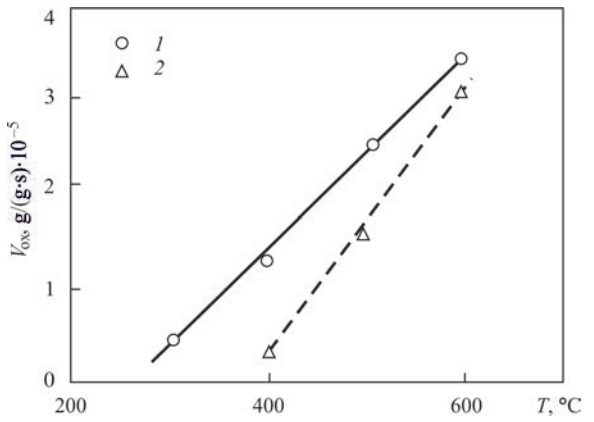

Figure 2. Effect of temperature on oxidation rate of ferromanganese particles of the size of 0–50 μm (*1*) and 0–100 μm (*2*) sieved from powders produced by grinding in the PALLA mill [1]

and chemical properties, as well as on the type and modes of operation of the grinding equipment.

Ferroalloys differ in their grinding capability, therefore, the powders of various ferroalloys produced using the same grinder differ in dispersity, as well as fire and explosion hazard. The same can be said about the powders of the same ferroalloy, produced using different grinders.

The fire and explosion hazard of the technology of ferroalloys grinding is evaluated according to the procedure, which provides a laboratory and production stage [1].

At the laboratory stage, the chemical composition, dispersion, kinetic indicators of powder oxidation, state of particles surface, as well as the characteristics of flammability and explosiveness, first of all of the most active dust fractions evolved from them, are determined.

At the production stage, the powders of ferroalloys for electrode coatings, produced under industrial conditions in different grinding installations, are tested. The flammability and explosiveness of powders, their dust fractions (smaller than 50 μm), the samples of which are taken from the aspirated gas (air) of the aspiration systems and from the dust deposits on building structures and technological equipment, are also investigated.

To characterize the fire and explosion hazard of grinding products, the following indicators are used [2–5].

Kinetic parameters of powder oxidation in the pre-inflammation period of heating: the temperature of the start of exothermic process $T_{s.e}$ and the oxidation rate V_{ox}.

Self-inflammation temperature is the lowest ambient temperature at which self-inflammation of sample is observed in the layer and in suspended state ($T_{s.ig}$, $T_{s.inf}$, °C). This indicator is found by introducing a certain mass of a substance into a vessel, heated to a stepwise rising temperature, and determining its minimum value at which self-inflammation occurs.

Lower flammability concentration limit (LFCL, g/m^3) and flame spreading (LCLS g/m^3) is the minimum content of a combustible substance in a homogeneous mixture with an oxidizing environment, at which the inflammation and spreading of the resulting flame through the mixture at any distance from the inflammation source is possible.

Maximum safe oxygen concentration in a gas environment, at which the inflammation of a substance and the flame spreading occur (MSOC, %).

Inflammation temperature of aerosol is the minimum temperature of an external source (usually a heated surface) at which the aerosol is inflamed (T_{inf}, °C).

During testing, aerosol of a certain concentration is brought into contact with a heated surface. For each concentration, the minimum inflammation temperature is determined, and then as the inflammation

Table 2. Indicators of pyrophornity and explosibility of powders of ferroalloys, used in the technology of electrode production [7]

Material	Powder in layer			Aerosol				
	Fraction share –005 %	$T_{s.ig}$, °C	T_{ig}, °C	T_{inf}, °C	LFCL, g/m^3	P_{max}, MPa	V_{max}, MPa/s	MSOC, vol.%
Ferromanganese FMn-92	12.5[1]	–	–	–	260	0.15	3.0	12.3
	100.0[2]	–	550	–	76	0.32	5.0	7.8
	100.0[3]	–	–	–	74	0.38	20.0	–
Ferrosilicon Fs = 45	17.0[1]	It is not inflamed by thermal (up to 1100 °C) and pyrotechnical source of ignition (burning temperature is 2500 °C)						
	100.0[2]							
Ferrotitanium Ft =30	14.5[1]	–	–	–	430	0.10	0.9	15.8
	95.0[2]	400	530	370	90	0.37	8.0	10.0
	100.0[3]	–	–	–	82	0.36	12.0	12.0
Manganese metal, d_{av} = 44 μm		240	450	–	130	0.33	3.0	–
Silicom metal, d_{av} = 74 μm		790	700	55	100	5.80	8.4	11.0

temperature, the lowest of these values is accepted at different concentrations.

The maximum explosion pressure is P_{max}, MPa, which represents the highest excessive pressure, occurring during the so-called deflagration, i.e. homogeneous, combustion of the dust-air mixture in a closed vessel at an initial atmospheric pressure of the mixture of 101.3 kPa. To determine P_{max}, the dust-air mixture of the preset composition is ignited in the volume of a reaction vessel and an excessive pressure is recorded, which is developing when the combustible mixture ignites. Changing the concentration of fuel in the mixture, the maximum value is chosen from the obtained results.

Rate of explosion pressure increment V_{max}, *MPa·s*$^{-1}$ is the derivative of the explosion pressure over time in the ascending region of the dependence of the explosion pressure of the combustible mixture on time. The principle of method of its evaluation is the experimental determination of maximum explosion pressure of a combustible mixture in a closed vessel, construction of a diagram of change in the explosion pressure over time and calculation of average and maximum speed using known formulas [3].

When categorizing the production grinding installations, the requirements of PUE7 are also taken into account [6].

Comparison of the kinetic parameters of the ferroalloys oxidation. Ferromanganese FMn 92, ferrotitanium FTi 30 and ferrosilicon FSi 45, which are used as deoxidizers of deposited metal, belong to alloys with a low activation energy. The tendency of their powders to oxidation in the pre-inflammation heating period (from 300 to 600, 700, and 1000 °C, respectively) is estimated from the values of $T_{s.e}$ and V_{ox}, obtained by the DTA method. The fractions with a particle size of 0–40 μm were investigated, which evolved by screening of powders produced by crushing and vibration grinding in laboratory installations. The heating rate of a sample in the DTA definitions amounted to 10 °C·min^{-1}. The oxidation rate was determined by graphical differentiation of DTA- and DTG-diagrams at a preset temperature of material heating.

The results of $T_{s.e}$ determination are presented in Table 1, and the dependence of their oxidation rate on temperature is shown in Figure 1.

From the abovementioned data it follows that the studied ferroalloys differ in their resistance to oxidation during the period of pre-inflammation heating. The process of ferromanganese oxidation, the most active among the tested ferroalloys, begins at the lowest temperature. Ferrosilicon is the most resistant to oxidation. Ferrotitanium takes intermediate position.

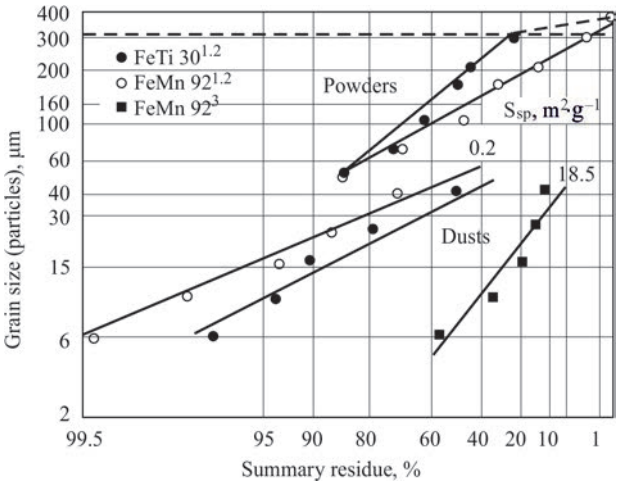

Figure 3. Grain compositions of powders of ferromanganese, ferrotitanium (*1*), dust deposits of ferromanganese in the air ducts of grinding installation (*2*) and dust fractions sieved from powders (*3*) of ferromanganese and ferrotitanium [7]

It is characteristic, that ferromanganese and ferrotitanium powders, produced by vibrating grinding, are more active than powders crushed by grinding. At the same time, the methods of ferrosilicon grinding do not affect the values of the temperatures of the exothermic reaction beginning.

With increase in temperature, the rate of oxidation is growing. Moreover, for ferromanganese powders it is so intensive, that when the inflammation temperature is reached, the crushed particles become more active than those produced by vibration grinding. The oxidation rate of ferrotitanium particles is growing with a rise in temperature to a lesser extent, and that of ferrosilicon particles is growing even more slowly. Moreover, their dust particles retain activity which is lower than that of their vibration grinded analogues throughout the whole pre-inflammation period.

Alongside with the powders prepared in laboratory conditions, at the MISiS [1], the samples were

Table 3. Effect of grinder type on indicators of fire and explosion hazard of powders [1, 8]

Ferroalloy	Fraction, μm	LFCL, g/m^3	$T_{s.ig}$, °C	T_{int}, °C
Laboratory ball mill*				
Ferromanganese	0–50	69	370	350
	50–100	106	540	420
Ferrosilicon	0–50	n.v	n.v	n.v
Ferrotitanium	0–50	n.v	590	470
	50–100	n.v	635	450
Laboratory disintegrator D95*				
Ferromanganese	0–50	190	600	450
	50–100	n.v	790	550
	Polydispersed	280	630	470
Ferrotitanium	0–50	n.v	n.v	n.v
	50–100	n.v	n.v	n.v

*Inert mixture of argon with air.

Table 4. Specified characteristics of fire hazard of powders of ferroalloys, produced in grinding installations in electrode production

Ferroalloy (and additive, 5 %)	Medium	Holding, days*	Fraction, μm	LFCL, g·mm^{-3}	$T_{s.ig}$, °C	T_{inf}, °C
Slotted ball mill						
Ferromanganese (marble 15)	Air	3	0–50	740	430	620
			Polydispersed	n.v*	460	760
Ferrotitanium (marble 7)			0–50	n.v	740	520
			Polydispersed	n.v	930	590
Ferromanganese (magnesite 10)	Nitrogen (92 %)	10	0–50	n.v	430	760
			Polydispersed	n.v	450	780
Ferrotitanium (marble 10)		–	0–50	740	420	600
			Polydispersed	n.v	850	640
Vibration rod mill						
Ferromanganese FMn 92	Nitrogen (92 %)	7	0–50	690	420	510
			Polydispersed	760	460	570
Ferrosilicon Fs 45			0–50	n.v	620	n.v
			Polydispersed	n.v	790	n.v
Ferrotitanium FTi30			0–50	n.v	710	520
			Polydispersed	n.v	870	610

*In accordance with plant technology to brake the chemical interaction with liquid glass in coating.
**n.v — value of LFCL exceeds 1000 g/m^3, and T_{inf} exceeds 1000 °C.

investigated, taken during grinding of ferroalloys in industrial vibratory mills PALLA. The fractions with a particles size of 0–50 and 0–100 μm were investigated. The results of investigations of ferromanganese powders are shown in Figure 2. They correlate with the abovementioned data, which characterize the kinetics of oxidation of dust particles of this ferroalloy, which were produced in grinders of a laboratory type. Indeed, a coarse disperse sample, as well as its laboratory analogue, is less active; therefore, it begins to oxidize noticeably at a higher temperature than the fine disperse one. With rise in temperature, the rate of its oxidation increases steeper.

Comparing Figures 1 and 2, it is seen that the increase in the oxidation rate of particles of 0–40 μm in size, caused by heating, which are taken from ferromanganese powders grinded in the laboratory, is the same as of the particles of 0–50 μm in size, taken from the powder produced in the industrial mill PALLA. Fractions with a particle size of 0–100 and 0–50 μm from the powders produced in the mill PALLA, as to oxidative ability, are qualitatively related to each other in the same way as the particles similar in size, which are taken from the powders produced by grinding and, accordingly, vibrating milling in laboratory installations.

By the nature of change in the relative position and inclination angle of the compared curves relative to the temperature scale, it may seem that the size of the particles affects their oxidation capacity more than the activation of their surface by vibration grinding, which should have occurred. Since the compared ferroalloys differ in density, the oxidation rate of the powders should be normalized, in our opinion, by the specific volume surface of particles, but not by the mass of the sample.

Regulatory characteristics of fire and explosion hazard of ferroalloys, established in laboratory conditions. The values of the pyrophoric and explosive indicators of the powders of ferromanganese, ferrosilicon and ferrotitanium are given according to the data of IPMS of the NAS of Ukraine in Table 2. For comparison, it also includes indicators of powders of metallic manganese and silicon.

The grain characteristics of the used powders of ferromanganese and ferrotitanium are compared in Figure 3.

Indexation of samples accepted in Table and in Figure 2 is the following: 1 — polydispersed powders of studied ferroalloys; 2 — fractions with particles sizes of less than 50 μm, screened from polydispersed powders; 3 — dust deposits in the air duct; d_{av} is the average weighted diameter of particles.

The mentioned data show that ferrosilicon powders are characterized by the highest resistance against inflammation and explosions. They are not ignited either by heat or pyrotechnic source of inflammation, neither in a layer, nor in a state of aerosol.

Ferromanganese and ferrotitanium powders in the layer are characterized by approximately the same values of T_{ig}. However, in the state of air suspension they differ significantly. Thus, with an increase in the share of tiny particles from 15 to 100 %, for ferrotitanium powder the values of LFCL (initially about 2 times higher than that of ferromanganese), almost 5 times decrease, and that of ferromanganese, only 3 times. At the same time, the MSOC value of the compared objects decreases only 1.5 times.

The explosion pressure of the aerosol of ferrotitanium and ferromanganese powders and especially the rate of increment of pressure during an explosion is changed at the same increase in the degree of dispersion to a much higher level. Thus, the value P_{max} of the compared ferroalloys in the state of aerosol increases by 2.5–3.0 times. Similarly, the value of the aerosol V_{max} of ferromanganese increases (from 3 to 5 MPa/s). At the same time, V_{max} of aerosol of ferrotitanium increases by 10 times (from 0.9 to 8 MPa/s).

From the point of view of increase in the V_{max} indicator, the role of dust particles in the composition of the depositions, the samples of which were taken for testing in the air duct, is especially dangerous As follows from the Table 2, the values of V_{max} of deposits of aerosol are 4 times, and those of ferrotitanium are 1.5 times higher than those of aerosols of under-sieve fractions of polydisperse powders of these ferroalloys.

Effect of type of grinder on fire explosion hazard of ferroalloy powders. In the works [1, 8], fire and explosion hazard of powders produced by dispersing the ferromanganese, ferrosilicon and ferrotitanium in a ball mill and a disintegrator of laboratory type D95 with shielding gas environment was considered. From the manufactured powders, two fractions (0–50 and 0–100 μm) were selected and tested. For comparison, a ferromanganese powder of polydispersed composition, made in the disintegrator D95, was used. The results of investigations are summarized in Table 3.

The given data show that the powders of compared fractions produced by grinding in a disintegrator are less active than in a ball mill. This is explained by their greater oxidation due to a higher energy of the grinding process in the disintegrator. With the increase in the share of large particles, the fire and explosion hazard of the powders of all the tested ferroalloys decreases.

From the results of studies of the dust fraction evolved from ferromanganese powders, MISiS [5] ranked the used laboratory grinding units according to LCLS as follows: KID (280), disintegrator D35 (190), ball mills ShB of drum type (70) and of vibration type VM (50 g·m^{-3}).

Comparative evaluation of industrial grinding installations used in electrode production. The general situation with preparation of ferroalloy powders, as well as actual values of their fire and explosion hazard indicators achieved in the technology of welding electrodes production can be characterized by the data given in the works [5, 8, 9]:

- extensive range of grinders types (chamber, bypass, slot-hole and vibratory ball and rod mills, as well as roller, hammer and cone crushers);
- variety of grinding schemes (with an inert additive, in a controlled gas or water environment);
- variety of ways of taking the target product (screening, continuous sieving together with screening, separation or centrifugation);
- different methods of interoperational transport of the finished powder in the technological cycle (Kibble, pneumatic transport, etc.).

The simplest and often a quite reliable technique for preventing explosion hazard situations during fine grinding of ferroalloys in batch mills is the loading of the so-called inert additive into the grinding chamber together with pieces of ferroalloy. This product can be any of the ore mineral components of the coating, added in the amount of at least 8 % of the mass of the ferroalloy being grinded. Even with this variant of grinding, to prevent the explosion, the mill can be depressurized only after a preliminary exposure for at least 15 min from the moment of stopping to guarantee the dust deposition.

Nowadays, mainly mills of continuous action are used, providing a high efficiency of the process and operating per pass with continuous sieving of the crushed product or its subsequent screening. In these mills, grinding is realized mainly in shielding gas media and the scheme and modes of supplying shielding gas (nitrogen or carbon dioxide with a regulated oxygen concentration) are selected taking into account:

- chemical activity of grinded ferroalloy;
- their dispersion in a grinded state;
- design of grinding installation, including the possibility of sealing the mill housing, as well as the path of the further movement of the finished powder outside its borders;
- design features of aspiration suctions, as well as opportunities of optimizing their aerodynamic interactions with the protective environment in order to maintain the partial pressure of oxygen in the protective atmosphere of the grinder at a preset level, necessary for the formation of a phlegmatizing oxide film on the newly formed surface.

In this regard, the characteristics of fire and explosion hazard of industrial powders of ferroalloys produced by different electrode making enterprises vary within fairly wide limits (Table 4). Evaluating them, it can be concluded that the powders produced in laboratory installations have a higher fire and explosion hazard than those produced in industrial installations.

Despite a fairly high degree of oxidation of the surface of particles, they, nevertheless, retain the ability to burn and explode. Especially ferromanganese powders, the LCLS values of which do not reach 1000 g·m^{-3}, and $T_{s.ig.}$ and $T_{inf.}$ of polydispersed powders are 460 and 570 °C, even if they are produced

in a protective medium of the necessary condition. Particularly dangerous are the fractions of industrial powders smaller than 50 μm. From Table 4 it follows that the LCLS values of this fraction are 690 g·m^{-3}, and $T_{s.ig}$ and T_{inf} are 420 and 510 °C, respectively. The efficiency of inert additive is low because it is more easily grinded and leaves the slotted mill chamber faster than the particles of ferroalloy powder.

Somewhat more passive are ferrotitanium powders of the same fraction, the value of LCLS of which exceeds 1000 °C, and $T_{s.ig}$ and T_{inf} is 710 and 520 °C, respectively.

Explosions of ferroalloy aerosol particles, occurring in grinding equipment with the participation of combustible gases, represent a particular danger [9].

Hydrogen evolved from the grinded ferroalloy together with hydrogen, acetylene, methane, arsenites and phosphines, formed as a result of interaction of alloys with moisture, which for any reason got to the grinding chamber, significantly decrease LCLS and MSOC, and also increase P_{max} and V_{max} of aerosols. It was established, that to reach an explosive hazard of the hydrogen concentration, which is accumulated in the grinding chamber as a result of desorption from ferroalloy particles and their interaction with moisture, it may take no more than 1 min [9]. In such conditions, the required efficiency of quick response of emergency gas analysis systems and timely blocking of equipment operation is not achieved.

Additional danger is represented by microparticles (satellites), which, accumulating on the surface of coarser ferroalloy grains, increase their specific surface. As a result, the value of LCLS of polydispersed powders may decrease by 1.5–2.0 times. In order to prevent the adverse effect of this factor, phlegmatizing additives of bonding and enveloping liquids are injected into the grinding equipment. They agglomerate microparticles into larger aggregates covered with a protective film of a chemically inert liquid [8, 10, 11]. On the example of ferromanganese powder, vibro-crushed for 3 h, it is shown that the fraction of free particles with a size smaller than 40 μm can be 5 times reduced in it, and its LCLS density — by 3 times [10].

The abovementioned results show that the fire and explosion hazard of each ferroalloy powder used in electrode technology should be determined for each type of grinding equipment, its operation mode, sampling place, as well as technological methods used to prevent inflammations and explosions. In other words, regular certification of each specific technology of grinding ferroalloys is necessary, just as it is done in the technology of welding production in order to regularly confirm the quality of manufactured products.

The author appreciates O.D. Nejkov for his useful opinions.

1. Toleshov, A.K. (2009) Method of evaluation of fire and explosion hazard of production processes of metal and alloy powders. *Metallurg*, **6**, 30–33 [in Russian].
2. Nedin, V.V., Nejkov, O.D., Alekseev, A.G. et al. (1971) *Fire hazard of industrial powders*. Kiev, Naukova Dumka [in Russian].
3. *(1990) GOST 12.1.044–89 SSBT*: Fire and explosion hazard of substances and materials. Range of blast data and methods of their determination. Moscow, Standarty[in Russian].
4. Toleshov, A.K. (1995) Standard characteristics of fire and explosion hazard of ferroalloys powder made in electrode production. *Metallurg*, **4**, 19–21 [in Russian].
5. Babajtsev, I.V., Toleshov, A.K., Derzhavets, A.A. (1995) Evaluation of inflammability of powders of metals and alloys. *Ibid*., **9**, 26–27 [in Russian].
6. *Rules of arrangement of electric units PUE7* [in Russian].
7. Nejkov, O.D., Vasilieva, G.D., Kuzub, A.P. et al. et al. (1971) *Examination of explosibility of ferrosilicon, ferromanganese, ferrotitanium, ferrochrome, silicocalcium and manganese powders. Prevention of sudden explosions of gas-dispersed systems*. Kiev, Naukova Dumka, 36–44 [in Russian].
8. Gridin, A.A., Serebryakova, V.V., Babajtsev, I.V. et al. (1985) Study of disintegrator processes of dispersion and activation of explosion and fire hazardous ferroalloys. *Stal*, **11**, 36–37 [in Russian].
9. Strizhko, L.S., Babajtsev, I.V., Toleshov, A.K. (1998) Prevention of explosions in refining of ferroalloys. *Metallurg*, **9**, 27–28 [in Russian].
10. Babajtsev, I.V., Gerusova, V.P., Delyan, V.I. (1983) Passivation of powders of silicocalcium. *Izv. Vuzov. Chyorn. Metallurgiya*, **5**, 151–152 [in Russian].
11. Babajtsev, I.V., Toleshov, A.K., Shchepelev, A.V. (1996) Decrease of explosion hazard of ferroalloys powders during vibrogrinding. *Ibid.*, **1**, 73–74 [in Russian].

Received 24.04.2019

INTERNATIONAL CONFERENCE «CONSUMABLES FOR WELDING, SURFACING, COATING DEPOSITION AND 3D TECHNOLOGIES»

International Scientific and Technical Conference «Consumables for welding, surfacing, coating deposition and 3D technologies» was held in Kyiv at E.O. Paton Electric Welding Institute on June 4–5, 2019. It was organized by E.O. Paton Electric Welding Institute, International Associations «Welding» and «Electrode» and Society of Welders of Ukraine. Proceedings of the Conference were published to the beginning of Conference work in form of special issue of Paton Welding Journal, No.6, 2019.

Scientists, lecturers and engineer-technical specialists of SRI, higher education institutions, industrial and commercial enterprises, representatives of associations from a series of cities of Ukraine as well as foreign participants from Poland, Germany, France participated in the Conference, in total more than 60 people.

A list of organizations and companies, specialists of which participated in the Conference, included: E.O. Paton Electric Welding Institute, Paton PWE, TM.Weltek LLC, Sumy-Electrode LLC, Vitapolis LLC, NTUU «Igor Sikorsky Kyiv Polytechnic Institute», Dnipro University of Technology, Z. I. Nekrasov Iron and Steel Institute of the NAS of Ukraine, SE Ivchenko-Progress, PLAN-T LLC, Additive Laser Technologies of Ukraine LLC, Tekhnologii Vysokikh Energij LLC, Zirast-Dnepr LLC, Dniprovsk State Technical University, VANT LLC, Institute of Welding in Gliwice (Poland), Dr. Rosert RCT Company (Germany), Welding Alloys Group (France) and others.

Deputy Director of PWI Prof. I.V. Krivtsun made a welcoming speech at the Conference opening. He conveyed greetings to the Conference participants on behalf of Prof. B.E. Paton, in short words described the main tendencies on the world's market of welding consumables and wished successful and fruitful work to the Conference. In particular, the importance of meetings and

Discussion during presentation of A.A. Mazur

During the visit to Paton PWE

discussions between the specialists in the field of welding consumables, which assist to rise the efficiency of welding engineering, was underlined.

16 presentations on a series of relevant for welding engineering topics were made at the Conference during plenary session. Without giving detailed attention to each of them (as it was mentioned, the presentations were included in the issue of Paton Welding Journal, No.6, 2019), we would like to note only those, which sparked the largest interest and provoked lively discussions. Thus, presentation of A.A. Mazur (PWI) «State and perspectives of world's market of welding consumables» it was noted that welding in foreseeable perspective is the basic technology in many branches of industry and construction. Industrialized countries are characterized with sufficiently stable dynamics of development of welding engineering and welding market, which is determined by stable growth of consumption of structural materials and expansion of their mix as well as appearance on welding market of new advanced materials, technologies and equipment for welding and related processes.

R. Rosert (Germany) in presentation «Welding and submerged-arc surfacing of high-alloy steels with flux-cored wires» in details outlined on several examples of realized projects on manufacture of unique welding equipment. Outlined technologies of welding and surfacing today are effectively used for welding of all classes of high-alloy steels and alloys, for surfacing of cobalt-based alloys.

Y. Nagaj (Poland) in presentation «Issues of certification of welding consumables in Poland and EU countries» outlined on the algorithm of action of any company having a goal to enter the European market. He in details highlighted the steps of Poland on a way of economic development, which allowed it to become EU equal partner.

Large interest was provoked by presentation of A.A. Kononenko (Dnipro University of Technology) «Investigation of conditions of deep penetration in manufacture of samples of high-temperature alloy Inconel 718 by method of selective laser melting». This method (Selective Laser Melting) allows manufacturing complex-profile products on a computer model virtually of any metallic powders.

The exhibition of manufacturers of welding consumables, with participation of PWI, Paton PWE, Sumy-Electrode LLC, VITAPOLIS LLC, VELMA LLC, PLAN-T LLC was held during the Conference.

A series of bilateral negotiations directed on cooperation and further collaboration, and performance of joint projects took place during the Conference and Exhibition work.

In the second day of the Conference its participants visited Paton Pilot Plant of Welding Equipment.

Drs A.T. Zelnichenko, V.N. Lipodaev, PWI

Calendar of July

JULY 1, 1957 Date of birth of Yu.S. Korobov, professor, honoured inventor of the Russian Federation. At his participation, new designs of holders for welding semiautomatic devices, technologies of submerged-arc welding of shells, surfacing of axes of balancers of special equipment were developed and implemented. Under his supervision, the technology of spraying by electrometallization of steel coating on the aluminum base of worn-out surface of the roller of a creeper tractor was developed. The conception of improving the quality of coatings during arc metallization based on the analysis of the results of modelling physicochemical processes and studying the properties of coatings was developed and scientifically grounded.

JULY 2, 1929 American inventor and businessman Edward Budd (1870–1946) received a patent on the technology of welding in the automotive industry. Edward Budd was a pioneer in the mass production of all-metal car bodies and founded his own company «Edward Budd Manufacturing Company». Preferring the frame metal structures, Edward Budd proceeded not only from the fact that they are stronger than wood ones and also more manufacturable. Edward Budd was the first who applied spot welding in the automotive industry.

JULY 3, 1960 At the beginning of July 1960, T.M. Slutskaya (1907–1987), a representative of the Paton School, developed for the first time the self-shielding activated electrode materials for arc welding. She developed the basis of alloying wires with rare earth and rare metals, due to which nitrogen was bound into refractory nitrides.

JULY 4, 1981 The largest Soviet nuclear-powered submarine in the world, a heavy strategic-purpose missile cruiser submarine of the Project 941 «Akula» with a length of more than 170 m was put into tests. Its pressure hulls were welded from sections (shells) of cylindrical, conical and elliptical shape with a wall thickness of 75 mm. A similar submarine at the same time was created in the United States and, later on was named «Ohio».

JULY 5, 1931 Date of death of Oscar Chelberg (1870–1931), a Swedish inventor and industrialist, founder of the company ESAB in 1904. Oscar Chelberg invented the electrode coating used for manual arc welding by immersion of a bare steel wire into the mixture of carbonates and silicates. The purpose of the coating is to protect the molten metal from the effect of oxygen and nitrogen, present in the atmosphere. His pioneering developments laid the foundation for beginning the investigations on the development of reliable welding electrodes. Today, ESAB produces welding materials, equipment for welding and cutting of metal for practically all the branches of industry.

JULY 6, 1935 The construction of the German heavy cruiser «Admiral Hipper» was started. After signing the Treaty of Versailles, Germany was restricted in the construction of large-capacity ships. In order to officially comply with the restrictions to weight, several radical innovations were included in the design of this type of a ship. Designers were the first to use welding in large military ships instead of riveting. Because of their heavy armament of eight 203 mm guns and small sizes, the British began referring to such vessels as «pocket battleships». The hull of the ship was built of transverse steel frames; more than 90 % of the structure was joined using welding, which reduced the total mass of the hull by 15 %.

JULY 7, 1962 The absolute speed record of 2681 km/h was set in the experimental all-weather interceptor E-166 of the Design Bureau «MiG». This flight was performed by the test pilot G.K. Mosolov. Unlike the Americans, who chose a titanium alloy as the basic material of their reconnaissance aircraft, the «Experimental Design Bureau named after A.I. Mikoyan» chose different grades of steels. Its application allowed refusing from riveted structures in favour of welded ones. This, in turn, required the creation of new technological cycles, taking into account the use of different welding methods during a large-panel assembly. The experimental operation of the E-166 aircraft allowed gaining an important flight experience at high supersonic speeds.

JULY 8, 1761 Date of birth of V.V. Petrov (1761–1834), a Russian physicist- experimenter, self-taught electrical engineer, academician of the St. Petersburg Academy of Sciences. One of the outstanding achievements of the scientist was the discovery of the phenomenon of an electric arc in 1802 and evidence of the possibility of its practical application for the purpose of melting, welding metals and their reduction from ores and for lighting. In 1802, he designed a large galvanic battery consisting of 2100 copper-zinc cells with an electromotive force of about 1700 V.

*The material was prepared by the Steel Work Company (Krivoy Rog, Ukraine) with the participation of the editorial board of the Journal. The Calendar is published every month, starting from the issue of «The Paton Welding Journal» No.1, 2019.

JULY 9, 2014 The first launch of the rocket-carrier of «Angara» family from the «Plesetsk» Cosmodrome was performed. The rocket is capable of delivering 35 tons of cargo into orbit. The requirements of strength and tightness of welds of the fuel tanks were the most fully satisfied by argon-arc welding. During the construction of the «Angara» rocket -carrier, it is supposed to gradually introduce friction stir welding for application. The «Angara» rocket-carrier replaces the outdated model «Proton-M».

JULY 10, 1905 During dispersal of the workers meeting, L.I. Borchaninov (1837–1905) was killed. He was a worker at the Motovilikh plants, one of the first welders in Russia. He was working under the supervision of N.G. Slavyanov, an inventor of arc welding of metals. Together with the worker P. Aspidov, he accompanied Slavyanov to the Fourth Electrical Exhibition in St. Petersburg, where they equipped a temporary workshop and demonstrated the process of restoring metallic parts using electric welding. He participated in the building of the largest in Russia and Europe tugboat «Kasogs Prince Rededya», where welding was used instead of riveting for the first time in the history of shipbuilding.

JULY 11, 1979 «Skylab», the first and only American space station, leaved the orbit, completing its work. During the flight, experiments were carried out on evaluation of the effect of zero gravity on the quality of welded joints produced by electron beam welding. The «Skylab» station was equipped with a complex which included multi-purpose electric furnaces and an electron beam installation. The experiments were conducted on the investigation of molten metal, photographing the behaviour of calcined materials in zero gravity, studying the crystal growth, treatment of immiscible alloys and brazing of stainless steel.

JULY 12, 1929 The first in the history of aviation the flight of the German giant flying boat «Dornier Do-X» took place. The aircraft was designed for service at the long-distance passenger airlines. On October 20, 1929, during a 40-minute demonstration flight, this plane took off from the Lake Constance with 169 passengers on board. This record remained unsurpassed in the first half of the XX century. Due to the low flight characteristics, the aircraft did not come to the series production but only made several demonstration flights to Africa, North and South America in 1930–1932. In order to reduce weight, welding was applied for joining aluminum parts.

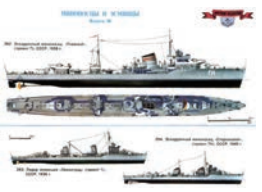

JULY 13, 1936 The destroyer of the project 7 «Gnevny» was launched. It was the main ship of the so-called Stalinist series, built for the Soviet Navy in the second half of the 1930s, one of the most popular types of destroyers in the history of the Soviet fleet. The thickness of the hull lining was 5–9 mm, the deck flooring was 3–10 mm, and the watertight bulkheads were only 3–4 mm. The structures were mainly riveted, but the electric welding was used for the assembly of bulkheads, platforms under the lower deck and a number of other elements.

JULY 14, 1969 An inhabited underwater apparatus designed to study the middle depths of the Gulf Stream (up to 1000 m), the Ben Franklin mesoscaphe, was submerged into the water. It was designed by Jacques Picard. A special attention was paid to welds. Numerous tests and examinations were carried out before it was allowed to use the apparatus. For welding, electrodes, alloyed with manganese and molybdenum, were used.

JULY 15, 2010 In the summer of 2010, the book «Paton School» was prepared for publication. It presents information about the world-famous Paton's scientific and engineering school in the field of welding and related technologies, which was organized by academician E.O. Paton, an outstanding scientist, and further developed by academician B.E. Paton, a worthy successor of his activities. In the book the formation and development of this school is highlighted and information about its famous representatives is given.

JULY 16, 1961 By decree of the Presidium of the Supreme Soviet of the USSR for great successes in the development of the rocket industry, science and technology, successful performance of the first flight of a Soviet man in space in the «Vostok» spacecraft-satellite, M.K. Yangel was re-awarded the title Hero of Socialist Labour.

JULY 17, 1964 By resolution of the Council of Ministers of the Ukr.SSR of 12.06.1964 No. 59.5 and resolution of the Presidium of the Academy of Sciences of the Ukr.SSR of July 17, 1964 No. 188 the E.O. Paton Prize of the National Academy of Sciences of Ukraine was established for outstanding scientific works in the field of developing the new metallic materials and methods for their treatment. This is one of the few examples where the award is named after a welder-scientist.

JULY 18, 1955 At Disneyland an amusement facility: a model of a space rocket called Moonliner, was opened. Since 1955 to 1962 Moonliner was located in the first futuristic exhibition. It was also an example of a new approach to modern advertising media. In order to build a 27-meter aluminum rocket the welding in inert gases was used. It is interesting that with the development of rocket construction, the same welding methods were used in the production of real space rockets. The construction of such a facility caused a wide resonance with the public already before the launch of the first satellite of Earth.

JULY 19, 1900 The opening of the Paris Metro took place. The opening was dated for the beginning of the 1900 World's Fair. The Paris Metro is one of the oldest metros in Europe (the fourth after the London, Budapest and Metro in Glasgow). The unsurpassed capabilities of thermit welding at that time were demonstrated visually during laying the tracks of the Paris Metro.

JULY 20, 1966 The crew commander Neil Armstrong and the pilot Edwin Aldrin of the American spacecraft «Apollo-11» landed a lunar module on the Moon. The accomplishment of this project could not be achieved without the use of modern welding technologies.

JULY 21, 2007 The skyscraper «Burj Khalifa» of 829.8 m height was officially recognized as the tallest building in the world during construction. The solemn opening ceremony took place on January 4, 2010 in Dubai, the largest city of the United Arab Emirates. During its construction the welding technologies were especially in demand. They were applied starting from the foundation and ending at the highest point, where everything was fastened either with bolts or electric arc welding. It is one of the records and demonstrates how large structures can be created by welding. The spire of «Burj Khalifa» is a complex steel structure with many columns and welded beams.

JULY 22, 1872 Date of birth of V.F. Mitkevich (1872–1951), an outstanding Russian and Soviet electrical engineer, academician of the Academy of Sciences of the USSR. In 1901, he proposed circuits of a single-phase full-wave rectifier (full-wave with two windings) for converting an alternating current into a direct current and a three-phase one-half-wave rectifier (half-wave with zero output). V.F. Mitkevich was the first in the world to propose a three-phase arc for welding metals.

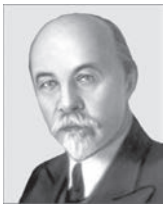

JULY 23, 1995 Date of death of N.A. Langer (1910–1995), a chemical scientist-analyst, representative of the Paton school. He made a significant contribution to the development of methods for protection of welded joints against corrosion. He proposed original electrochemical methods for studying the corrosion resistance of welded joints. They allow predicting the stability of joints during operation in the environments with a high corrosion activity. Langer investigated the conditions for the occurrence of particularly threatening corrosion of welded joints, the so-called crevice corrosion, and also identified methods for its elimination. The results of a number of works have found application in industry.

JULY 24, 1967 In St. Louis the Arch was opened, also known as a Gateway to the West. It is a memorial, which is the hallmark of St. Louis. Its height is 192 m at the highest point and the width of its base is also 192 m. The arch is the highest monument at the territory of the United States. Builders, together with the company «Lincoln Electric», successfully manufactured and joined 142 parts of one of the most complex building structures in the US history. During its construction the manual arc welding, semi-automatic gas-shielded welding and submerged-arc welding were used.

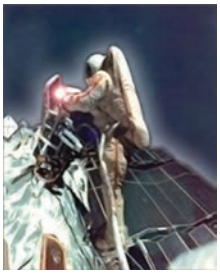

JULY 25, 1984 In open space outside the board of the orbital station «Salyut-7», experiments in electron beam welding were carried out using a welding device URI (a versatile hand tool) designed at the E.O. Paton Electric Welding Institute. This device allowed welding, cutting, brazing metal and depositing coatings. The cosmonauts V. Dzhanibekov and S. Savitskaya went into outer space to perform welding technological works. For three and a half hours, the cosmonauts conducted the entire complex of planned experiments.

JULY 26, 1845 The ship «United Kingdom» with an all-metal hull started its first voyage across the Atlantic. The vessel was distinguished by its enormous sizes: its length was almost 100 m. In the «United Kingdom» for the first time, a screw propeller was used instead of paddle-wheels. That was a real event in shipbuilding. When creating a huge crankshaft for the ship, a new modernized «welding hammer» was used, invented by Joseph Stenster.

JULY 27, 1942 The American interceptor «Mustang NA-73X» took the first air battle. The need in accelerated production of military machinery forced the use of welding even wider. It was estimated that during the transition to welding in an aircraft weighing 4 tons, where it was usually necessary to apply up to 100,000 rivets of 112.5 mg each, a weight reduction of about 10 % is achieved. At the same time, aerodynamics, tightness and corrosion resistance are improved, and the time for manufacturing the whole structure is shortened by 60 %.

JULY 28, 1883 Date of birth of V.P. Vologdin (1883–1950), a Soviet scientist and engineer, a pioneer in the use of electric welding in ship building. He designed and built the first all-welded ship in the USSR. A tugboat of the series «ZhS» (iron welded) was built. It turned out that a hull of the ship became lighter, the labour intensiveness of the ship building was reduced by a third.

JULY 29, 1993 A certificate on registration of the Society of Welders of Ukraine was issued. It was founded in November 1992 by the initiative of the E.O. Paton Electric Welding Institute (Kiev). The organization unites all scientists, teachers, specialists, craftsmen and workers in the field of welding and related processes in Ukraine. The main task of the Society is informational, consulting, legal support of all workers employed in the welding industry of Ukraine.

JULY 30, 1904 The longest battle of the Russian-Japanese War, the defence of Port Arthur (July 30–December 23, 1904) began. The sailors of the Russian fleet and the workers of the Baltic Ship Repair Plant, located in the besieged city, successfully used arc welding by a coal electrode to repair the ship hulls.

JULY 31, 1962 Date of death of Nils Miller (1899–1962). He left after him a large company «Miller Electric». In the 1920s almost all electric arc welding was carried out using a bulky and expensive three-phase generator. In 1929, Nils Miller realized the need in designing a small and inexpensive welding machine, operating from the power mains. In 1935, the company «Miller Electric» was founded. Next year, El Mulder, the chief engineer of the «Miller Electric», invented the first in the world high-frequency industrial welding device at alternating current. This invention significantly improved the quality of welding and allowed using welding at alternating current.